Received June 26, 2018, accepted July 6, 2018, date of publication July 10, 2018, date of current version August 7, 2018.

Digital Object Identifier 10.1109/ACCESS.2018.2854820

Towards Studying the Two-Tier Intra-Frequency X2 Handover Based on Software-Defined Open LTE Platform

JIANXIN JIA[1], GUANGZHONG LIU[1], DEZHI HAN[1], AND JUN WANG[2], (Senior Member, IEEE)
[1]College of Information Engineering, Shanghai Maritime University, Shanghai 201306, China
[2]Department of Electronic Engineering and Computer Science, University of Central Florida, Orlando, FL 32816, USA

Corresponding author: Guangzhong Liu (gzhliu@shmtu.edu.cn)

This work was supported by the National Natural Science Foundation of China under Grant 61672338 and Grant 61373028.

ABSTRACT The next generation cellular systems are rapidly evolving from a homogeneous macrocell deployment to a heterogeneous deployment of macrocells overlaid with femtocells, which is referred to as heterogeneous networks (HetNets). In macro-femto HetNets, the handover issue is more important than that in macrocell networks. On one hand, more frequent handovers are triggered because the coverage range of the femtocell is small, and the multiple femtocells are overlaid with macrocells. On the other hand, some schemes, such as load balancing, aimed at improving network performance, will also cause frequent handover in macro-femto HetNets. Therefore, the study on handover is of great importance, especially in macro-femto HetNets. In this paper, based on the software-defined open long-term evolution (LTE) platform, we propose an analytical model to study the two-tier intra-frequency X2 handover in realistic macrocell-femtocell HetNets scenario. Specifically, we first construct the software-defined open LTE platform. Based on the open LTE platform, we then characterize the relation between the handover failure and the ping-pong rates in a macro-femto HetNets scenario as a function of the relevant system parameters such as the time-to-trigger, user equipment velocity, etc. Finally, we derive the handover failure and ping-pong rates in closed-form expressions. The handover experiment results have verified the accuracy of our analytical derivations, which shed new light on key aspects of the handover process in macro-femto HetNets.

INDEX TERMS Macro-femto HetNets, software-defined, open LTE platform, X2 handover, long-term evolution.

I. INTRODUCTION

The wireless data traffic is increasing dramatically due to proliferation of smart devices and the high dependency on mobile communications in everyday life. Among the possible techniques to overcome the capacity crunch problem, network densification is seen as the most promising solution [1]. As a result, Femtocells are being deployed within the macrocell coverage to offload some of the users associated with the latter. This is referred to as macro-femto heterogeneous networks (i.e., macro-femto HetNets) and it is being considered for the Long-Term Evolution Advanced (LTE-A) and beyond. It has been estimated that 50 million base stations will be deployed as soon as 2020 [2]. Typically, a femtocell base station has a radio coverage of 5 to 100 meter-radius, and a macrocell base station with a radio coverage area of 0.5 to 2 kilometer-radius may overlap with a large number of femtocells. With the deployment of ultra-dense femtocells, the femtocells provide wireless transmission services with higher data rate, offload data traffic from a macrocell, and expand the service area of a macrocell. However, along with dense femtocell deployments in hot-spot coverages, macro-femto HetNets come with challenges in terms of mobility management [3], [4]. Fig.1 illustrates a typical cross-tier handover scenario. With the dense deployment of macrocells and femtocells, those cells are overlaid with each other. Also, due to the small and non-continuous service areas of the small, frequent handover executions occur in the macro-femto HetNets. As a consequence, the UE will experience a high handover rate (i.e., frequent handover from macrocell to femtocell, then to macrocell again). According to the standard discussions and evaluation results by the 3rd Generation Project

2169-3536 © 2018 IEEE. Translations and content mining are permitted for academic research only.
Personal use is also permitted, but republication/redistribution requires IEEE permission.
See http://www.ieee.org/publications_standards/publications/rights/index.html for more information.

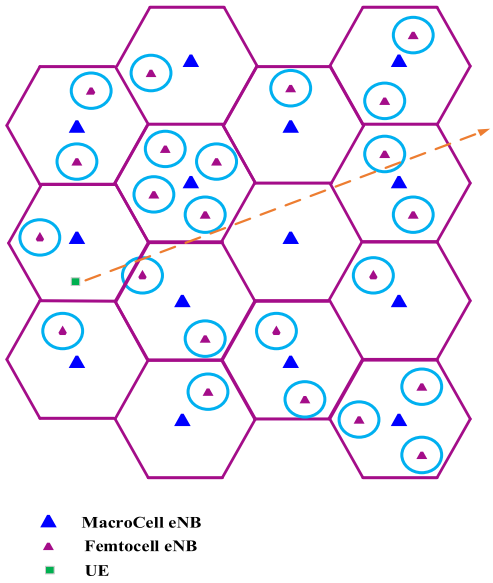

FIGURE 1. An instance of the cross-tier handover in macrocell-femtocell scenarios, where the purple hexagon and light blue circle are the macrocell boundary and femtocell boundary, respectively.

Partnership (3GPP), the cross-tier (i.e., from macrocell to femtocell) handover rate and handover failure rate in macro-femto HetNets are observed to be much higher than in a macro cell only network [5]. Frequent handovers in macro-femto HetNets not only brings heavy signaling overhead on the network, but also degrades the user experience. Therefore, the cross-tier handover is treated as the bottleneck of dense macro-femto HetNet deployments, which need to be analyzed in details.

In general, the handover process, standardized by the 3rd Generation Partnership Project (3GPP) [6], is triggered by the UE, which periodically measures the Reference Signal Received Power (RSRP) from the surrounding cells. When the difference between the RSRP of a neighboring cell and that of the serving cell is higher than a fixed handover hysteresis value (i.e., event A3 in [7]), the handover process starts. If this condition holds for a period of time equal to the Time-To-Trigger (TTT) parameter, the handover is finalized and the user equipment connects to the base station with the strongest RSRP. The handover process allows a UE in connected mode to transfer its connection from its serving cell to a target cell, while guaranteeing quality of service. Since the handover process depends on a large number of different parameters (e.g., hysteresis margin, time-to-trigger (TTT), UE velocity, etc.), its optimization is an intricate problem. Indeed, the handover optimization problem has received large attention from the cellular community and standardization bodies. However, due to the recent development of macro-femto HetNets, the handover problem should be revisited.

In traditional homogeneous networks (i.e., macrocells), mobile UE typically uses the same set of handover parameters for handing over a target cell. However, in a macro-femto HetNets, using the same set of handover parameters for all cells and for all UEs may increase the rate of handover failures and ping-pongs. Despite some recent results analyzing mobility performance in macro-femto HetNets [8]–[10], to our best knowledge, the theoretical analysis of handover failure and ping-pong probabilities based on software-defined open LTE platform in macro-femto HetNets is not available yet in the prior works. In this paper, in order to better understand the impact of macro-femto HetNets roll-outs on the handover process, we derive closed-form expressions for handover failure and ping-pong rates as functions of relevant system parameters such as TTT and UE velocity in a macro-femto HetNet scenario. In our analysis, the femtocell coverage and radio link failure areas are modeled as circular regions, and the UEs trajectories are linear, which are aligned with the macro-femto HetNets mobility experiment assumptions in a related study item in 3GPP [11].

There are two main handover modes in macrocell-femtocell HetNets scenario, which are S1 handover and X2 handover. Many works have been done comparing the S1 and X2 handover in terms of the EPC signaling load and the results proofs that X2 handover can reduce EPC signaling load more than six times compared with S1 handover. X2 handover can be a sort of solution to decrease the load impact to the EPC and to increase the reliable inbound handover (i.e., from the macrocell to the femtocell) [12], [13]. Therefore, this paper will focus on intra-frequency X2 handover in two-tier (i.e., macro-femto) HetNets that happens between eNBs. In most of the cases, both source and target eNBs are connected to the same MME and are located in the same tracking area (TA). The measurement cases cover the handover between two cells supporting the X2 interface between the eNBs.

To sum up, the goal of this paper is to analyze and characterize the performance of the intra-frequency X2 handover in macro-femto HetNets scenario. Our contributions can be summarized as follows:

- Base on the current version Evolved Packet Core (EPC) source code in the OpenAirInterface Software Alliance (OSA) which is a non-profit consortium fostering a community of industrial as well as academic contributors for open source software and hardware development for the core network (EPC), access network and user equipment (i.e., the EUTRAN) of 3GPP cellular networks, we propose a software-defined open LTE platform which is composed of the commercial UEs, commercial eNBs, and the soft EPC. Specifically, since the current version EPC cannot support the X2 handover, we first supplement the codes in the MME module and the Service &Packet Gateway (SPGW) modules based on the X2 handover sequence defined in the 3GPP protocol. We then carry out the X2 handover experiment to validate our supplement functions in EPC. The uninterruption application session in UE and the complete signaling messages captured by the Wireshark Application have demonstrated that what we have contributed in the EPC.

- Based on the software-defined open LTE platform, we propose a small cell coverage model through intra-frequency X2 handover experiment where the small cell boundary and the cross-tier handover failure boundary can be roughly represented by two biased circles. Based on the proposed model, we derive analytical closed-form expressions for cross-tier (i.e., two-tier) no handover rate, macrocell to femtocell handover failure rate, femtocell to macrocell handover failure rate, and ping-pong rate as functions of relevant system parameters, including the Time to Trigger (TTT), the Radio Frequency (RF) Transmission (Tx) power (i.e., the Tx power is proportion to the eNB's signal radius) of each tier eNB (i.e., the macrocell eNB and the femtocell eNB), and the UE mobility velocity. These analytical results could provide support for improving the mobility management in HetNets.
- Based on the software-defined open LTE platform, the accuracy of the analytical results is verified through the two-tier intra-frequency X2 handover experiment. Moreover, the effects of system parameters, such as the eNBs' RF Tx power, the TTT, the A3 offset, and the UE velocity, are studied on the handover performance, which would provide guidance for actual network planning in densely deployed HetNets scenarios which are comprised of coexisting macrocells and small cells (e.g., the femtocells).

The remainder of this paper is organized as follows. We briefly review the related works and the state of the art in Section II. Section III presents the system architecture and X2 handover procedure with deployed femtocells. In section IV, the construction process of the software defined open LTE platform is presented, the small cell coverage and handover failure boundary model are derived, and the handover failure rate and ping-pong rate with closed-form expressions are presented. Section V provides experiment evaluations with verifications to the analytical results. Finally, Section VI provides concluding remarks and future directions.

II. RELATED WORK

In recent years, some works have specifically investigated the handover procedure in macro-femto heterogeneous cellular networks [2], [3]. These works divided the handover procedure in macro-femto heterogeneous cellular networks into three categories: hand-out, hand-in, and hand-inter. A hand-out is the handover procedure from a femtocell to a macrocell, a hand-in is the handover procedure from a macrocell to a femtocell, and a hand-inter is the handover procedure between different femtocells. Different handover procedures are based on different handover decisions and different cell selection algorithms, but the signaling flow for these handover procedures is almost the same as shown in Fig. 4. In this paper, we mainly focus the handover from the macrocell to the femtocell (i.e., hand-in).

The authors in [6] proposes a distance-based handover scheme. In this scheme, a mobile user obtains his moving distance d in a femtocell coverage area. Then d is compared with a threshold *TTHR*, and handover is triggered according to the comparison result. The moving distance is calculated according to the change rate of Received Signal Strength (RSS) measurement. Oh *et al.* [12] propose an algorithm that, while keeping the TTT and hysteresis margin constant, adaptively modifies the Cell Individual Offset (CIO) parameter, which is a margin to be added to the RSRP for load management purposes. The authors show that a UE can detect changes in its mobility pattern by monitoring the changes of the type of handover failure events (e.g., too early or too late handover events, handover failures, or handover to the wrong cell) and, hence, can adjust the specified CIO parameter to minimize both the handover failure and the ping-pong rates. For a macro-femto HetNet with dense femtocell deployment, [10] proposes an algorithm to make a minimum but appropriate number of neighboring femtocells to increase successful handover. This algorithm considers received signal level, access modes, and detected frequency from neighboring femtocells. As a femtocell does not support high-speed mobility, and the coverage of a femtocell is small, Perez *et al.* [3] make handover decisions according to the mobile speed of users and selecting the target cell according to the RSS or available resource. There are also some works that jointly consider RSS, SoT, and NoF to make switching decisions. In [2], the handover decision is made according to both the measurement parameters (e.g., RSS indicator, RSSI, and Interference-plus-Noise Ratio (INR)) included in the handover requests and the femtocell's special parameters such as access mode, traffic load, and capability.

Reference [18] analyzes the Cell Range Expansion (CRE) technique that consists in enlarging the small cell coverage in order to balance the users load. The authors simulate the effect of both CRE bias and hysteresis margin on the handover failure and ping-pong rates, while fixing the TTT parameter. A different approach is presented in [19] where the handover decision is based on a mobility prediction algorithm that estimates the residence time of the UE in the possible target cell. The proposed policy allows the UE to switch to the target cell only when the estimated residence time is above a certain threshold. Jeong *et al.* [20], present a mobility state estimation algorithm which groups UEs into three speed classes and assigns a fixed TTT value to each of them, such that high speed UEs avoid the handover to Picocells, while lower speed UEs perform handover in order to minimize their Radio Link Failure (RLF) rate. Choi [24], instead, propose a joint algorithm that, on the one hand, tunes TTT and the hysteresis parameters to optimize the hand over performance metric (defined as a weighted sum of RLF, ping pong and handover failure) and, on the other hand, adapts the handover margin to achieve a load balancing condition. Considering the resource constraints in a target femtocell, which can cause handover failure, [7] proposes a multi-objective handover solution for LTE macro-femto HetNets, which considers both signal strength and available bandwidth when selecting the optimal target cell. In [8], an efficient handover decision

algorithm based on available data volume, which indicates the amount of data that the UE can receive from the macrocell or femtocell, is proposed for macro-femto HetNets. It uses users' mobility to estimate the time that users stay in a femtocell. Then a user computes available data volume from the macrocell and femtocell during estimated time. If the available data volume from the femtocell is greater than the available data volume from the macrocell, the UE performs a handover from the macrocell to the femtocell. Otherwise, the UE keeps the macrocell connection. A study of more general user trajectories is presented in [17], where the authors propose a realistic user mobility model, and present analytic expressions for the handover rate, i.e., the expected number of handovers per unit time, and the cell sojourn time, i.e., the expected duration that the user stays within a particular serving cell.

Although the state of the art solutions improves the efficiency of handover in HetNets with respect to the special setting of the handover related parameters, in these works, however, all users utilize the simulator to validate their HetNet handover analytical model and evaluate the experiment results, which may not suitable when it comes to the realistic scenario. To our best knowledge, the experiment validation for the handover analytical model, which based on the realistic HetNet (i.e., macrocell-femtocell) scenario (i.e., software defined open LTE platform) rather than based on the simulator, has not been proposed in the literature, which is one of the main contributions of this paper.

III. THE MACRO-FEMTO HetNets SYSTEM ARCHITECTURE AND X2 HANDOVER PROCEDURE WITH DEPLOYED FEMTOCELLS

A. THE MACRO-FEMTO HetNets SYSTEM ARCHITECTURE

In this section, we first introduce the macro-femto heterogeneous network scenario, and then we detailly depict the X2 handover procedure. The overall LTE system architecture with femtocell deployment is shown in Fig.2. In the context of LTE, a macrocell station is referred to as evolved Node B (i.e., eNB) and a femtocell station as home eNB (i.e., HeNB). As illustrated in Fig. 2, two of the evolved packet core (EPC) network entities are involved in the support of eNBs and HeNBs, the Mobility Management Entity (MME) and the Serving Gateway (SGW). The MME implements the functions of core network (CN) signaling for Mobile Management (MM) between 3GPP access networks, idle state mobility handling (e.g., paging), tracking area list management, roaming, bearer control, security and authentication. On the other hand, the SGW hosts the functions of lawful interception, charging, accounting, packet routing and forwarding, as well as mobility anchoring for intra and inter-3GPP Mobile Management. In the presence of femtocells, the E-UTRAN architecture consists of eNBs, HeNBs, and HeNB gateways (i.e., HeNB-GW). The eNBs provide user and control plane protocol terminations towards the UE, while they support the functions of radio resource

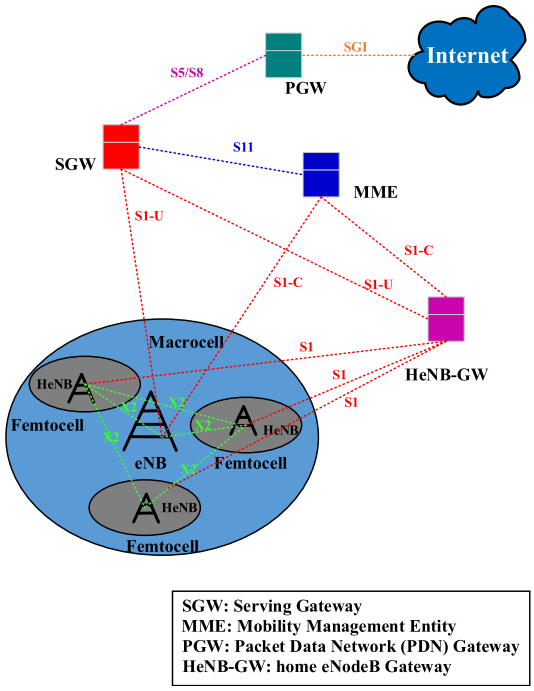

FIGURE 2. The Macro-Femto heterogeneous network architecture.

management, admission control, scheduling and transmission of paging/broadcast messages, measurement configuration for mobility and scheduling, as well as routing of user plane data towards the SGW. The functions supported by the HeNBs are the same as those supported by the eNBs, while the same implies for the procedures run between the HeNBs and the EPC. The HeNB GW acts as a concentrator for the control plane to support a large number of HeNBs in a scalable manner. The deployment of HeNB-GW is optional, however, if present, it appears to the HeNBs as an MME and to the EPC as an eNB. The eNBs and HeNBs interconnect with each other through the X2 interface [26], [27], while they also connect to the EPC through the S1 interface [28], [29].

Moreover, shown in Fig.2, six standard interfaces (i.e., S1, X2, S5, S8, S11, SGI) are specified by the Third Generation Partnership Project (3GPP). The S1 interface supports interconnection between the mobility management entity (MME) and the eNB, specifically, the S1-C interface is responsible for the control plane communication between the eNB and the MME, while the S1-U interface is responsible for the data plane communication between the eNB and the SGW. The X2 interface describes functionalities for mobility and defines information exchanged between different eNBs. In 3GPP Release 11, the X2 interface is also defined between HeNBs. The S5/S8 interface is used for transporting the data plane and user plane packets between a Serving GW and a PDN GW. The S11 interface is responsible for delivering the control plane packets between the MME and the SGW. The SGI interface supports the interconnection between the PGW and the Internet, which is used for transmitting/receiving the data plane packets to/from the Internet. Here, we mainly focus on the X2 interface.

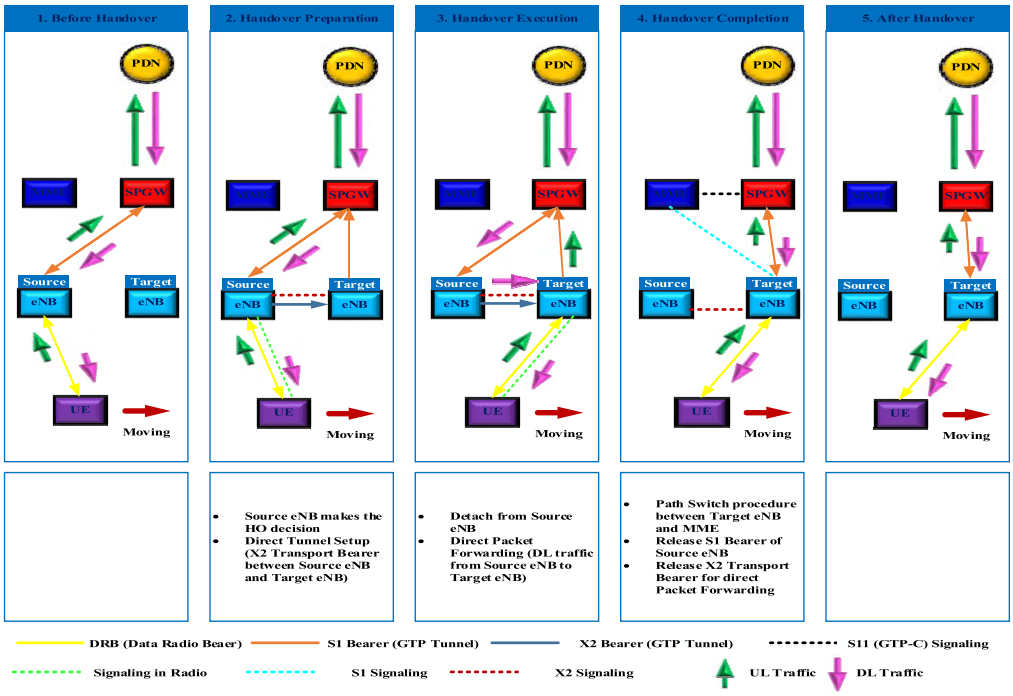

FIGURE 3. The packets forwarding process under X2-based handover scenario.

B. THE X2 HANDOVER PROCEDURE WITH DEPLOYED FEMTOCELLS

For the handover procedure in LTE system, a connection has to be established among eNBs in order to signal with each other for handover. This is managed through X2 interface, using X2 Application Protocol (X2-AP). To be specific, the X2 handover key features, the packets forwarding process under X2 handover scenario, and the X2 handover procedure sequence diagram will be detailly presented in the next.

The X2 handover key features are [30]:

- The whole procedure is directly performed between the two eNBs.
- MME is involved only after the handover procedure is completed for the path switch procedure contrary to the S1 handover that is MME assisted decreasing the delay and the network signaling overhead.
- The release of source eNB resources is triggered via the target eNB at the end of the path switch procedure.

Fig. 3 shows packets forwarding process under X2 handover scenario. As illustrated in Fig.3, there are five phases in the X2 handover process, which are ''Before Handover'', ''Handover Preparation'', ''Handover Execution'', ''Handover Completion'', and ''After Handover''. In the first phase, the direct packets forwarding tunnel for uplink and downlink packets traffic are established among the UE, the source eNB, and the SGW. As UE moving, the X2 handover process step into the second phase, during this phase, the source eNB make the handover decision and send the ''handover request'' signaling message to the target eNB. After the source eNB received the ''Handover Request Ack'' signaling message form the target eNB, the X2 transport bearer between the source eNB and the target eNB is established. Then the X2 handover procedure step into the third phase, in this phase, the UE detach from the source eNB and the direct uplink data plane packets forwarding tunnel is established. But at this moment, the path of the downlink data plane packets is SGW - source eNB - target eNB - UE, which demonstrates that the direct downlink data plane tunnel is not established. Once the UE has successfully sent the handover complete message to the target eNB, the X2 handover process step into the fourth phase, then the target eNodeB can start sending downlink packets directly to the UE. The target eNodeB indicates to the Mobility Management Entity (MME) that the S1-U interface needs to be switched from the source eNodeB to the target eNodeB. The MME updates the SGW with the new address information for the downlink of the user plane and confirms the relocation of the S1-U interface towards the target eNodeB with signaling message ''Path Switch Ack''. There can be a time interval between packets forwarded by source eNodeB and those coming from the SGW which may give a rise of the out-of-order packet delivery impacting badly on TCP performance. When the SGW receives the command to switch the user plane to the target eNodeB, SGW switches the downlink data path to the target side. SGW sends one or more ''end marker'' packets on the old path to source eNodeB and then releases any user plane resources towards source eNodeB. Once ''end marker'' reaches target eNodeB, it can start sending downlink payload data coming from the SGW. It is desirable that during inter-eNodeB handover the initially negotiated quality

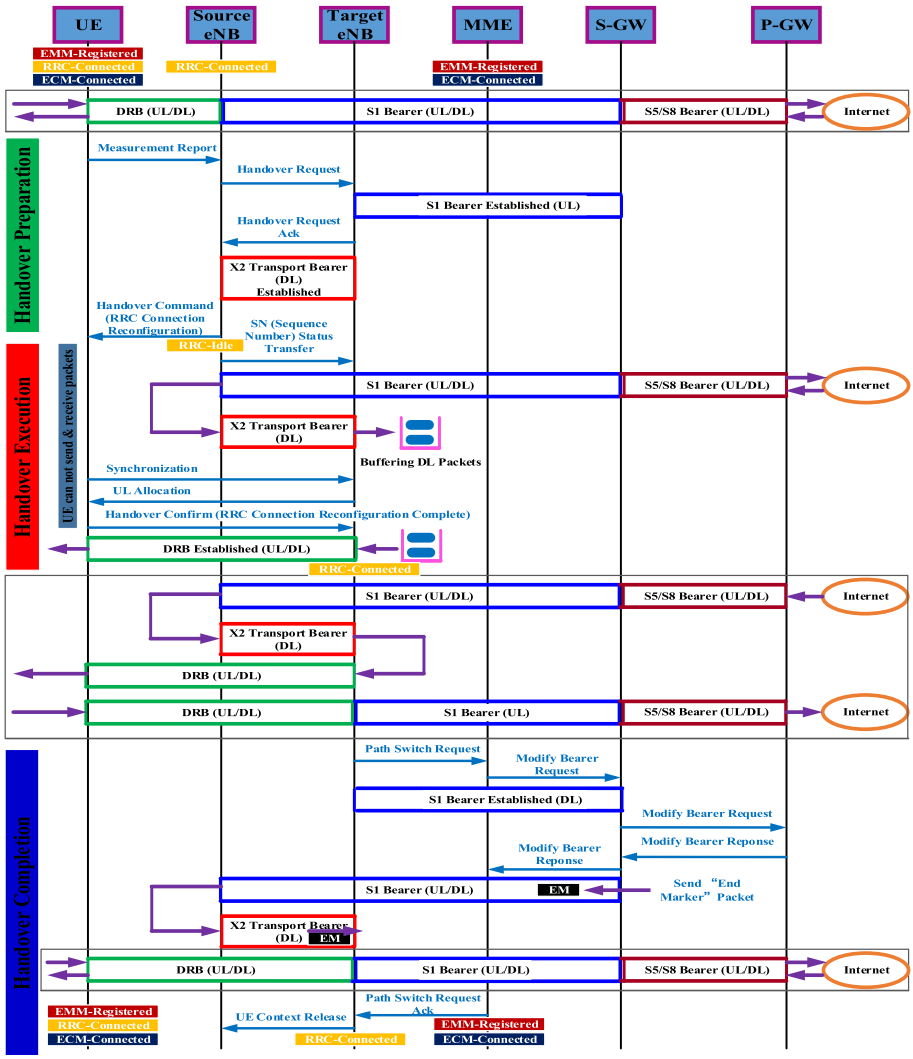

FIGURE 4. The X2 handover procedure sequence diagram.

of service be maintained, i.e. packets are delivered to the target eNodeB in sequence, there is not any duplicate or lost packet, and the interruption time does not affect the applications running. Finally, in the fifth phase, the direct packets forwarding tunnel for uplink and downlink packets traffic are successfully established among the UE, the target eNB, and the SGW, which indicates that the UE has successfully handover from the source eNB to the target eNB.

Based on Fig.3 and its related description, in the next, we will analyze the intra-frequency X2 handover from another dimension (i.e., the signaling sequence diagram). As shown in Fig.4, the three tunnels in those three rectangles are referred to the user data plane, which is established between the UE and the PGW.

The X2 handover procedure can be described in five phases, as shown in Fig. 4:

(1) Before Handover: UE is attached to the source eNB. The Dedicated Radio Bearers (DRBs) and Signaling Radio Bearers (SRBs) are established and UL or DL traffic is transmitted between the source eNB and the UE. The UE remains in the Radio Resource Control (RRC)-Connected, EMM-Registered, and ECM-connected states with respect to the source eNB. Also, UE keeps all the resources allocated by EUTRAN and EPC.

(2) Handover Preparation: The UE sends the periodical measurement report to the source eNB, this report contains information about the neighboring cells. The source eNB triggers the handover based on the reported measurement results, i.e., A3 event [31] and chooses the best reported target cell by the UE. Then, the source eNB sends an X2 "Handover Request" signaling message to the target eNB. This message contains the information needed to perform the handover. Considering the QoS in the RAB context, the target eNB performs call admission control and if it is able to provide the requested resources for the new UE, it sends a "Handover Request Acknowledgment" signaling message to the source

eNB through the X2 direct tunnel setup. The source eNB receives this message that includes the configuration of the GTP-U tunnels per radio access data radio bearer as well as the RRC Connection Reconfiguration message in a transparent container that the source eNB has to forward to the UE. In the RRC message, the parameters in Layer 1 or Layer 2 are provided to the UE in order to be synchronized with the target eNB. Finally, the source eNB sends the ''Handover Command'' signaling message that encloses the signaling message ''RRC Connection Reconfiguration'' to the UE. If the target eNB cannot accept the handover request, it responds to the source eNB with an X2 failure message. During this step, the UE states remain unchanged.

(3) Handover execution: The UE receives the signaling message ''RRC Connection Reconfiguration'' sent from source eNB to UE and transits to the RRC idle state, which trigger the detachment from the source eNB. The source eNB sends the signaling message ''Sequence Number (SN) status transfer'' that contains the Packet Data Convergence Protocol (PDCP) sequence numbers to the target eNB through X2 interface. Then, UE is synchronized with the target eNB based on the given parameters, and the target eNodeB accepts the request and responds back with a timing adjustment and an uplink resource grant. Based on the above procedures, the UE sends the handover confirm message that encloses the ''RRC Connection Reconfiguration Complete'' to acknowledge the successful handover to the target eNB. As a result, the UE transits to the RRC connected state with respect to the target eNB.

(4) Handover Completion: The target eNB receives the ''RRC Connection Reconfiguration Complete'' sent by UE. At this point, the UE is receiving and transmitting data. The downlink data transmission towards the UE is still being routed via the source eNodeB. The path will now be switched to remove the source eNodeB from the path. Then the MME requests the SGW to switch the path to the target eNodeB, and then the SGW asks the PGW to switch the path. The PGW responds back to the SGW signaling the completion of the path switch, and the SGW then responds back to the MME signaling the completion of the path switch. The SGW also inserts an end marker towards the source eNodeB. This marker will be used to sequence the data received from the source eNodeB and the new data received from the target eNodeB. It should be noted that the target eNodeB does not release its data forwarding tunnels from the source eNodeB until it has received an ''end marker'' packet indicating that all forwarded packets have been received. Before the end marker is received by the source eNB, the UE Keep receiving the data from the zigzag path. Once the target eNB receives the end marker, the new path UE - target eNodeB - PGW is established. At the same time, the target eNB sends the downlink packets to UE from the new path. Based on the above-mentioned procedure, the MME responds back to signal the completion of the path switch. Finally, the target eNB asks the source eNodeB to release the UE Context.

(5) After Handover: After the handover is completed, the UE is attached to the target eNB. The new DRB and SRB are established, and the UL/DL traffic is transmitted as in the initial step. At this time, the UE remains in the RRC-Connected, EMM-Registered, and ECM-connected states with respect to the target eNB, and it keeps all the resources allocated by E-UTRAN and EPC.

IV. SOFTWARE-DEFINED OPEN LTE PLATFORM

A. THE CONSTRUCTION PROCESS OF SOFTWARE-DEFINED OPEN LTE PLATFORM

The current generation of hardware and software for radio access network (RAN) consists of large numbers of proprietary elements that stifle innovation and increase the cost for the operators to deploy new services in an ever-changing fast paced cellular network. Open source software running on general purpose processors (e.g., x86, ARM) can greatly simplify network access, reduce cost, increase flexibility, improve innovation speed and accelerate time-to-market for introduction of new services. There is already a movement going on within the industry on the development of Software Defined Networking (SDN) concepts to open the proprietary interfaces to control the hardware and software of the RAN. The open source implementation of fully real-time stack (i.e., soft eNB, soft UE, and core network (i.e., soft EPC)) on general purpose processors when combined with SDN, Network Function Virtualization (NFV) and OpenStack can bring significant efficiency in RAN design from both innovation and cost perspective [32].

As mentioned above, the progressive shift of functionality from hardware to software has been a steady trend in the electronic industry, and when nowadays demand for a new RAN functionality materializes, a software implementation on a flexible platform becomes often the preferred choice. In this section, we propose the software-defined open LTE platform which composed by commercial user equipment (e.g., mobile phone), commercial eNBs, and the soft EPC. Strictly speaking, the software-defined open LTE platform should be composed by software-defined UE (i.e., soft UE), software-defined eNBs (i.e., soft eNB), and soft EPC. Although the current version (i.e., the milestone labeled with the black words in Fig.5) of the open LTE platform is not completely opening due to the UE and eNB are hard-coded commercial equipment, we will develop the software-defined UE and software-defined eNB in our future work. Moreover, we have defined some new features for the software-defined UE and software-defined eNB, such as the Automatic Gain Control (AGC) which used for the soft UE handover. As shown in Fig.5, the current version of LTE platform is the milestone step of the final version (i.e., completely software-defined) with the reason that the commercial equipment can help us to figure out what the features of soft UE, soft eNB, and soft EPC should be through testing experiments. Then, based on the feature requirements analysis, we can develop the final version more effectively.

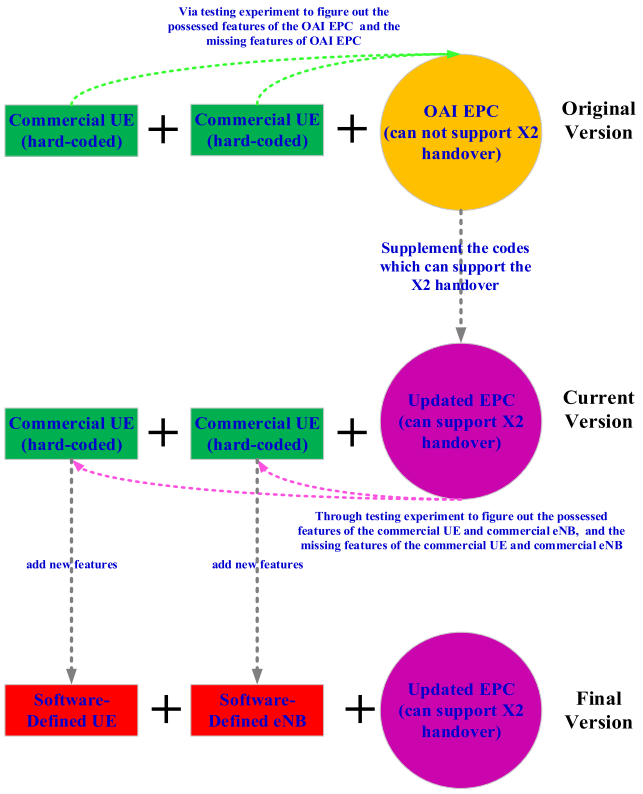

FIGURE 5. The evolution of the software-defined open LTE platform.

In this paper, we mainly focus on the study of two-tire intra-frequency X2 handover based on the software-defined open LTE platform (i.e., the real experiment scenario). To this end, we need first construct a mixed real-time software-hardware architecture, i.e., a software defined open LTE platform. Then, we propose the X2 handover analytical model and carry out the X2 handover performance study experiment based on the software-defined open LTE platform. To be specific, we have done the following works. We choose the OpenAir-Interface (OAI) EPC, the commercial UE, and the commercial eNB to compose the original version open LTE platform (i.e., the first phase in Fig.5). The reason for choosing the OAI EPC is that it is a mature product which is completely implemented based on the 3GPP protocol. However, through EPC performance testing experiment, we found that the current version OAI EPC cannot support the X2 handover function. To be specific, based on the captured signaling messages in Wireshark during the EPC performance testing experiment, we have figured out the reason of the unsuccessful handover is that the original version EPC lacks the function related to the ''handover completion'' phase (i.e., lack the processing modules for the signaling messages ''PathSwitchRequest'' and its subsequent signaling messages''). Therefore, we need supplement the codes which can support the X2 handover in the OAI EPC and evolve the original version to the current version (i.e., the second phase in Fig.5).

For generally speaking, the supplement function should include three main sub-functions which are the MME module requests the SGW module to switch the path to the target eNodeB, the SGW module asks the PGW module to switch the path, and the SPGW modules respond back to the MME module signaling the completion of the path switch. Base on the analysis, in the subsequent sub-sections, we will detailly illustrate how to evolve the original version OAI EPC to the current version EPC.

Based on the X2 handover sequence diagram shown in Fig.4, once the MME receives the signaling message ''Path Switch Request'' from the target eNB, it will first handle this message and then send the signaling message ''Modify Bearer Request'' to the SGW. Fig.6 briefly demonstrates our supplemented functions in MME after the MME receives the signaling message ''Path Switch Request''.

Shown in Fig.6, the pink words in the first rectangle are the formal parameter, and this formal parameter is a structure data type. Apparently, from this formal parameter name, we can learn that this is an S1AP signaling message between the eNB and the MME, and the S1AP is the protocol stack name used for the communication between the MME and eNB. The definition of the formal parameter is shown in Fig.7, note that there is a union data type ''union msg'' embedded in the structure data type ''struct s1ap_message_s'', and this union data type ''union msg'' includes all the S1AP signaling messages between the eNB and the MME.

In Fig.6, the three variables defined in the second rectangle are the signaling message ''S1ap_PathSwitchRequestIEs_t'' which is corresponding to the highlighted part in Fig.7, the structure data type ''ue_description_t'' is used for describing the context of the UE, and the integer data type ''enb_ue_s1ap_id_t'' is used for uniquely identifying the UE over the S1 interface within an eNB, respectively.

In Fig.6, the first code line in the third rectangle indicates the ''S1ap_PathSwitchRequestIEs_t'' has been assigned by the passing actual argument through the formal parameter (i.e., the pink part in the first rectangle). Then, based on the first code line, the second line calculates the ''enb_ue_s1ap_id'' and then assigns this value to the variable ''enb_ue_s1ap_id_t''. Here, we want further explain the second code line. Note that the ''S1ap_PathSwitchRequestIEs_t'' (i.e., the highlighted part in Fig.7) is also a structure data type and the ''S1ap_ENB_UE_S1AP_ID_t'' is the member field. The red part ''ENB_UE_S1AP_ID_MASK'' is a macro with the definition of ''#define ENB_UE_S1AP_ID_MASK 0x00FFFFFF'', which is use for ''AND'' operation (i.e., &).

In the fourth rectangle, we first use the value of another member filed ''sourceMME_UE_S1AP_ID'' defined in ''S1ap_PathSwitchRequestIEs_t'' to make sure this ''ue_description_t'' is not equals to NULL, which indicates the ''MME UE S1AP ID'' provided by the eNB points to the valid UE ID stored in the MME. Then, we use the determine statements in the second code line to make sure the value of ''enb_ue_s1ap_id'' defined in ''ue_description_t'' matches to the value of ''enb_ue_s1ap_id'' calculated in the third rectangle.

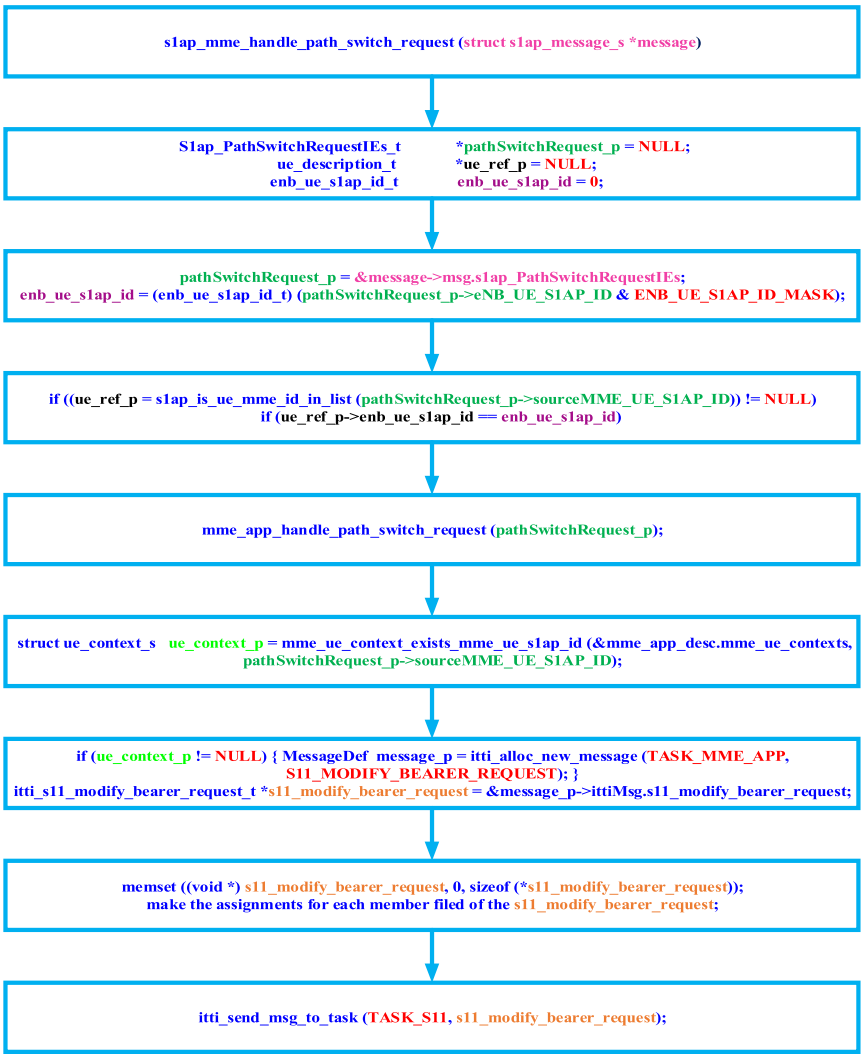

FIGURE 6. The sketch of the supplement functions in MME.

Based on the processing procedures mentioned above, in the fifth rectangle, the function ''mme_app_handle_path_switch_request'' is called with the actual argument ''pathSwitchRequest_p'' which is originally defined in the first rectangle, assigned in the second rectangle, and determined in the fourth rectangle.

The contents shown from the sixth rectangle to the ninth rectangle are the processing steps defined in the function ''mme_app_handle_path_switch_request'' (i.e., shown in the fifth rectangle). In the sixth rectangle, we utilize the passing actual argument ''pathSwitchRequest_p'' and the function ''mme_ue_context_exists_mme_ue_s1ap_id'' to make sure the ''ue_context_p'' is not equals to NULL. In the seventh rectangle, We define the structure data type variable ''s11_modify_bearer_request'' which is sent from the MME to the SGW (i.e., the signaling message ''Modify Bearer Request'' shown in the handover sequence diagram in Fig.4). Then, the code lines in the eighth rectangle indicates the initial assignment process and the detailed assignment process, respectively. Specifically, the initial assignment value for the ''s11_modify_bearer_request'' is 0 and then the detailed assignment processes are conducted. Here, we mainly focus on five member fields defined in the ''s11_modify_bearer_request'' and they are the GTP version, the UE address, the eNB address, the GTP tunnel inputting port id, and the GTP tunnel outputting tunnel port id, respectively. Since these five member fields are important for the further processing in the SPGW modules, which will be described in the next part. Finally, in the ninth rectangle, the function ''mme_app_handle_path_switch_request'' exploits the function ''itti_send_msg_to_task'' to send the signaling message ''s11_modify_bearer_request'' to the SPGW modules for further processing.

As illustrated in Fig.8, those rectangles labeled with the dark blue words refer to the key functions used for handling the signaling message received from the MME module, those pink circles refer to the key codes between each two key functions, and those little purple circles refer to the

FIGURE 7. The definition of the structure data type "struct s1ap_message_s *message.

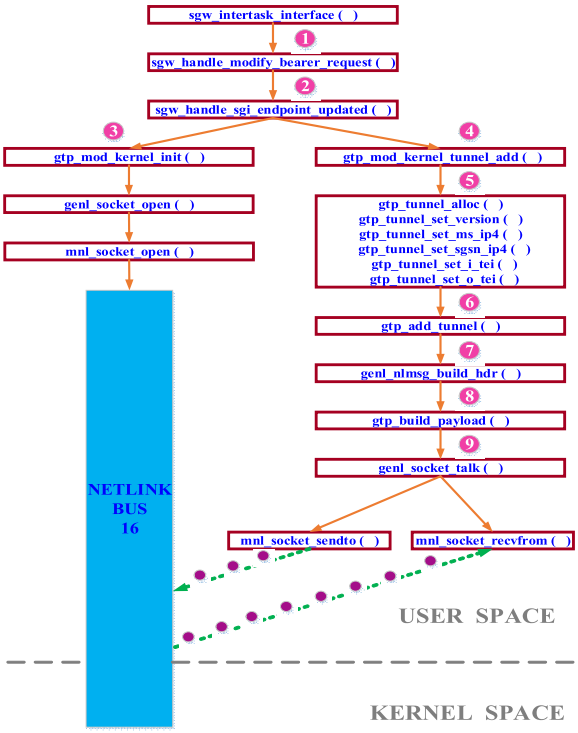

FIGURE 8. The processing procedures in SPGW (i.e., SGW+PGW) module after receiving the signaling message "s11_modify_bearer_request".

Netlink messages received from/sent to the NETLINK BUS (i.e., the light blue rectangle in Fig.8). Moreover, the SPGW module is divided into two parts of which one is located in the user space and the other is located in the kernel space (i.e., as part of the OS kernel). The user space module communicates with the kernel space module by means of Netlink, which is a special IPC (Inter-Process Communication) used for transferring information between the kernel and user space processes.

The first rectangle in Fig.8 is the interface of the SPGW module to receive the signaling message "s11_modify_bearer _request" transmitted from the MME module. The key codes (i.e., the first pink circle) between the first rectangle and the second rectangle is shown in Fig.9. Note that the "while" statement indicates the "sgw_intertask_interface ()" continuously receive the signaling message through the S11 interface (i.e., sent from the MME). The "switch-case" statement is used for selecting the detailed handling function based on the received message's ID. The highlighted part in Fig.9 have demonstrated that the signaling message "s11_modify_bearer_request" has been received by the function "sgw_handle_modify_bearer_request ()"and this message will be further processed.

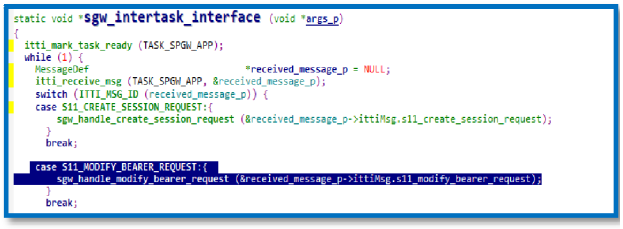

FIGURE 9. The key codes between the functions "sgw_intertask_interface" and "sgw_handle_modify_bearer_request".

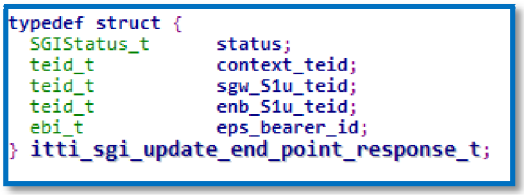

FIGURE 10. The structure data type "itti_sgi_update_end_point_response_t".

In the key codes between the second rectangle and the third rectangle in Fig.8 (i.e., the second pink circle), we define a structure data type "itti_sgi_update_end_point_response_t" shown in Fig.10 and define a variable "sgi_update_end_ point_resp". The first member field "status" indicates the Status of endpoint creation, the second member field "context_teid" indicates the tunnel endpoint identifier for S11 tunnel (i.e., the tunnel between the MME and SGW), the third member field "sgw_S1u_teid" and the fourth member field "enb_S1u_teid" indicate the tunnel endpoint identifier for S1-U tunnel (i.e., between the eNB and SGW), and the last member field "eps_bearer_id" indicates the Evolved Packets System (EPS) bearer identifier (i.e., the tunnel established between the UE and SGW (i.e., UE - eNB - MME - SGW)). Then we make some assignments to the structure variable "sgi_update_end_point_resp" and pass the actual argument "s11_modify_bearer_request" (i.e., received from the MME module) to the function "sgw_handle_sgi_endpoint_updated" (i.e., the third rectangle in Fig.8) for further processing.

In Fig.8, the third pink circle and the fourth circle (i.e., pink circle refers to the key codes between

each two key functions), we define a structure data type ''sgw_eps_bearer_entry_t'' and define a variable ''eps_bearer_entry_p'' which indicates the EPS bearer (i.e., UE - source eNB – MME - SGW) need to be mo-dified. Here, we focus on the five member fields in structure variable ''eps_bearer_entry_p'' and they are the UE address, the source eNB address, the GTP version, and the tunnel endpoint identifier for S1-U tunnel between the eNB and SGW (i.e., the member fields ''sgw_S1u_teid'' and ''enb_S1u_teid defined in ''sgi_update _end_point_resp''). We then use the two received actual arguments ''sgi_update_end_point_resp'' and ''s11_modify_bearer_request'' to make the assignments for those five member fields defined in ''eps_bearer_entry_p'' (i.e., the eps_bea-rer_entry_p.UE_address= s11_modify_bearer_request.UE_ad-dress, eps_bearer_entry_p.Enb_address= s11_modify_bearer_request.eNB_address eps_bearer_entry_p.GTP_version= s11-_modify_bearer_request.GTP_version, eps_bearer_entry_p. sgw_S1u_teid= sgi_update_end_point_resp. sgw_S1u_teid, eps-_bearer_entry_p.enb_S1u_teid= sgi_update_end_point_resp.enb_S1u_teid).

```
int gtp_mod_kernel_tunnel_add(struct in_addr ue,
struct in_addr enb, uint32_t i_tei, uint32_t o_tei)
{
  struct gtp_tunnel *t;
  int ret;
  t = gtp_tunnel_alloc();
  if (t == NULL)
    return RETURNerror;
  gtp_tunnel_set_version(t, 1);
  gtp_tunnel_set_ms_ip4(t, &ue);
  gtp_tunnel_set_sgsn_ip4(t, &enb);
  gtp_tunnel_set_i_tei(t, i_tei);
  gtp_tunnel_set_o_tei(t, o_tei);
  ret = gtp_add_tunnel(t);
  gtp_tunnel_free(t);
  return ret;
}
```

FIGURE 11. The key codes in the fifth pink circle in Fig.8.

Based on the above-mentioned processing procedures, the function ''sgw_handle_sgi_endpoint_updated'' calls the function ''gtp_mod_kernel_init'', the function ''gtp_mod _kernel_tunnel-_add'', and passes in five actual arguments which are ''eps_be-arer_entry_p.UE_address'', ''eps_bearer_entry_p.Enb_address'', ''eps_bearer_entry_p.GTP_version'', ''eps_bearer_entry_p.sgw-_S1u_teid'', and ''eps _bearer_entry_p. enb_S1u_teid''. Once t-he function ''mnl_socket_open'' done, the Netlink tunnel with t-he BUS ID 16 between the kernel space and user space will be established. Then the function ''gtp_mod_kernel_tunnel_add'' calls those six functions shown in the rectangle below the fifth pink circle. The key codes in the fifth pink circle is illustrated in Fig.11, note that there is a structure data type ''structure gtp_tunnel'' which has five main member fields corresponding to t-he five received actual arguments (i.e., UE the address, the eN-B address, the enb_S1u_teid, the sgw_S1u_teid, and the GTP version). The function ''gtp_tunnel_set_version'' is used to assi-gn the GTP version for the ''structure gtp_tunnel'', the function ''gtp_tunnel_set_ms_ip4'' is used to assign the UE address for the ''structure gtp_tunnel'', the function ''gtp_tunnel_set_sgs-n_ip4'' is used to assign the source eNB address for the ''structure gtp_tunnel'', the function ''gtp_tunnel_set_i_tei'' is used to assign the S1-U tunnel inputting endpoint ID for the ''structure gtp_tunnel'', and the function ''gtp_tunnel_set_o_tei'' is used to assign the S1-U tunnel outputting endpoint ID for the ''structure gtp_tunnel''. Then the function ''gtp_add_tunnel'' is called and the actual argument ''structure gtp_tunnel *t'' is passed into it.

Since the received actual argument ''structure gtp_tunnel *t'' in function ''gtp_add_tunnel'' need to be further encapsulated as a Netlink message. Therefore, the function ''genl_nlmsg_build_hdr'' (i.e., the function below the seventh pink circle in Fig.8) is first called, which is used for building the Netlink message header (i.e., the red part and green part in Fig.12) and then the function ''gtp_build_payload'' (i.e., the function below the eighth pink circle in Fig.8) is called, which is used for making up the Netlink message payload (i.e., the blue part in Fig.12). Once those two functions done, the Netlink message shown in Fig.12 will be made.

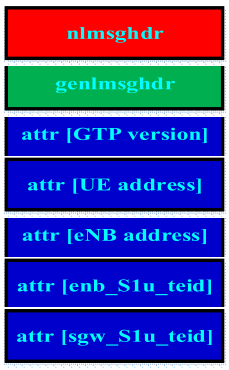

FIGURE 12. The Netlink message.

Shown in Fig.8, the ''nlmsghdr'' is the outer Netlink message header, the ''genlmsghdr'' is the inner Netlink message header used for indicating the Netlink BUS, and the ''attr [ ]'' are the Netlink message attributes used for encapsulating the received actual arguments. Then the function ''genl_socket_talk'' (i.e., the function below the ninth pink circle in Fig.8) utilize the function ''mnl_socket_sendto'' to send those Netlink messages to the kernel space for further processing and use the function ''mnl_socket_recvfrom'' to receive the Netlink messages from the kernel space.

Shown in Fig.13, the kernel space receives the Netlink messages from the user space. The function ''gtp_genl_get_net'' and function ''gtp_find_dev'' are used for examining the link attributes and figuring out which network namespace we are talking about. Then the function ''ipv4_pdp_add'' is called which is the final destination of the signaling message ''s11_modify_bearer_request'' transmitted from the MME module. Here, we give a detailed description for the function

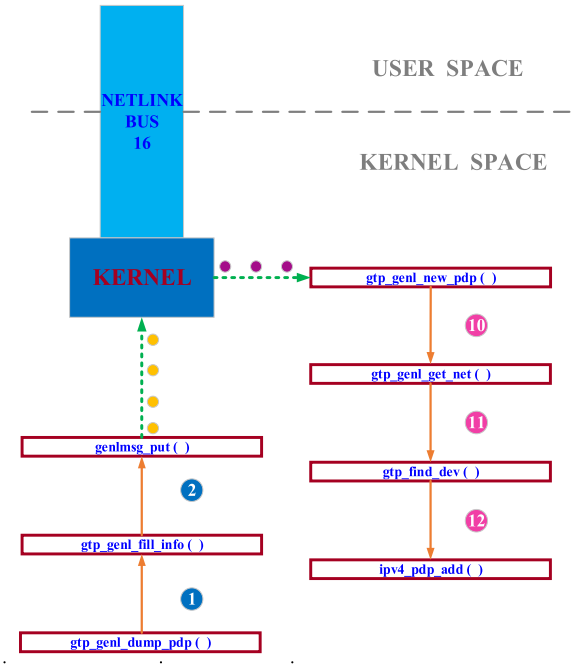

FIGURE 13. The processing procedures in kernel space.

"ipv4_pdp_add", and the key codes of "ipv4_pdp_add" are shown in Fig.14.

Shown in Fig.14, the second formal parameter "struct genl_info * info" is the Netlink message received from the user space (i.e., the purple circle). In code line 1, we define an important structure data type "struct pdp_ctx". A Packet Data Protocol (PDP) context offers a packet data connection over which the UE and the network can exchange IP packets (i.e., UE - eNB - SGW - PGW - IP network backbone). In code line 2, we use the attribute value "info-> [UE address]" to calculate the UE address index located in the UE address hash table stored in the kernel space. Then, from code line 3 to code line 8, we use the determine statements to make sure whether the received UE address matches to the UE address stored in the hash table. If the determine statements condition is true, then from line 9- line 20, we utilize the function "ipve_pdp_fill" to update PDP context (i.e., the i_tei is now updated to the target eNB arress) which stores the S1-U tunnel endpoint information (i.e., the SI-U inputting endpoint (i_tei) and the S1-U outputting endpoint (o_tei)). If the determine statements condition is false, then in line 21, we first use the function "malloc" to allocate a new "struct pdp_ctx" and we then utilize the function "ipve_pdp_fill" to fill the new PDP context (i.e., now is UE - target eNB - SGW – PGW - IP backbone). In addition, along with the new PDP context, two hash tables (i.e., the UE address hash table and the i_tei hash table) will be respectively added with two new items, which are the new UE address and the new S1-U input endpoint ID (i.e., the target eNB address). We can see that now the EPS bearer has been successfully updated (i.e., the fourth phase shown in Fig.3), and the signaling message "modify bearer response" will be sent through the function "gtp_genl_dump" to the user space for further processing. To be specific, the function "gtp_genl_fill_info" is used for converting the PDP context to the Netlink message and the function "genlmsg_put" is used for sending the Netlink messages to the Netlink BUS.

Till now, we have described the main part of our current version open LTE platform, in the next section, we will conduct the testing experiment to validate the supplement functions used for the X2 handover.

B. THE VALIDATION PROCESS FOR THE CURRENT VERSION OPEN LTE PLATFORM

Till now, we have constructed the software-defined open LTE platform, the next step is that we need to verify this platform (i.e., whether it can work effectively with the supplemented functions). As above-mentioned, the original version did not support the handover function, and we have supplemented this function. Therefore, we need to test what we have done. We choose the commercial UE (i.e., Redmi mobile phone), the commercial cellular base station (i.e., the Sunnada Nanocell Base Station), and the updated EPC supplemented with handover function to carry out our handover testing experiment. We first start up the open LTE platform attached with two commercial eNBs and open the Wireshark application in the Host PC where the EPC locates. Let the Redmi mobile phone connect to Internet via eNB #1 and then let the mobile phone play a video. Then we move from eNB #1 to eNB #2. Based on two rules, we can draw the conclusion that the UE has successfully handover from eNB#1 to eNB #2. One is the signaling messages captured by the Wireshark must be right and complete (i.e., based on 3GPP protocol), the other is the video is still played fluently on the mobile phone. In most testing cases, we first check out whether the video is still playing as we moving, then we analyze the captured information shown in Wireshark. The detailed experiment parameters and experiment procedures are illustrated in Section VI. Here, this experiment mainly focuses on the handover function testing (i.e., whether the handover function can work). However, the experiments conducted in section.VI mainly focus on the handover performance metrics (i.e., the no handover probabilities, the handover failure probabilities, and the ping-pong probabilities). In another word, the experiment carried out in this part is the foundation of the experiments conducted in section.VI. In the next, we analyze the Wireshark information which are captured during the handover experiment. Before we start the analysis process, we first demonstrate the protocol stacks in Evolved Packet System (i.e., EPC + eNBs) shown in Fig.15. Note that in Fig.15, the protocol stack between the eNB and the MME has five layers (i.e., the control plane), which are S1 application protocol layer (S1-AP), Stream Control Transmission Protocol layer (i.e., SCTP), Internet Protocol (IP) layer, Layer 2 (e.g., the ethernet layer), and Layer 1 (e.g., the physical layer). The protocol stacks between the eNBs has five layers, which are X2 application protocol

```
static int ipv4_pdp_add(struct net_device *dev, struct genl_info *info)
{
        struct gtp_dev *gtp = netdev_priv(dev); u32 hash_ms, hash_tid = 0;struct pdp_ctx *pctx; bool found = false;__be32 ms_addr;   //1
        ms_addr = nla_get_be32(info->attrs[GTPA_MS_ADDRESS]);hash_ms = ipv4_hashfn(ms_addr) % gtp->hash_size;                    //2
        hlist_for_each_entry_rcu(pctx, &gtp->addr_hash[hash_ms], hlist_addr) {                                                    //3
                if (pctx->ms_addr_ip4.s_addr == ms_addr) {                                                                        //4
                        found = true;                                                                                             //5
                        break;                                                                                                    //6
                }                                                                                                                 //7
        }                                                                                                                         //8
        if (found) {                                                                                                              //9
                if (info->nlhdr->nlmsg_flags & NLM_F_EXCL)                                                                        //10
                        return -EEXIST;                                                                                           //11
                if (info->nlhdr->nlmsg_flags & NLM_F_REPLACE)                                                                     //12
                        return -EOPNOTSUPP;                                                                                       //13
                ipv4_pdp_fill(pctx, info);                                                                                        //14
                if (pctx->gtp_version == GTP_V0)                                                                                  //15
                        netdev_dbg(dev, "GTPv0-U: update tunnel id = %llx (pdp %p)\n", pctx->u.v0.tid, pctx);                     //16
                else if (pctx->gtp_version == GTP_V1)                                                                             //17
                        netdev_dbg(dev, "GTPv1-U: update tunnel id = %x/%x (pdp %p)\n", pctx->u.v1.i_tei, pctx->u.v1.o_tei, pctx);//18
                return 0;                                                                                                         //19
        }                                                                                                                         //20
        pctx = kmalloc(sizeof(struct pdp_ctx), GFP_KERNEL);                                                                       //21
        if (pctx == NULL)                                                                                                         //22
                return -ENOMEM;                                                                                                   //23
        ipv4_pdp_fill(pctx, info);                                                                                                //24
        atomic_set(&pctx->tx_seq, 0);                                                                                             //25
        switch (pctx->gtp_version) {                                                                                              //26
        case GTP_V0:                                                                                                              //27
                hash_tid = gtp0_hashfn(pctx->u.v0.tid) % gtp->hash_size;                                                          //28
                break;                                                                                                            //29
        case GTP_V1:                                                                                                              //30
                hash_tid = gtp1u_hashfn(pctx->u.v1.i_tei) % gtp->hash_size;                                                       //31
                break;                                                                                                            //32
        }                                                                                                                         //33
        hlist_add_head_rcu(&pctx->hlist_addr, &gtp->addr_hash[hash_ms]);                                                          //34
        hlist_add_head_rcu(&pctx->hlist_tid, &gtp->tid_hash[hash_tid]);                                                           //35
        switch (pctx->gtp_version) {                                                                                              //36
        case GTP_V0:                                                                                                              //37
                netdev_dbg(dev, "GTPv0-U: new PDP ctx id=%llx ssgn=%pI4 ms=%pI4 (pdp=%p)\n", pctx->u.v0.tid, &pctx->sgsn_addr_ip4,&pctx->ms_addr_ip4, pctx);   //38
                break;                                                                                                            //39
        case GTP_V1:                                                                                                              //40
                netdev_dbg(dev, "GTPv1-U: new PDP ctx id=%x/%x ssgn=%pI4 ms=%pI4 (pdp=%p)\n", pctx->u.v1.i_tei, pctx->u.v1.o_tei,  &pctx->sgsn_addr_ip4, &pctx->ms_addr_ip4, pctx);  //41
                break;                                                                                                            //42
        }                                                                                                                         //43
        return 0;                                                                                                                 //44
}                                                                                                                                 //45
```

FIGURE 14. The key codes of "ipv4_pdp_add".

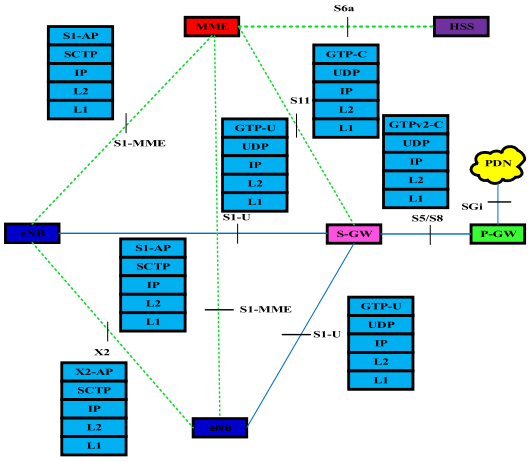

FIGURE 15. The protocol stacks in Evolved Packet System (EPS).

layer (X2-AP), Stream Control Transmission Protocol layer (i.e., SCTP), IP layer, Layer 2 (e.g., the ethernet layer), and Layer 1 (e.g., the physical layer). The protocol stack between the eNB and the SGW has five layers (i.e., the data plane), which are General Packet Radio Service (GPRS) Tunneling Protocol user plane (GTP-U) layer, User Datagram Protocol (UDP) layer, IP layer, Layer 2 (e.g., the ethernet layer), and Layer 1 (e.g., the physical layer). The protocol stack between the SGW and the MME has five layers, which are General Packet Radio Service (GPRS) Tunneling Protocol control plane (GTP-C) layer, User Datagram Protocol (UDP) layer, IP layer, Layer 2 (e.g., the ethernet layer), and Layer 1 (e.g., the physical layer). The protocol stack between the SGW and the PGW has five layers, which are General Packet Radio Service (GPRS) Tunneling Protocol version 2 control plane (GTPv2-C) layer, User Datagram Protocol (UDP) layer, IP layer, Layer 2 (e.g., the ethernet layer), and Layer 1 (e.g., the physical layer). Based on Fig.15 and the Wireshark captured information, we give the following analysis for the handover testing experiment.

We open the Wireshark log file and chronologically sort the logs. Since the Wireshark application is located in the Host PC where the EPC locates, therefore we can capture the information between the eNB and the MME via "eth0" or "eth1" (the detailed experiment plan and experiment procedures are described in Section.VI) and capture the information among the MME, the SGW and PGW via "loopback" with the reason that those three function modules are located in the same Host PC (i.e., the experiment plan shown in Section.VI). Then we input the filtering key words "x2ap"to filter the Wireshark logs, and analyze the captured information in the X2 interface (i.e., between the source eNB and the target eNB). Shown in Fig.16, the four signaling messages in the red rectangle are exchanged between the two eNBs. The first two signaling messages "Handover Request" and "Handover Request Ack" (i.e., the frame 11237 and 11296) in the red rectangle are corresponding to the related signaling messages of "Handover Preparation" phase in X2 handover procedure sequence diagram shown in Fig.4. The third signaling message "SNStatusTransfer" (i.e., the frame 11306) in the red rectangle is corresponding to the related signaling messages of "Handover Execution" phase in X2 handover procedure sequence diagram shown in Fig.4. The fourth signaling message "UEContextRelease" (i.e., the frame 11716) in the red rectangle is corresponding to the related signaling messages of "Handover Completion" phase in X2 handover procedure sequence diagram shown in Fig.4.

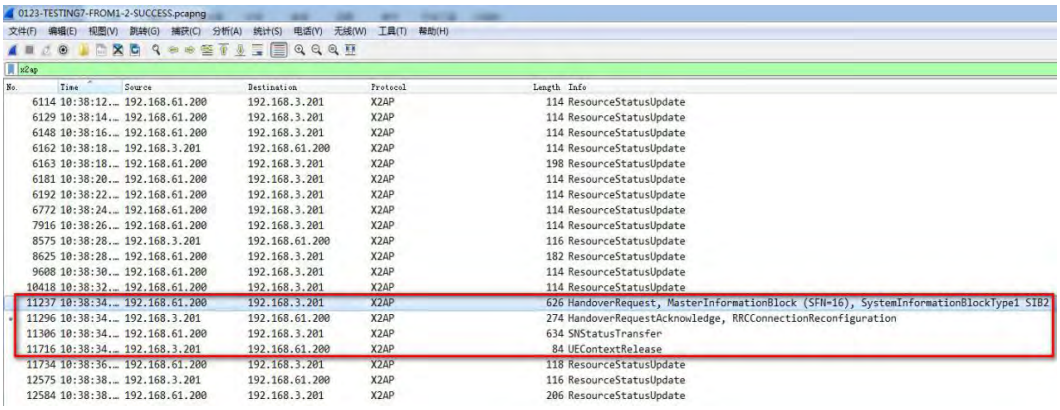

FIGURE 16. The filtered signaling messages related to X2AP.

Based on the above-mentioned analysis and the X2AP protocol stack shown in Fig.17, we pick those four packets and further analyze them.

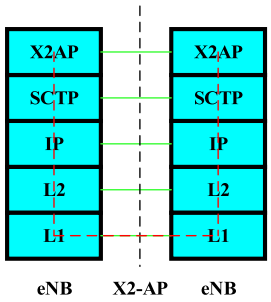

FIGURE 17. The protocol stack between the source eNB and the target eNB (i.e, via X2 interface).

Those four frames 11237, 11296, 11306 and 11716 are shown from Fig.18 to Fig.21, and they are respectively the signaling messages "Handover Request", "Handover Request Ack", "SNStatusTransfer", and "UEContextRelease". Here, we give the detailed descriptions for those different color rectangles in the figures. The purple rectangles demonstrate those four frames' number. The red rectangles indicate those four messages are based on the X2AP protocol stack, and the layers separations (i.e., from bottom to the top are X2AP, SCTP, IP, and Ethernet) are corresponding to the X2AP protocol stack shown in Fig.17. The dark blue rectangles of frame 11237 and frame 11306 indicate the source address of those two messages is 192.168.61.200 (i.e., the ip address of eNB #1 shown in section.VI) and the destination of those two messages is 192.168.3.201 (i.e., the ip address of eNB #2 shown in section.VI). Be differ from frame 11237 and frame 11306, the dark blue rectangles of frame 11296 and frame 11716 indicate the source address of those two messages is 192.168.3.201 and the destination of those two messages is 192.168.61.200, which means those two signaling messages are sent from eNB #2 to eNB #1.

We have finished the analysis process for the signaling messages related to the X2AP protocol stack (i.e., the signaling messages between two eNBs). In the next, we input the filtering key words "s1ap" in the WireShark log file to filter the logs and analyze the captured information of the S1 interface (i.e., between the target eNB and the MME). Shown in Fig.22, the two signaling messages in the dark blue rectangle are exchanged between the target eNB and the MME. The first signaling message 11705 "PathSwitchRequest" is sent from 192.168.3.201 (i.e., the target eNB) to 192.168.61.105 (i.e., the MME) and the second message 11714 "PathSwitchRequestAck" is sent from 192.168.61.105 (i.e., the MME) to 192.168.3.201 (i.e., the target eNB), and those two messages are corresponding to the related signaling messages of "Handover Completion" phase in X2 handover procedure sequence diagram shown in Fig.4.

Based on the S1AP protocol stack shown in Fig.23, we pick those two signaling messages (i.e., No.11705 and No.11714) and analyze them. To be specific, the light green part in Fig.23 is the S1AP protocol stack between the eNB and the MME (i.e., the control plane). The dark orange part is the protocol stack between the UE and the eNB, the pink part is the non-access stratum protocol stack, and the dashed light blue line is the path of the packets flow from the UE to the MME.

Those two frames 11705 and 11714 are shown in Fig.24 and Fig.25, they are respectively the signaling messages "PathSwitchRequest" and "PathSwitchRequestAck". The purple rectangles demonstrate those two frames' number. The red rectangles indicate those two messages are based on the S1AP protocol stack, and the layers separations (i.e., from bottom to the top are S1AP, SCTP, IP, and Ethernet) are corresponding to the S1AP protocol stack shown in the light green part of Fig.23. The dark blue rectangle of frame 11705 indicates this signaling message is sent from eNB #2 (i.e., the target eNB #2 with ip address 192.168.3.201) to MME with ip address 192.168.61.105 and the dark blue rectangle of frame 11714 indicates this signaling message is transmitted in an inverse direction (i.e., from MME to eNB #2).

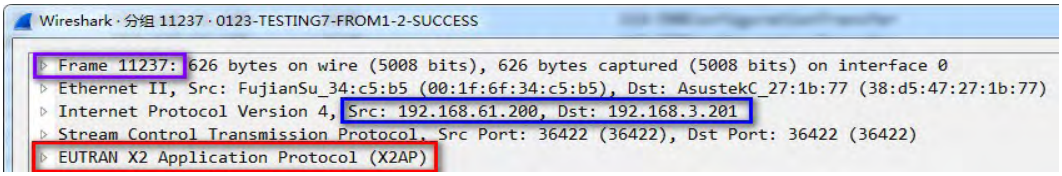

FIGURE 18. The detailed information of the frame 11237.

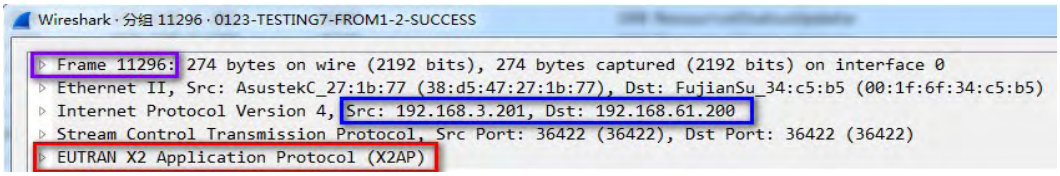

FIGURE 19. The detailed information of the frame 11296.

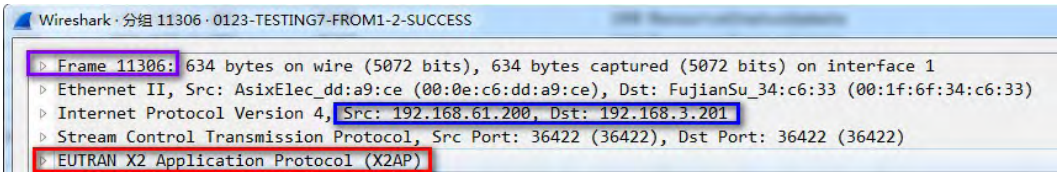

FIGURE 20. The detailed information of the frame 11306.

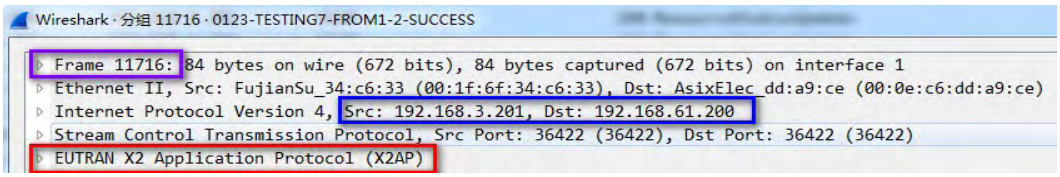

FIGURE 21. The detailed information of the frame 11716.

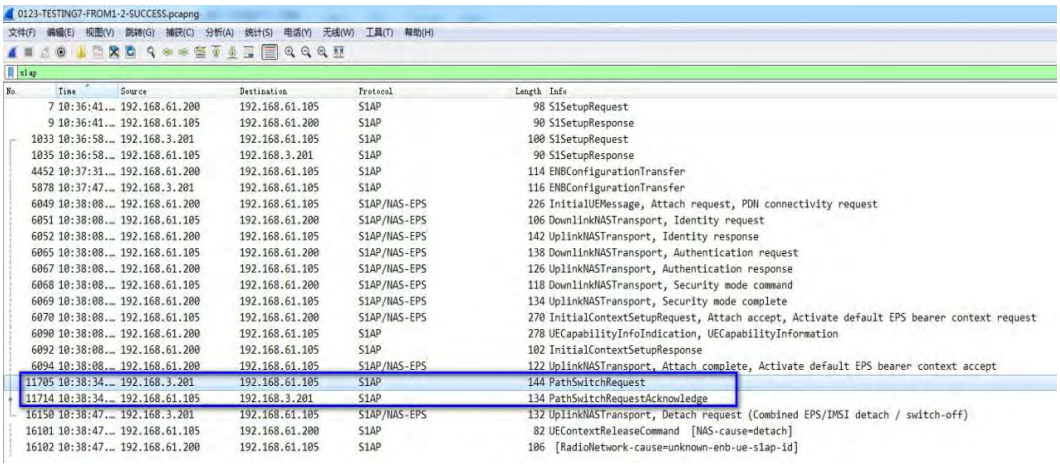

FIGURE 22. The filtered signaling messages related to S1AP.

We have finished the analysis process for the signaling messages related to the S1AP protocol stack (i.e., the signaling messages between the eNB and the MME). In the next, we input the filtering key words "gtpv2" in the Wireshark log file to filter the logs, and analyze the captured information of the S5/S8/S11 interface (i.e., between the MME, the SGW,

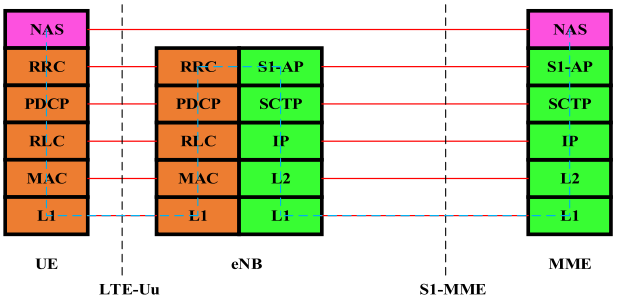

FIGURE 23. The control plane protocol stack between the eNB and the MME (i.e., via S1 interface).

and the PGW). Shown in Fig.26, the four signaling messages in the red rectangle are exchanged among the MME, the SGW, and the PGW. Specifically, the first two signaling message "Modify Bearer Request" and "Modify Bearer Response" in the red rectangle are exchanged between the MME with the ip address of 127.0.11.1 and the SGW with the ip address of 127.0.11.2 (i.e., the ip address 127.0.11.x indicates that the Host PC send the signaling messages to itself with the reason that the MME and the SGW are located in the same Host PC), and those signaling message are corresponding to the related signaling messages of "Handover Completion" phase in X2 handover procedure sequence diagram shown in Fig.4. The last two signaling message "Modify Bearer Request" and "Modify Bearer Response" in the red rectangle are exchanged between the SGW with the ip address of 127.0.11.1 and the PGW with the ip address of 127.0.11.2 (i.e., the ip address 127.0.11.x indicates that the Host PC send the signaling messages to itself with the reason that the SGW and the PGW are located in the same Host PC), and those signaling message are corresponding to the related signaling messages of "Handover Completion" phase in X2 handover procedure sequence diagram shown in Fig.4.

Based on the protocol stacks among the MME, the SGW, and the PGW shown in Fig.27 (i.e., the red part), we pick those four signaling messages (i.e., No.6089, No. 6096, No.11728, and No. 11732) and analyze them.

Those four frames 6089, 6096, 11728 and 11732 are shown from Fig.28 to Fig.31, frames 6089, 11728 are the signaling message of" Modify Bearer Request" and frames 6096, 11732 are the signaling message of "Modify Bearer Response". The purple rectangles demonstrate those four frames' number. The red rectangles of frames 6089, 6096 indicate those two messages are based on the protocol stack between MME and SGW, and the layers separations (i.e., from bottom to the top are GTPv2, UDP, IP, and Ethernet) are corresponding to the protocol stack shown in the red part of Fig.27. The red rectangles of frame 11728 and frame 11732 indicate those two messages are based on the protocol stack between SGW and PGW, and the layers separations are also corresponding to the protocol stack shown in the red part of Fig.27. The dark blue rectangle of frame 6089 indicates that this signaling message is sent from MME with the ip address of 127.0.11.1 to SGW with the ip address of 127.0.11.2 and the dark blue rectangle of frame 6096 indicates this message is transmitted in an inverse direction (i.e., from SGW to MME). The dark blue rectangle of frame 11728 indicates that this signaling message is sent from SGW with the ip address of 127.0.11.1 to PGW with the ip address of 127.0.11.2 and the dark blue rectangle of frame 11732 indicates this message is transmitted in an inverse direction (i.e., from PGW to SGW).

We have finished the analysis for the control plane (i.e., the signaling messages between the eNBs (i.e., X2AP), the signaling messages between the eNB and the MME (i.e., S1AP), and the signaling messages among the MME, the SGW, and the PGW (i.e., GTPv2)) of the handover process. Those signaling messages are correct and complete, and they are chronologically happens based on the event sequence defined in the X2 handover procedure sequence diagram shown in Fig.4. In next, we analyze the data plane (i.e., three black rectangles shown in the X2 handover procedure sequence diagram) of the handover process. Specifically, in order to clearly check out those three phases related to the downlink and uplink data plane traffic (i.e., the three black rectangles shown in the sequence diagram) between the UE with the ip address of 192.168.9.2 and the Internet via the virtual interface gtp0 (highlighted with the light blue line shown in Fig.32, which is created after the EPC.sh has been run) with the ip address of 192.168.9.1. We then input the filtering key words "s1ap or x2ap or gtpv2 or gtp" in the Wireshark log file to filter the logs and we pick up one group of uplink and downlink data plane packets shown in Fig.33.

Note that in Fig.33, the dark blue rectangle demonstrates the uplink (i.e., from 192.168.9.2 to 192.168.9.1) and downlink (i.e., from 192.168.9.1 to 192.168.9.2) data plane packets between the UE and the gtp0. The red rectangle has verified (i.e., before the signaling message "HandoverRequestAck") that now the data plane packets path is UE-eNB#1-SGW-PGW (i.e., the first black rectangle shown in the sequence diagram in Fig.4). Based on the protocol stack between the UE and the PGW shown in Fig.34. We further analyze the frame (11293, 11294), and observe the uplink and downlink data plane traffic path.

To be specific, the light purple part in Fig.34 is the upper protocol stack between the UE and the PGW. The blue part is the protocol stack between the UE and the eNB. The green part is the protocol stack between the eNB and the SGW (i.e., S1-U), and the protocol stack between the SGW and the PGW (i.e., S5/S8). Moreover, the red dashed line indicates the packets path from the UE to the PGW.

Those two frames 11293, 11294 are shown in Fig.35 and Fig.36, they are respectively the uplink data plane packet sent from UE to Internet and the downlink data plane packet sent from Internet to UE. The purple rectangles demonstrate those two frames' number. The red rectangles indicate those two messages are based on the protocol stack between UE and PGW, and the layers separations (i.e., from bottom to

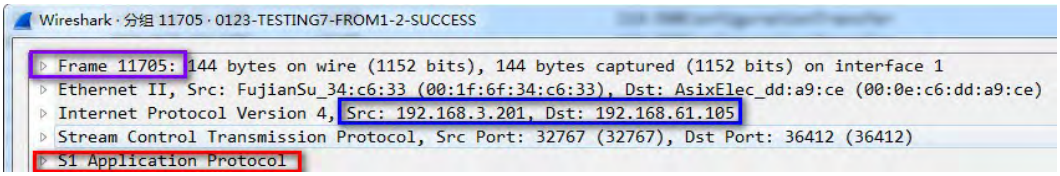

FIGURE 24. The detailed information of the frame 11705.

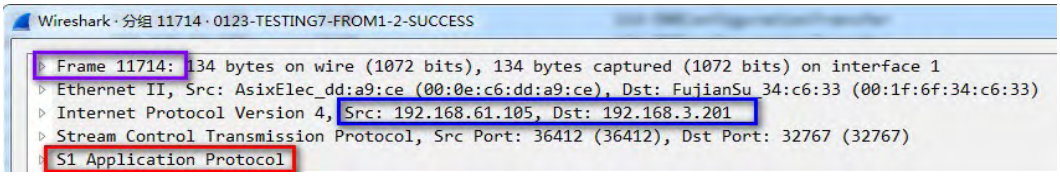

FIGURE 25. The detailed information of the frame 11714.

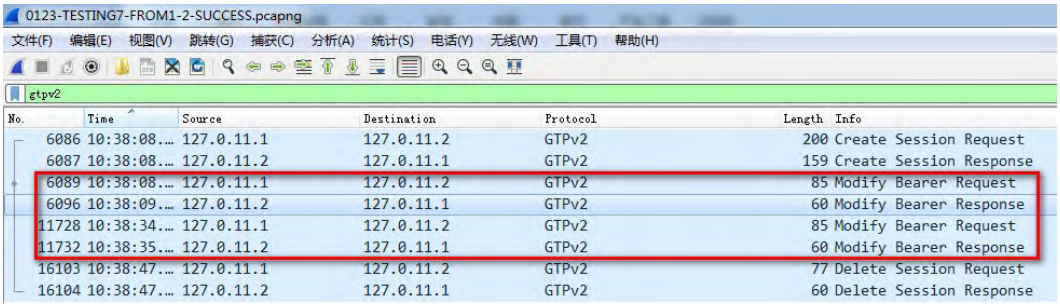

FIGURE 26. The filtered signaling messages related to GTPv2.

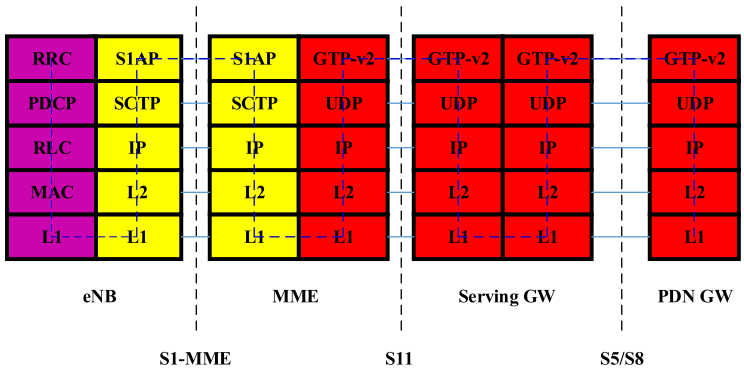

FIGURE 27. The protocol stacks among the MME, the SGW, and the PGW.

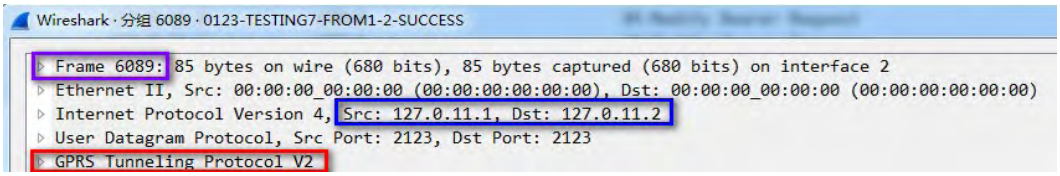

FIGURE 28. The detailed information of the frame 6089.

the top are TCP, IP, GTP, UDP, IP, and Ethernet) are corresponding to the purple part and green part in Fig.34. The dark blue rectangle of frame 11293 indicates the path of this packet from UE to Internet is 192.168.9.2 (i.e., the UE) - 192.168.61.200 (i.e., the eNB #1) - 192.168.61.103 (i.e., the SGW) - 192.168.61.104 (i.e., the PGW) - 192.168.9.1

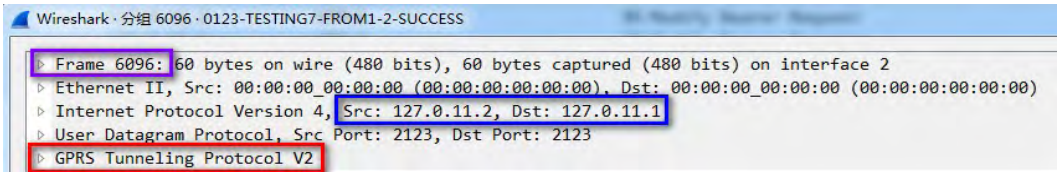

FIGURE 29. The detailed information of the frame 6096.

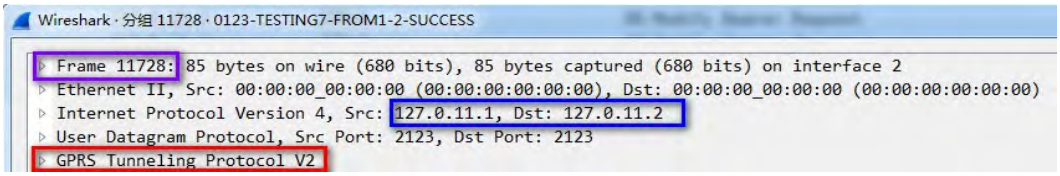

FIGURE 30. The detailed information of the frame 11728.

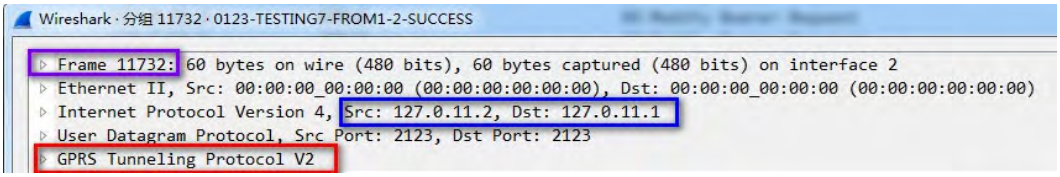

FIGURE 31. The detailed information of the frame 11732.

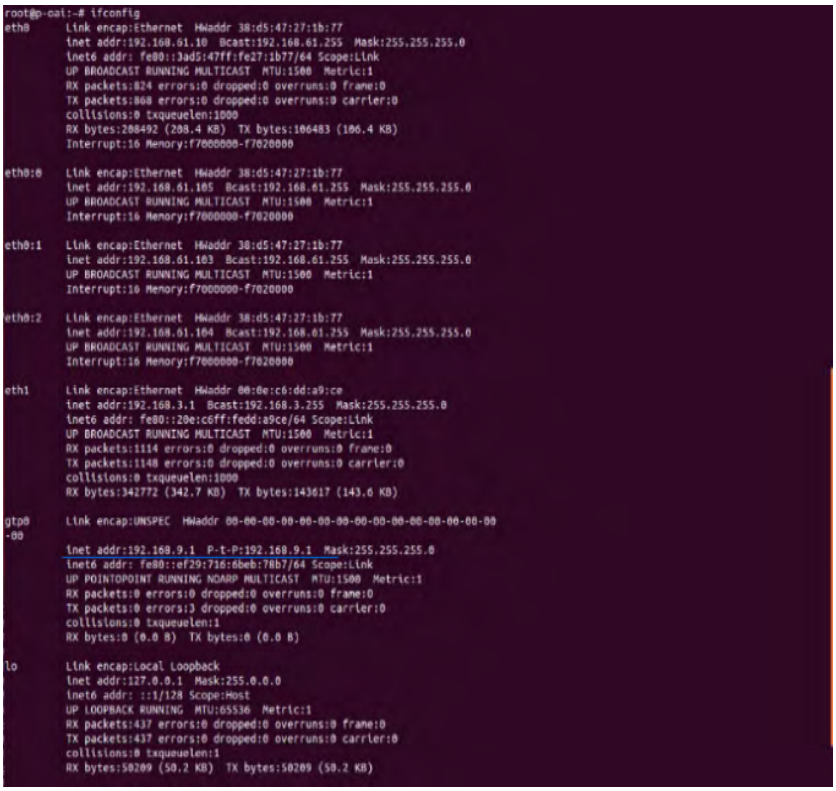

FIGURE 32. The ip address of the gtp0.

(i.e., the virtual interface gtp0), and it is corresponding to the first black rectangle in Fig.4 (i.e., the sequence diagram). The dark blue rectangle of frame 11294 indicates the path of this packet from Internet to UE is 192.168.9.1 - 192.168.61.104 - 192.168.61.103 - 192.168.61.10 (i.e., the eth0 shown in the experiment plan in section.VI) - 192.168.61.200 - 192.168.9.2, and it is corresponding to the first black rectangle in Fig.4.

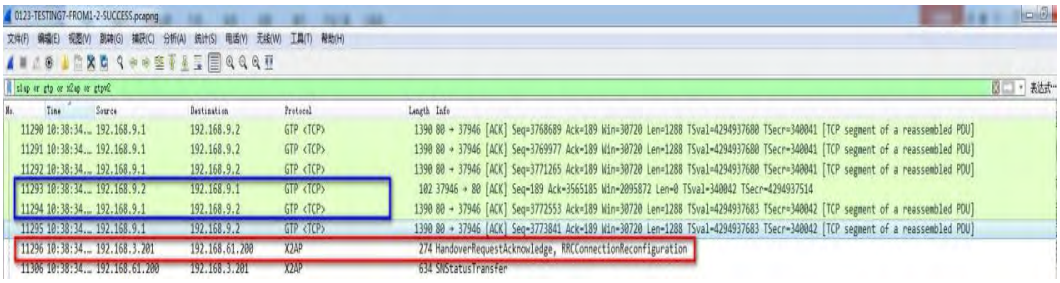

FIGURE 33. The uplink and downlink data plane packets path before the signaling message "HandoverRequestAck".

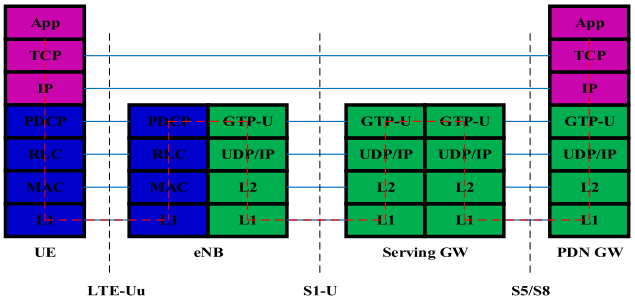

FIGURE 34. The protocol stack between the UE and the PGW.

The black part in Fig.37 is the logs filtered by the key words "gtp or s1ap or x2ap or gtpv2", and it is the downlink data plane packets flow between the "Handover Execution" phase and the "Handover Completion" phase (i.e., the second black rectangle shown in the sequence diagram in Fig.4). Moreover, the red rectangle has verified (i.e., before the signaling message "PathSwitchRequest") that the downlink data plane packets path is Internet - gtp0 - PGW - SGW - eNB#1 - eNB#2 - UE (i.e., the second black rectangle shown in sequence diagram in Fig.4) right now. Based on the protocol stack between the UE and the PGW shown in Fig.34. We mainly analyze the frame 11703 and observe the downlink data plane packets path.

The frame 11703 is shown in Fig.38, and it is the downlink data plane packet sent from the Internet to the UE. The purple rectangle demonstrates the frame number. The dark blue rectangle indicates the path of this packet from the Internet to the UE is 192.168.9.1 (i.e., the virtual interface gtp0) -192.168.61.104 (i.e., the PGW) - 192.168.61.103 (i.e., the SGW) - 192.168.61.200 (i.e., the eNB #1) - 192.168.3.201 (i.e., the eNB #2) - 192.168.3.1 (i.e., the eth1) - 192.168.9.2 (i.e., the UE), and it is corresponding to the downlink packets path shown in the second black rectangle shown in Fig.4. The red rectangle indicates that this signaling message is based on the protocol stack between the UE and the PGW. Moreover, the layers separation shown in Fig.38 (i.e., from bottom to the top are TCP, IP, GTP, UDP, IP, and Ethernet) is corresponding to the protocol stack shown in Fig.34 (i.e., the purple part and the green part).

The black part in Fig.39 is the logs filtered by the key words "gtp or s1ap or x2ap or gtpv2", and it is the uplink (i.e., from 192.168.9.2 to 192.168.9.1) and downlink (i.e., from 192.168.9.1 to 192.168.9.2) data plane packets between the UE and the Internet. The red rectangle has verified (i.e., after the signaling message "PathSwitchRequestAck") that now the downlink data plane packets path is Internet - gtp0 - PGW - SGW - eNB#2 - eth1 - UE and the uplink data plane packets path is UE - eth1 - eNB#2 - SGW - PGW - gtp0 - Internet (i.e., the third black rectangle shown in Fig.4). Based on the protocol stack between the UE and the PGW shown in Fig.34. We further analyze the frame (11733, 11737), and observe the uplink and downlink data plane traffic path.

Those two frames 11733, 11737 are shown in Fig.40 and Fig.41, they are respectively the downlink data plane packet sent from Internet to UE and the uplink data plane packet sent from the UE to the Internet. The purple rectangles demonstrate those two frames' number. The red rectangles indicate those two messages are based on the protocol stack between UE and PGW, and the layers separations (i.e., from bottom to the top are TCP, IP, GTP, UDP, IP, and Ethernet) are corresponding to the purple part and green part in Fig.34. The dark blue rectangle of frame 11733 indicates the path of this packet from Internet to UE is 192.168.9.1 (i.e., the virtual interface gtp0) -192.168.61.104 (i.e., the PGW) - 192.168.61.103 (i.e., the SGW) - 192.168.3.1 (i.e., the eth1) - 192.168.3.201 (i.e., the eNB #2) - 192.168.9.2 (i.e., the UE), and it is corresponding to the downlink packets path shown in the third black rectangle in Fig.4 (i.e., the sequence diagram). The dark blue rectangle of frame 11737 indicates the path of this packet from UE to Internet is 192.168.9.2 -192.168.3.1 - 192.168.3.201 - 192.168.61.103 - 192.168.61.104 - 192.168.9.1 - Internet, and it is also corresponding to the uplink packets path shown in the third black rectangle in Fig.4.

To sum up, based on the above-mentioned analysis for the handover testing experiment, we can kindly conclude that the handover function supplemented in the current version open LTE platform can successfully work.

V. CROSS-TIER HANDOVER ANALYTICAL MODEL BASED ON SOFTWARE-DEFINED OPEN LTE PLATFORM

A. SMALL CELL COVERAGE MODEL AND THE CROSS-TIER HANDOVER FAILURE BOUNDARY MODEL

In this section, we first propose the small cell coverage model and the cross-tier handover failure boundary model through the handover experiment based on the current version open

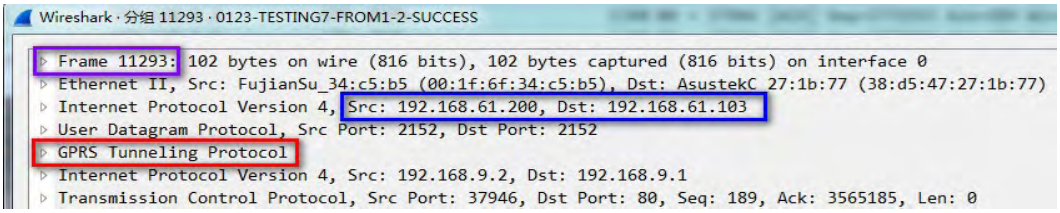

FIGURE 35. The detailed information of the frame 11293.

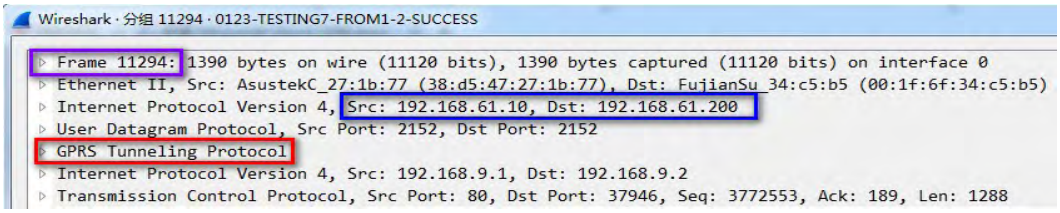

FIGURE 36. The detailed information of the frame 11294.

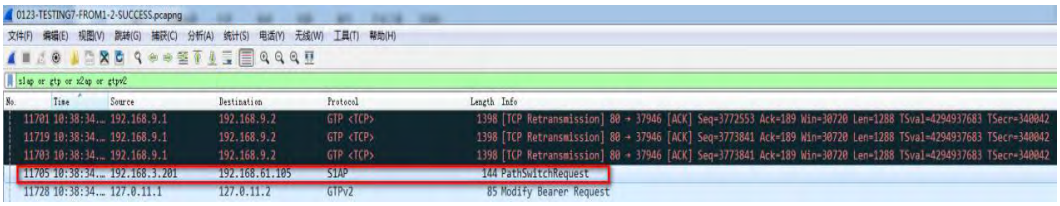

FIGURE 37. The downlink data plane packets path before the signaling message "PathSwitchRequest".

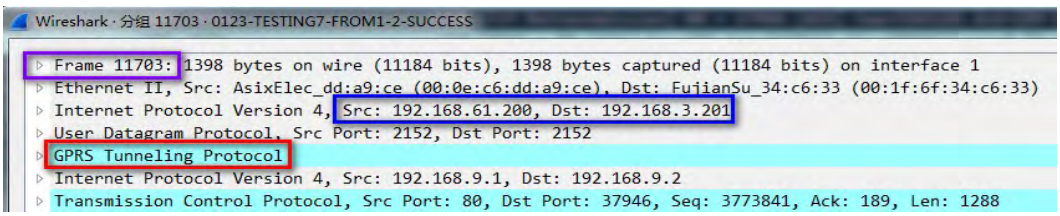

FIGURE 38. The detailed information of the frame 11703.

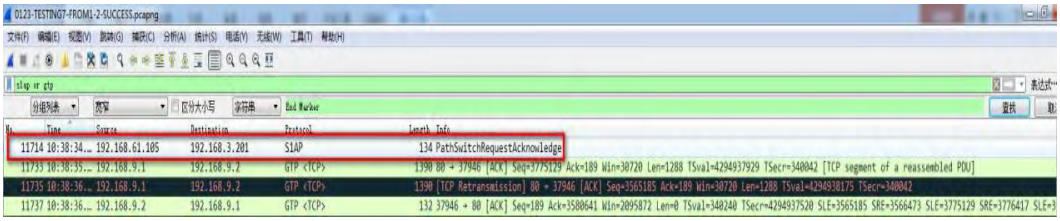

FIGURE 39. The uplink and downlink data plane packets path before the signaling message "PathSwitchRequest".

LTE platform (i.e., shown in Fig.5) which is composed by the commercial eNBs, commercial UEs, and the updated EPC (i.e., the X2 handover function has been supplemented). Then, we propose the cross-tier handover sketch and describe the derivation processes of the handover performance metrics.

Fig.42 illustrates the roughly cross-tier handover trigger locations and handover failure locations of which the red circles refer to the macrocell to femtocell handover trigger locations and the light blue triangles refer to the handover failure locations. The dark blue cross refers to the location of eNB #2 (i.e., the femtocell eNB). Since the signal strength

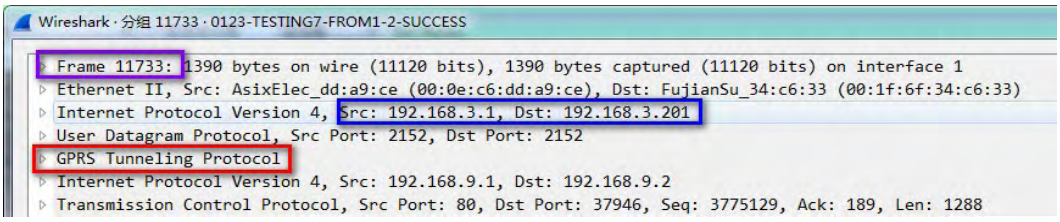

FIGURE 40. The detailed information of the frame 11733.

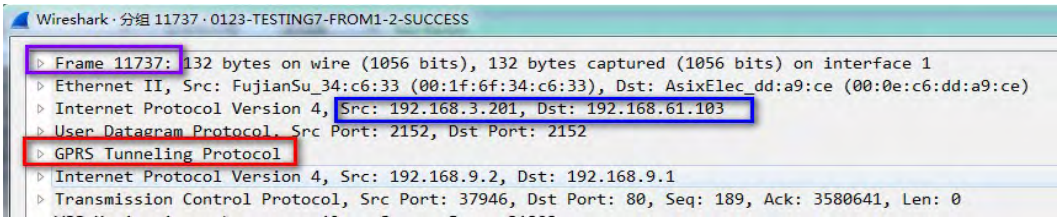

FIGURE 41. The detailed information of the frame 11737.

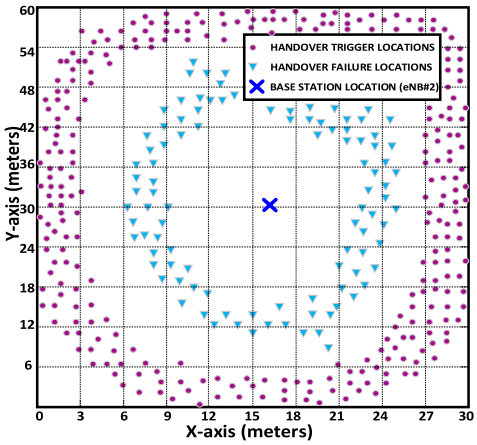

FIGURE 42. The cross-tier handover failure locations and handover trigger locations captured through the handover experiment.

and the signal radius are proportion to the base station's Tx power. Therefore, we turn larger the eNB #1's Tx power (i.e., act as the macrocell base station) and turn lower the eNB #2's Tx power (i.e., act as the femtocell base station). That location information is obtained via the handover experiment based on the current version open LTE platform. Specifically, for each handover experiment (The detailed experiment parameters and procedures are illustrated in section VI), we initially start a session (e.g., play a video) on the commercial UE, then we move from the macrocell coverage to the femtocell coverage. Based on the status of the UE session (i.e., whether continuous play), the signaling messages captured by the Wireshark (i.e., to observe different handover cases, like no handover, handover failure, ping-pong, and successful handover), and the events occurrence location (i.e., the location calculated based on our laboratory's area and the square floor tile with 0.6 meters in length). After conducting several experiments, we obtain some handover failure locations and handover trigger locations, and draw the roughly graph shown in Fig.42. Moreover, note that in Fig.42, the handover failure locations look like a deformed circle with the reason of the sector antennas installed in the cellular base stations (i.e., eNBs). Based on Fig.42, in the subsequent sections, we exploit a geometry-based model for the theoretical analysis of those four handover performance metrics (i.e., the no handover probability, macrocell to femtocell handover failure probability, femtocell to macrocell handover failure probability, and ping-pong probability).

B. CROSS-TIER HANDOVER ANALYSES

For the proposed small cell coverage and handover failure boundary model, four handover performance metrics are derived in this subsection, including the no handover probability, the macrocell to femtocell handover failure probability, the femtocell to macrocell handover failure probability, and the ping-pong probability.

Based on the small cell model and the cross-tier handover failure boundary model shown in Fig. 42, we give the sketch of the cross-tier handover scenario illustrated in Fig. 43. In order to jointly study those four handover performance metrics. Here, we focus on a single UE which starts as a macrocell UE and moves along a straight line towards an arbitrary direction. The macrocell UE becomes a femtocell UE if it is successfully handed over to the femtocell (i.e., cross-tier), and then becomes a macrocell UE again if it is successfully handed over to the macrocell. The radius of the femtocell coverage circle is denoted by R_{at}, while the radius of the handover failure circles for macrocell UE and for femtocell UE are denoted by R_{am} and R_{af}, respectively, where $R_{af} > R_{am}$. The above-mentioned parameters can be obtained through the reference signal received power (RSRP) testing results.

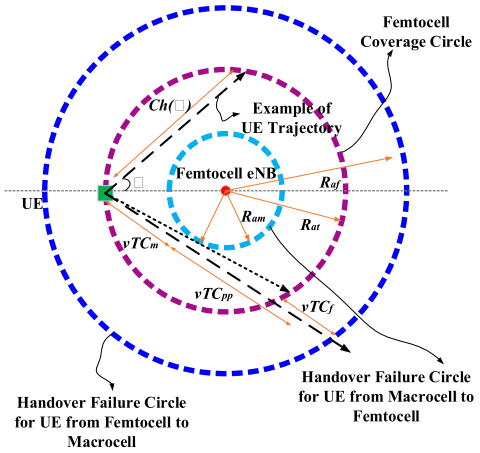

FIGURE 43. The sketch of the cross-tier handover scenario.

The sketch of the cross-tier handover scenario is illustrated in Fig.43, we use the equation (1) shown below to calculate the length of the chord determined by the intersection points between the UE trajectory and the femtocell coverage circle.

$$ch(\psi) = 2R_{at}\cos(\psi) \tag{1}$$

Let Assume v is the velocity of the UE on the calculated chord, which obtained via equation (1). Let $\psi \sim [-\pi/2, \pi/2)$ represent the angle of the chord (i.e., UE trajectory) with respect to the horizontal axis. Let ch be the chord length variable, and the probability density function of ch is shown below [33].

$$\mathrm{g}(ch) = \frac{2}{\pi\sqrt{4R_{at}^2 - ch^2}} \tag{2}$$

Then, based on equation (2), we can learn that if we want obtain the probability of $ch(\psi)$ under the condition that the length of ch is between $ch1$ and $ch2$ with (i.e., $ch1 \leq ch2$), we can utilize the equation (3) to calculate it. Moreover, the derivation process from equation (3) to equation (2) is illustrated in Appendix A.

$$\mathrm{P}(ch_1 < ch(\psi) < ch_2) = \frac{2}{\pi}\arctan\left(\frac{ch}{\sqrt{4R_{at}^2 - ch^2}}\right)\Big|_{ch_1}^{ch_2} \tag{3}$$

Based on equation (3) and the handover sketch shown in Fig.43, we can calculate the no handover probability, the handover failure probability (including the macrocell handover failure probability and femtocell handover failure probability), and the ping-pong probability. In Fig.43, when the macrocell UE enters the femtocell coverage circle, the parameter Time To Trigger (TTT) TC_m, which is used to mitigate potential ping-pong effect due to fast channel fluctuations, is initiated. For a successful handover, the RSRP of the target femtocell should be larger than that of the serving microcell throughout the duration of TC_m. A larger TTT can reduce ping-pong effect, but it may also increase handover failures. Therefore, the value of TC_m should be carefully selected. In the following, handover failure and ping-pong effect probabilities will be derived as functions of TTT, UE velocity, and other important network parameters.

Here, we first to calculate the probability of no handover for the macrocell UEs. To be specific, as macrocell UE moving from the macrocell to the femtocell, after TTT is triggered, the macrocell UE does not make an handover to the target eNB (i.e., the femtocell eNB) if it leaves the femtocell coverage circle before the end of TTT, in which case there is no macrocell UE handover failure, i.e., the macrocell UE does not make an handover to the femtocell eNB if the product vTC_m is larger than the chord length $ch(\psi)$, and the chord does not intersect with the macrocell UE handover failure circle. Therefore, we can express the no handover (N-HO) probability K_{N-HO} as follows.

$$K_{\text{N-HO}} = \begin{cases} \mathrm{P}(ch(\psi) < 2\sqrt{R_{at}^2 - R_{am}^2}), \\ \qquad vTC_m \geq 2\sqrt{R_{at}^2 - R_{am}^2} \\ \mathrm{P}(ch(\psi) < vTC_m), \\ \qquad vTC_m < 2\sqrt{R_{at}^2 - R_{am}^2} \end{cases} \tag{4}$$

The equation (5) shown below is the chord length when the UE's trajectory is tangent to the macrocell UE handover failure circle shown in Fig.43.

$$2\sqrt{R_{at}^2 - R_{am}^2} \tag{5}$$

Till now, we can note that equation (3) has provided a way to derive equation (4) as follows.

$$\begin{aligned} &K_{\text{N-HO}} \\ &= \begin{cases} \mathrm{P}(ch(\psi) < 2\sqrt{R_{at}^2 - R_{am}^2}), & vTC_m \geq 2\sqrt{R_{at}^2 - R_{am}^2} \\ \mathrm{P}(ch(\psi) < vTC_m), & vTC_m < 2\sqrt{R_{at}^2 - R_{am}^2} \end{cases} \\ &= \begin{cases} \frac{2}{\pi}\arctan\left(\frac{ch}{\sqrt{4R_{at}^2 - ch^2}}\right)\Big|_{-\infty}^{2\sqrt{R_{at}^2 - R_{am}^2}} \\ \quad vTC_m \geq 2\sqrt{R_{at}^2 - R_{am}^2} \\ \frac{2}{\pi}\arctan\left(\frac{ch}{\sqrt{4R_{at}^2 - ch^2}}\right)\Big|_{-\infty}^{vTC_m} \quad vTC_m < 2\sqrt{R_{at}^2 - R_{am}^2} \end{cases} \\ &= \begin{cases} \frac{2}{\pi}\arctan\left(\frac{ch}{\sqrt{4R_{at}^2 - ch^2}}\right)\Big|_{0}^{2\sqrt{R_{at}^2 - R_{am}^2}} \\ \quad vTC_m \geq 2\sqrt{R_{at}^2 - R_{am}^2} \\ \frac{2}{\pi}\arctan\left(\frac{ch}{\sqrt{4R_{at}^2 - ch^2}}\right)\Big|_{0}^{vTC_m} \quad vTC_m < 2\sqrt{R_{at}^2 - R_{am}^2} \end{cases} \\ &= \begin{cases} \frac{2}{\pi}\arctan\left(\frac{\sqrt{R_{at}^2 - R_{am}^2}}{R_{am}}\right), & vTC_m \geq 2\sqrt{R_{at}^2 - R_{am}^2} \\ \frac{2}{\pi}\arctan\left(\frac{vTC_m}{\sqrt{4R_{at}^2 - v^2(TC_m)^2}}\right), \\ \quad vTC_m < 2\sqrt{R_{at}^2 - R_{am}^2} \end{cases} \end{aligned} \tag{6}$$

According to equation (5), if the product υTC_m is sufficiently large, the probability of no handover is equivalent to the probability of the UE's trajectory not intersecting with the macrocell UE's handover failure circle. We have done the theoretical analysis process of no handover for the macrocell UEs when they are moving from the macrocell to the femtocell. Then we calculate the probability of handover failure probability for the macrocell UEs when they are moving from macrocell to the femtocell. Specifically, if $ch(\psi) \geq$ equation (5), the macrocell UE's trajectory intersects with the macrocell UE's handover failure circle, and thus the possibility of macrocell UE handover failure exists. In this case, in order to avoid macrocell UE handover failure, the TTT should expire before it reaches the macrocell UE handover failure circle, which depends on the macrocell UE velocity. As a result, if $ch(\psi) \geq$ equation (5), an macrocell UE handover failure occurs if the distance υTC_m travelled by the macrocell UE during the TTT is larger than the distance $X_{HF-M}(\psi, R_{at}, R_{am})$ between the location where the TTT is triggered and the location where the macrocell UE trajectory intersects with the macrocell UE handover failure circle. In order words, a macrocell UE handover failure occurs if the following condition is satisfied

$$\upsilon TC_m \geq X_{\text{HF-M}}(\psi, R_{at}, R_{am}) \tag{7}$$

where

$$X_{\text{HF-M}}(\psi, R_{at}, R_{am}) = R_{at}\cos\psi - \sqrt{R_{am}^2 - R_{at}^2\sin^2\psi} \tag{8}$$

We can note that for the special case of ψ =0, macrocell UE handover failure is observed if $\upsilon TC_m \geq R_{at} - R_{am}$.

Then, the macrocell UE handover failure probability K_{HF-M} can be expressed as follows

$$\begin{aligned} K_{\text{HF-M}} &= A \times B \\ A &= \text{P}(ch(\psi) > 2\sqrt{R_{at}^2 - R_{am}^2}) \\ B &= \text{P}(\upsilon TC_m \geq \text{X}_{\text{HF-M}}(\psi, R_{at}, R_{am})) \end{aligned} \tag{9}$$

Based on equation (2), equation (3), equation (7), and equation (8), the second item (i.e., B) in equation (9) can be derived to equation (10). The detailed derivation process is illustrated in Appendix B.

$$\begin{aligned} &\text{P}(\upsilon TC_m \geq X_{\text{HF-M}}(\psi, R_{at}, R_{am})) \\ &= -\int_{-\arccos\frac{(\upsilon TC_m)^2 + R_{at}^2 - R_{am}^2}{2\upsilon R_{at} TC_m}}^{\arccos\frac{(\upsilon TC_m)^2 + R_{at}^2 - R_{am}^2}{2\upsilon R_{at} TC_m}} \frac{2}{\pi}\text{d}\psi \\ &= -\frac{4}{\pi}\arccos\frac{(\upsilon TC_m)^2 + R_{at}^2 - R_{am}^2}{2\upsilon R_{at} TC_m} \end{aligned} \tag{10}$$

Furthermore, for the first item (i.e., A) in equation (9), we use equation (4) to derive it. Based on equation (4), we can get the equation (11) shown below.

$$\begin{aligned} &\text{P}(ch(\psi) > 2\sqrt{R_{at}^2 - R_{am}^2}) \\ &= 1 - \text{P}(ch(\psi) < 2\sqrt{R_{at}^2 - R_{am}^2}) \\ &= 1 - \frac{2}{\pi}\arctan(\frac{\sqrt{R_{at}^2 - R_{am}^2}}{R_{am}}) \end{aligned} \tag{11}$$

Finally, using equation (10) (i.e., second item in equation (9)) and equation (11) (i.e., first item in equation (9)), we can obtain the macrocell UE handover failure probability K_{HF-M}.

$$\begin{aligned} K_{\text{HF-M}} = (1 - \frac{2}{\pi}\arctan(\frac{\sqrt{R_{at}^2 - R_{am}^2}}{R_{am}})) \\ \times (-\frac{4}{\pi}\arccos\frac{(\upsilon TC_m)^2 + R_{at}^2 - R_{am}^2}{2\upsilon R_{at} TC_m}) \end{aligned} \tag{12}$$

We can note that for the same value of product υTC_m, equation (12) shows that the macrocell handover failure probability is the same regardless of the specific values of υ and TC_m. However, the femtocell handover failure probability and the ping-pong probability may differ depending on distinct values of υ and TC_m, which will be detailly illustrated in the subsequent sections.

When comes to the femtocell handover failure probability, the macrocell UE should perform a successful handover to the femtocell at first (i.e., the microcell UE become the femtocell UE). Then, after such a handover is performed, as soon as the femtocell UE enters the coverage of the macrocell again, TTT of duration TC_f is initiated. In this case, if the femtocell UE reaches the femtocell UE handover failure circle before the TTT expires, a femtocell UE handover failure occurs. Let $X_{HF-F}(\psi, R_{at}, R_{af})$ denote the distance between the location where the TTT (i.e., TC_f) is triggered and the location where the femtocell UE trajectory intersects with the femtocell UE handover failure circle, which has the following expression.

$$X_{HF-F}(\psi, R_{at}, R_{af}) = R_{at}\cos\psi + \sqrt{R_{af}^2 - R_{at}^2\sin^2\psi} - ch(\psi) \tag{13}$$

Based on equation (13) and the probabilities obtained in the previous sections, we can derive the femtocell handover failure probability and the ping-pong probability for diverse values of the product υTC_m, to be specific, we give the following three cases.

The first case: $\upsilon TC_m \geq$ equation (5). In this case, based on equation (6) and equation (12), we can learn that the macrocell UE never makes a handover to the femtocell either due to existing the femtocell coverage circle before TTT expires, or due to macrocell UE handover failure. Therefore, femtocell UE handover failure and ping-pong probabilities of such a UE are $K_{HF-F} = K_{P-P}$ =0.

The second case: equation (5) > υTC_m > 0.5 × equation (5). In this case, when the chord $ch(\psi) \geq$ equation (5), an macrocell UE always suffers from macrocell UE handover failure and thus is never able to perform a handover to the femtocell eNB. Therefore, femtocell UE handover failures only occur for the condition $ch(\psi) <$ the equation (5), and their probabilities is shown as follows.

$$\begin{aligned} K_{HF-F} &= \text{P}(CD_{14-1}, CD_{14-2}) \\ CD_{14-1} &= \upsilon TC_m < ch(\psi) < 2\sqrt{R_{at}^2 - R_{am}^2} \\ CD_{14-2} &= \upsilon TC_f > X_{HF-F}(\psi, R_{at}, R_{af}) \end{aligned} \tag{14}$$

Note that in equation (14), the first item (i.e., CD_{14-1}) is the condition which represents the macrocell UE to make a handover to the femtocell eNB, and the second item (i.e., CD_{14-2}) is the condition which denotes the femtocell UE suffers from a femtocell UE handover failure. Then, based on equation (13), we can obtain the equation (15) shown below, and the detailed derivation process is illustrated in Appendix C.

$$\begin{aligned} vTC_f &> X_{HF-F}(\psi, R_{at}, R_{af}) \\ &\Rightarrow ch(\psi) > \frac{R_{af}^2 - R_{at}^2}{vTC_f} - vTC_f \end{aligned} \tag{15}$$

Based on equation (15) and the condition $ch(\psi) <$ equation (5), we can give that if $vTC_f <$ equation (16), a femtocell UE will never have a femtocell UE handover failure.

$$\sqrt{R_{af}^2 - R_{am}^2} - \sqrt{R_{at}^2 - R_{am}^2} \tag{16}$$

On the other hand, if $vTC_f >$ equation (16), the probability of the femtocell UE suffering from a femtocell UE handover failure is shown as follows.

$$\begin{aligned} K_{HF-F} &= \mathrm{P}(SE_{17-1} < ch(\psi) < SE_{17-2}) \\ &= \frac{2}{\pi}\arctan\left(\frac{ch}{\sqrt{4R_{at}^2 - ch^2}}\right)\Big|_{SE_{17-1}}^{SE_{17-2}} \\ SE_{17-1} &= \max\left(vTC_m, \frac{R_{af}^2 - R_{at}^2}{vTC_f} - vTC_f\right) \\ SE_{17-2} &= 2\sqrt{R_{at}^2 - R_{am}^2} \end{aligned} \tag{17}$$

The ping-pong probability for the second case mentioned above can be derived as the probability that the femtocell UE do not suffer from any handover failure and that femtocell UE stay less than TC_{pp} time units within the femtocell coverage circle, where TC_{pp} is fixed by the ping-pong definition (e.g., $TC_{pp} = 1$s in [34]). As a result, the ping-pong probability can be written after some manipulation as follows.

$$\begin{aligned} K_{P-P} &= \mathrm{P}(SE_{18-1} < ch(\psi) < \min \\ &\quad (SE_{18-2}, SE_{18-3}, SE_{18-4}, SE_{18-5})) \\ &= \mathrm{P}(vTC_m < ch(\psi) < \min(SE_{18-1}, SE_{18-2}, SE_{18-4})) \\ &= \frac{2}{\pi}\arctan\left(\frac{ch}{\sqrt{4R_{at}^2 - ch^2}}\right)\Big|_{vTC_m}^{\min(SE_{18-1}, SE_{18-2}, SE_{18-4})} \end{aligned}$$

$$SE_{18-1} = 2\sqrt{R_{at}^2 - R_{am}^2}, \quad SE_{18-2} = \frac{R_{af}^2 - R_{at}^2}{vTC_f} - vTC_f$$

$$\begin{aligned} SE_{18-3} &= \frac{R_{at}^2 - R_{am}^2}{vTC_m} + vTC_m, \\ SE_{18-4} &= v(TC_m - TC_f + TC_{pp}) \\ SE_{18-5} &= 2R \end{aligned} \tag{18}$$

Then, if $vTC_f < 0.5^*$ equation (5), the macrocell UE might not observe handover failure even when $ch(\psi) \geq$ equation (5), this is because it will successfully handover to the femtocell eNB before reaching the macrocell UE handover failure circle. In this case, after some manipulation, the femtocell UE handover failure probability can be shown as follows.

$$\begin{aligned} K_{HF-F} &= \mathrm{P}(CD_{19-1}, CD_{19-2}, CD_{19-3}) \\ &\quad + \mathrm{P}(CD_{19-4}, CD_{19-5}) \\ CD_{19-1} &= ch(\psi) \geq 2\sqrt{R_{at}^2 - R_{am}^2} \\ CD_{19-2} &= vTC_m < X_{HF-M}(\psi, R_{at}, R_{am}) \\ CD_{19-3} &= vTC_f > X_{HF-F}(\psi, R_{at}, R_{af}) \\ CD_{19-4} &= vTC_m < ch(\psi) < 2\sqrt{R_{at}^2 - R_{am}^2} \\ CD_{19-5} &= vTC_f > X_{HF-F}(\psi, R_{at}, R_{af}) \end{aligned} \tag{19}$$

We can see the CD_{19-2} in equation (19) can be calculated in the same way as that in equation (15), and the detailed derivation process is shown in Appendix.C. After calculation, we can obtain the following equation to represent CD_{19-2}.

$$\begin{aligned} CD_{19-2} &= vTC_m < X_{HF-M}(\psi, R_{at}, R_{am}) \\ &\Leftrightarrow ch(\psi) < \frac{R_{at}^2 - R_{am}^2}{vTC_m} + vTC_m \end{aligned} \tag{20}$$

Then, based on equation (15) and equation (20), the first item in equation (19) can be expressed as follows.

$$\begin{aligned} &\mathrm{P}(CD_{19-1}, CD_{19-2}, CD_{19-3}) \\ &\quad \Leftrightarrow \mathrm{P}(\max(SE_{21-1}, SE_{21-2}) < ch(\psi) < \min \\ &\quad (SE_{21-3}, SE_{21-4})) \\ SE_{21-1} &= 2\sqrt{R_{at}^2 - R_{am}^2} \\ SE_{21-2} &= \frac{R_{af}^2 - R_{at}^2}{vTC_f} - vTC_f \\ SE_{21-3} &= \frac{R_{at}^2 - R_{am}^2}{vTC_m} + vTC_m \\ SE_{21-4} &= 2R \end{aligned} \tag{21}$$

The equation (21) can be further calculated based on equation (3). After calculation, it can be expressed as follows.

$$\begin{aligned} &\mathrm{P}(\max(SE_{21-1}, SE_{21-2}) < ch(\psi) < \min(SE_{21-3}, SE_{21-4})) \\ &= \frac{2}{\pi}\arctan\left(\frac{ch}{\sqrt{4R_{at}^2 - ch^2}}\right)\Big|_{\max(2\sqrt{R_{at}^2 - R_{am}^2}, \frac{R_{af}^2 - R_{at}^2}{vTC_f} - vTC_f)}^{\min(\frac{R_{at}^2 - R_{am}^2}{vTC_m} + vTC_m, 2R)} \end{aligned} \tag{22}$$

The second item in equation (19) can be derived based on equation (15), then we can obtain the following equation (23).

$$\begin{aligned} &\mathrm{P}(CD_{19-4}, CD_{19-5}) \\ &\quad = \mathrm{P}(SE_{23-1} < ch(\psi) < SE_{23-2}) \\ &\quad = \frac{2}{\pi}\arctan\left(\frac{ch}{\sqrt{4R_{at}^2 - ch^2}}\right)\Big|_{SE_{23-1}}^{SE_{23-2}} \\ SE_{23-1} &= \min\left(vTC_m, \frac{R_{af}^2 - R_{at}^2}{vTC_f} - vTC_f\right) \\ SE_{23-2} &= 2\sqrt{R_{at}^2 - R_{am}^2} \end{aligned} \tag{23}$$

Based on equation (22) and equation (23), we can obtain the following equation (24) to represent equation (19).

$$\begin{aligned} &K_{HF-F} \\ &= \mathrm{P}(CD_{19-1}, CD_{19-2}, CD_{19-3}) + \mathrm{P}(CD_{19-4}, CD_{19-5}) \\ &= \frac{2}{\pi}\arctan\left(\frac{ch}{\sqrt{4R_{at}^2 - ch^2}}\right)\Big|_{\max(2\sqrt{R_{at}^2-R_{am}^2}, \frac{R_{af}^2-R_{at}^2}{vTC_f} - vTC_f)}^{\min(\frac{R_{at}^2-R_{am}^2}{vTC_m}+vTC_m, 2R)} \\ &\quad + \frac{2}{\pi}\arctan\left(\frac{ch}{\sqrt{4R_{at}^2 - ch^2}}\right)\Big|_{\min(vTC_m, \frac{R_{af}^2-R_{at}^2}{vTC_f} - vTC_f)}^{2\sqrt{R_{at}^2-R_{am}^2}} \end{aligned} \tag{24}$$

We can further show that if $vTC_f <$ equation (16), a femtocell UE will never have a femtocell UE handover failure. The ping-pong probability for this case can be expressed as follows.

$$\begin{aligned} K_{P-P} &= \mathrm{P}(CD_{25-1}, CD_{25-2}, CD_{25-3}) + \mathrm{P}(CD_{25-4}) \\ CD_{25-1} &= 2\sqrt{R_{at}^2 - R_{am}^2} < ch(\psi) < TC_m - TC_f + TC_{pp} \\ CD_{25-2} &= vTC_m < X_{HF-M}(\psi, R_{at}, R_{am}) \\ CD_{25-3} &= vTC_f < X_{HF-F}(\psi, R_{at}, R_{af}) \\ CD_{25-4} &= vTC_m < ch(\psi) \\ &< \min(2\sqrt{R_{at}^2 - R_{am}^2}, SE_{25-1}, SE_{25-2}) \\ SE_{25-1} &= \frac{R_{af}^2 - R_{at}^2}{vTC_f} - vTC_f \\ SE_{25-2} &= v(TC_m - TC_f + TC_{pp}) \end{aligned} \tag{25}$$

The second item in equation (25) can be further calculated based on equation (3), which can be expressed as follows.

$$\begin{aligned} &\mathrm{P}(CD_{25-4}) \\ &\quad = \frac{2}{\pi}\arctan\left(\frac{ch}{\sqrt{4R_{at}^2 - ch^2}}\right)\Big|_{vTC_m}^{\min(2\sqrt{R_{at}^2-R_{am}^2}, SE_{25-1}, SE_{25-2})} \\ &SE_{25-1} = \frac{R_{af}^2 - R_{at}^2}{vTC_f} - vTC_f \\ &SE_{25-2} = v(TC_m - TC_f + TC_{pp}) \end{aligned} \tag{26}$$

The first item in equation (25) can be further derived based on equation (3), equation (15), and equation (20). After derivation, we can obtain the first item of equation (25) as follows.

$$\begin{aligned} &\mathrm{P}(CD_{25-1}, CD_{25-2}, CD_{25-3}) \\ &\quad = \mathrm{P}(2\sqrt{R_{at}^2 - R_{am}^2} < ch(\psi) \\ &\quad < \min(SE_{27-1}, SE_{27-2}, SE_{27-3}, SE_{27-4})) \\ &\quad = \frac{2}{\pi}\arctan \\ &\quad \times \left(\frac{ch}{\sqrt{4R_{at}^2 - ch^2}}\right)\Big|_{2\sqrt{R_{at}^2-R_{am}^2}}^{\min(SE_{27-1}, SE_{27-2}, SE_{27-3}, SE_{27-4})} \\ &SE_{27-1} = \frac{R_{at}^2 - R_{af}^2}{vTC_f} + vTC_f \\ &SE_{27-2} = \frac{R_{at}^2 - R_{am}^2}{vTC_m} + vTC_m \\ &SE_{27-3} = v(TC_m - TC_f + TC_{pp}) \\ &SE_{27-4} = 2R_{at} \end{aligned} \tag{27}$$

Then, based on equation (26) and equation (27), we can obtain the following equation to represent equation (25).

$$\begin{aligned} K_{P-P} &= \mathrm{P}(CD_{25-1}, CD_{25-2}, CD_{25-3}) + \mathrm{P}(CD_{25-4}) \\ &= SE_{28-1} + SE_{28-2} \\ SE_{28-1} &= \frac{2}{\pi}\arctan \\ &\quad \times \left(\frac{ch}{\sqrt{4R_{at}^2 - ch^2}}\right)\Big|_{vTC_m}^{\min(2\sqrt{R_{at}^2-R_{am}^2}, SE_{25-1}, SE_{25-2})} \\ SE_{28-2} &= \frac{2}{\pi}\arctan \\ &\quad \times \left(\frac{ch}{\sqrt{4R_{at}^2 - ch^2}}\right)\Big|_{2\sqrt{R_{at}^2-R_{am}^2}}^{\min(SE_{27-1}, SE_{27-2}, SE_{27-3}, SE_{27-4})} \\ SE_{25-1} &= \frac{R_{af}^2 - R_{at}^2}{vTC_f} - vTC_f \\ SE_{25-2} &= v(TC_m - TC_f + TC_{pp}) \\ SE_{27-1} &= \frac{R_{at}^2 - R_{af}^2}{vTC_f} + vTC_f \\ SE_{27-2} &= \frac{R_{at}^2 - R_{am}^2}{vTC_m} + vTC_m \\ SE_{27-3} &= v(TC_m - TC_f + TC_{pp}) \\ SE_{27-4} &= 2R_{at} \end{aligned} \tag{28}$$

Based on those above-mentioned equations, we can note that the handover failure and the ping-pong probabilities can be plotted as functions of system parameters, e.g., UE velocity (for a given Time To Trigger), Time To Trigger (for a given velocity), base station coverage areas (e.g., R_{at}, R_{af}, R_{am}), etc. In next section, we will conduct extensive experiments to study the handover performance metrics under the different system parameters setting.

VI. EXPERIMENTATION AND EVALUATION

A. X2 HANDOVER EXPERIMENT

In this section, based on the software defined open LTE platform, we conduct the two-tier intra-frequency X2 handover experiment to verify the analytical results illustrated in section. V. To be specific, we mainly focus on the impact of the UE velocity, the TTT, and the Hysteresis for the handover performance. The detailed experiment parameters are shown in Table 1. Furthermore, the detailed experiment parameters are shown in Fig.44 (i.e., one Redmi 3 Mobile Phone) and Fig.45 (i.e., the device information screen of the Sunnada Nanocell Base Station), respectively.

Fig.44 demonstrates some important parameters of the Redmi 3 Mobile Phone, such as the operating system version (i.e., Android 5.1.1 LMY47V), the eight-core processor with maximum 1.5GHz, the RAM is 2.00GB, the total storage

TABLE 1. The experiment parameters.

Experimen t Time	Experiment Devices	Hardware Platform	Software Platform
January 23th, 2017	1 Redmi 3 Mobile Phone (ip address: 192.168.9.1) 2 Sunnada Nanocell Base Stations	1 PC: Processor: Intel(R)Core(TM)i5-6500CPU@ 3.20 GHz RAM: 16.0 GB (15.9 GB available) OS type: 64 bits Hard disk: 1200 GB	OS version: Ubuntu-14.04 Open LTE Platform

FIGURE 44. The Redmi 3 mobile phone.

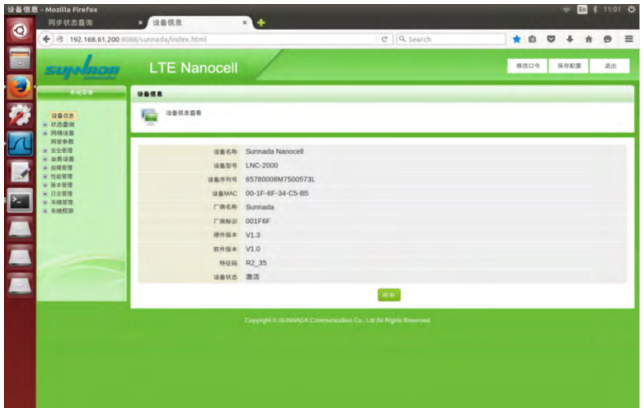

FIGURE 45. The device information screen of the Sunnada Nanocell Base Station.

space is 16GB (3.33 GB available), the baseband version (i.e., 14-M8936F *AAA* ANUZM1.41886_V011), and the OS kernel (i.e., 3.10.49-perf-g6241083).

Fig.45 appears in the telnet base station configuration interface, this figure demonstrates some important parameters of the Sunnada Nanocell Base Station, such as the device type (i.e., LNC-2000), the device sequence number (i.e., 65780008M7500573L), the device MAC address (i.e., 00-1F-6F-34-C5-B5), the manufacture identity (i.e., 001F6F), and etc.

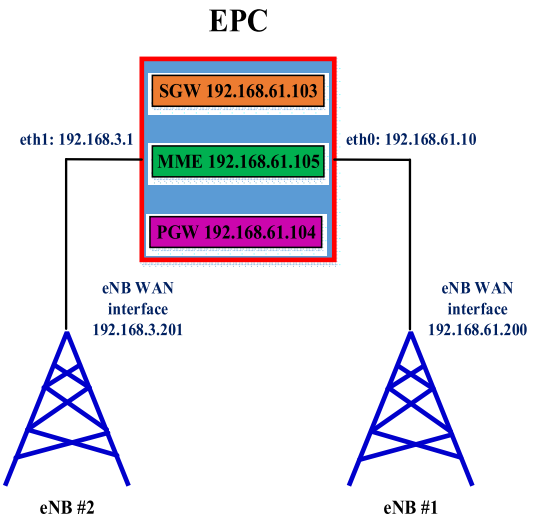

FIGURE 46. The detailed experiment plans.

Based on the above-mentioned experiment parameters, we then propose the detailed experiment plan shown in Fig.46. Note that there are two eNBs, which are the macrocell eNB and the femtocell eNB. To be specific, let the eNB #1 as the macrocell eNB (configure its Tx power larger than eNB #2), and the ip address of this eNB is set to 192.168.61.200. Let the eNB #2 as the femtocell eNB (configure its Tx power smaller than eNB #1), and the ip address of this eNB is set to 192.168.3.201. Let the EPC locate on a server with two Ethernet interfaces (i.e., eth0 and eth1), which are set to 192.168.3.1 and 192.168.61.10, respectively. The eNB #1 and the eth0 are in the same network segment from 192.168.61.10 to 192.168.61.200. The eNB #2 and eth1 are in another network segment from 192.168.3.1 to 192.168.3.201. Moreover, the MME, SGW, and the PGW are set to 192.168.105, 192.168.1.104, and 192.168.1.103, respectively.

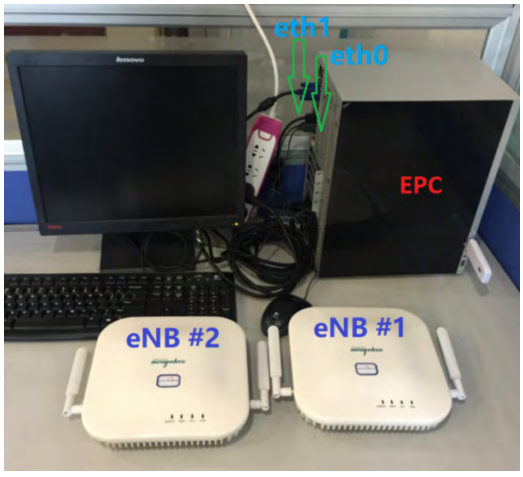

FIGURE 47. The real experiment scenario.

Based on the experiment plan, we then demonstrate the real experiment scenario shown in Figure.47, and carry out the following detailed experiment procedures.

The experiment procedures are:

(1). We first implement the software-defined open LTE platform (i.e., the EPC) into the host PC. We then write an easy starting script called EPC.sh which is used for easy starting the EPC.

(2). Shown in Fig.47, there are two Sunnada Nanocell Base Stations, which are labled by eNB #1 and eNB2, respectively. Since this PC only has one RJ45 interface, therefore, we need use the USB 3.0 to RJ45 Ethernet Network Cable Adapter (Shown in Fig.48) to increase the number of the RI45 interfaces (i.e., the eth1 shown in Fig.47). We use the twisted pairs to connect eNB #1 with eth0, and connect eNB #2 with eth1.

FIGURE 48. The USB 3.0 to RJ45 Ethernet Network Cable Adapter.

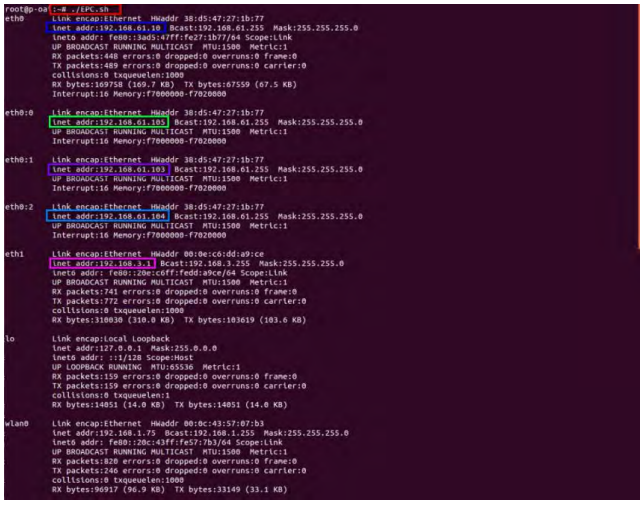

FIGURE 49. The configuration information.

(3). Based on the above-mentioned procedures, we turn on the Host PC and turn on two eNBs. For the Host PC, we press the combination buttons "Ctrl+Alt+T" to open the command window, and then we type the command "./EPC.sh" to easy start the EPC. We can see that the Fig.49 shown below is first demonstrated. The red rectangle indicates the command line, the dark blue rectangle indicates the ip address of eth0, the light green rectangle indicates the ip address of the MME, the purple rectangle indicates the ip address of the SGW, the light blue rectangle indicates the ip address of the PGW, and the pink rectangle indicates the ip address of eth1. Those configuration information are corresponding to our experiment plan shown in Fig.46. Then we open the "Wireshark" application installed in the Host PC to catch the packets flow in eth0, eth1, and loopback. Since in eth1, we can catch the packets flow between EPC and eNB#2 (e.g., the S1AP protocol stack (i.e., Fig.23) shown in earlier section and the S1-U protocol stack (i.e., GTP) shown in earlier section (i.e., Fig.34)). In eth0, we can catch the packets flow between EPC and eNB#1 (e.g., the S1AP protocol stack (i.e., Fig.23) shown in earlier section and the S1-U (i.e., GTP) shown in earlier section (i.e., Fig.34)). In loopback, we can catch the packets flow between the MME and the SPGW.

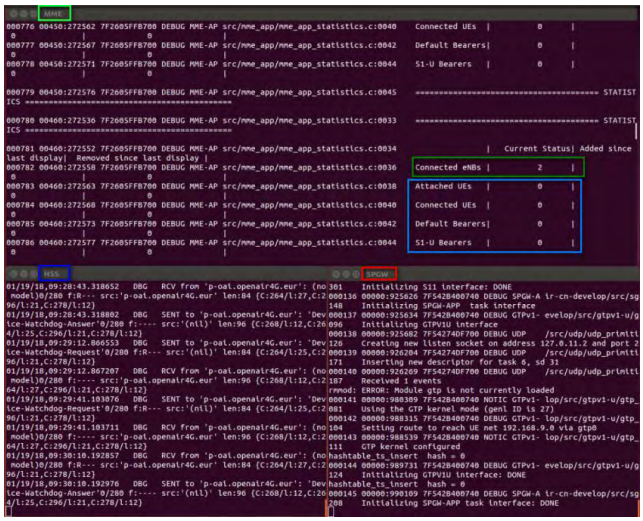

FIGURE 50. The open LTE platform startup information.

Following Fig.49, another three screens appear, which are the MME startup screen, the SPGW startup screen, and the HSS startup screen. The detailed information is shown in Fig.50, note that the light green rectangle indicates the MME startup screen, the dark blue rectangle indicates the HSS startup screen, and the red rectangle indicates the SPGW (i.e., SGW+PGW) startup screen. The full name of the noun abbreviation "HSS" is Home Subscriber Server used for storing the user equipment's' information, and the HSS not belong to the EPC. Moreover, note that there are two bigger rectangles of which one indicates that the number of connected eNB is 2 and the other indicates that the number of attached UE is 0.

(4). For the two startup eNBs, we need further to configure some parameters to support the handover experiment. To be specific, since those two eNBs and the Host PC are in the same network segment (i.e., eth0-eNB1, eth1-eNB2), we open a web browser in the Host PC and type the two URLs "http://192.168.61.200:8088/sunnada/index.html" (i.e., eNB #1) and "http://192.168.3.201:8088/sunnada/index.html" (i.e., eNB #2) to respectively login the two eNB's configuration page. Then we can see the configuration page illustrated in Fig.51 and Fig.52.

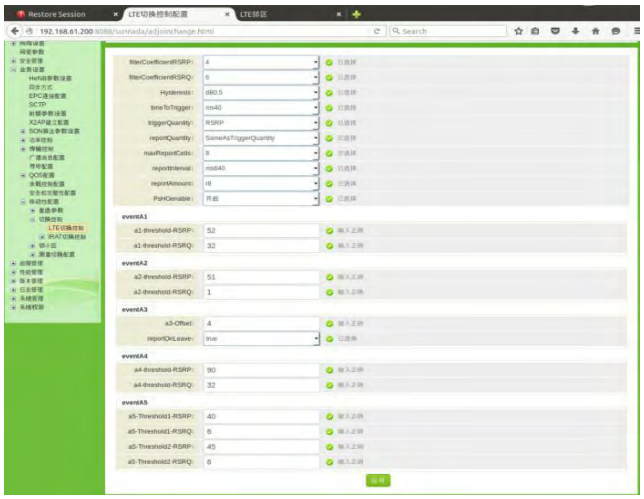

FIGURE 51. The configuration page of eNB #1.

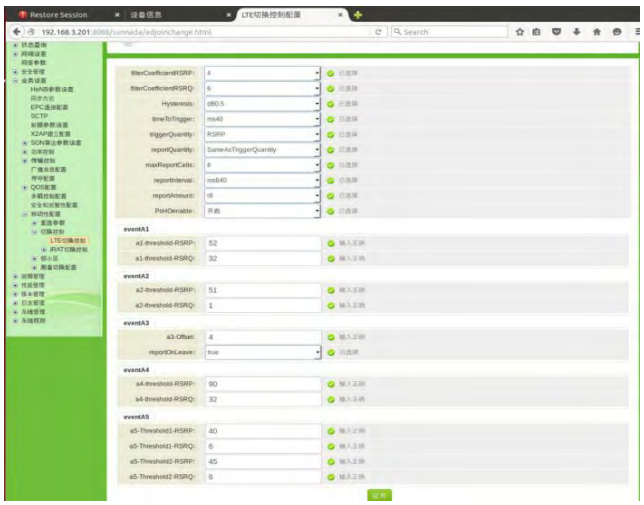

FIGURE 52. The configuration page of eNB #2.

Shown in Fig.51 and Fig.52, Fig.51 is the handover configuration page of eNB #1, and the Fig.52 is the handover configuration page of eNB #2. Since in this paper, we mainly focus on the intra-frequency handover, therefore we just need to adjust some related parameters. Once the parameters have been set, the eNBs will send the configuration information to UE via signaling message. Here, table 2 summaries some important configuration parameters related to intra-frequency handover and the value ranges of these parameters.

Based on the handover trigger event defined in [35]–[37]. We can learn that in LTE, UEs perform reference signal received power (RSRP) measurements to assess the proximity of neighboring cells, once the measurements are performed, the UE checks for the handover event entry condition, i.e., when the signal strength from a target cell is larger than the signal strength from the serving cell plus a hysteresis threshold. Also, when this condition is satisfied for the first time, and the UE waits for a duration of TTT, before sending

TABLE 2. Units for magnetic properties.

Configuration Parameters	Value Range
Hysteresis (dB)	[0,15]
FilterCoefficientRSRP (dB)	0, 1, 2, 3, 4, 5, 6, 7, 8, 9, 11, 13, 15, 17, 19
Time To Trigger (ms)	0, 40, 64, 80, 100, 128, 160, 256, 320, 480, 512, 640, 1024, 1280, 2560, 5120,
A3 offset (dB)	[-30dB,30dB]

a measurement report to its serving cell to initiate the actual handover. To be specific, we use equation (29) to sum up the entering condition of the measurement report triggering.

$$Mn + Ofn + Ocn - Hys > Mp + Ofp + Ocp + Off \quad (29)$$

where Mn is the measurement result of the neighbor cell, Ofn is the frequency specific offset of the frequency of the neighbour cell, Ocn is the cell specific offset of the neighbour cell, Mp is the measurement result of the service cell, Ofp is the frequency specific offset of the primary frequency, Ocp is the cell specific offset of the service cell, Hys is the hysteresis parameter for this event, Off is the a3 offset parameter for this. Note that in table 2, two configuration parameters (i.e., Hysteresis and A3 offset) appear in equation (29). Here, we give the following explanation of each parameter described in Table 2. The configuration parameter ''FilterCoefficientRSRP'' in table 2 is used for Layer 3 filtering. The Layer 3 filtering should be conducted before the measurement serving cell signal strength and neighbour cell signal strength obtained by UE (i.e., before equation (29) conducted). To sum up, according to Table 2, we can configure diverse combinations of parameters to carry out the intra-frequency handover experiment.

(5). Based on above-mentioned procedures, we place the eNB #1 at different distances from the eNB #2 and configure the Tx powers of those two eNBs through the configuration pages. Since each floor tile in our laboratory is a square shape with 0.6 meters in length, we can easily calculate the distance between eNB #1 and eNB#2. Moreover, we need to obey one rule that the Tx power of eNB #1 should be always set larger than eNB #2, since the eNB #1 acts as the macrocell eNB and the eNB #2 acts as the femtocell eNB in our experiment. We then exploit the Redmi 3 Mobile Phone to start an application session (e.g., play a video) in eNB #1 (i.e., macrocell eNB) and start moving to eNB #2 (i.e., femtocell eNB). Moreover, we open a traffic observation application on the Mobile Phone. At this time, we can observe that there are some changes in MME screen. As shown in Fig.53, the red rectangle indicates the number of the attached eNB is 2, the red rectangle indicates that the mobile phone is initially attached to the eNB #1, and the green rectangle indicates the S1 Bearer (i.e., S1-U) has been established between the SGW and the eNB #1 (i.e., the ''Before Handover'' phase described in Fig.3 and Fig.4).

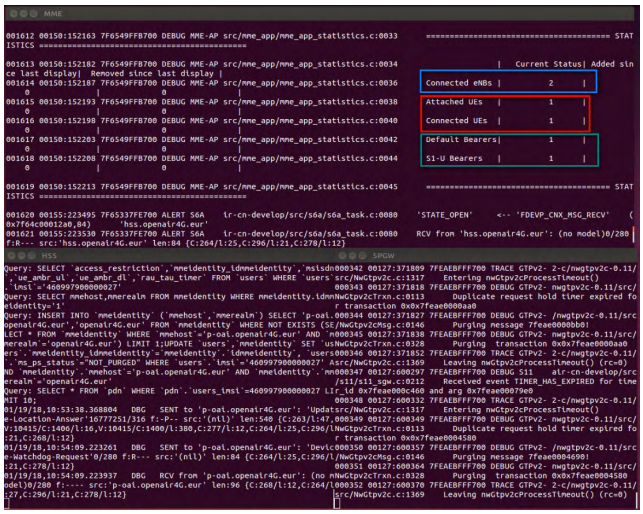

FIGURE 53. The information shown in MME screen when in the "Before Handover" phase.

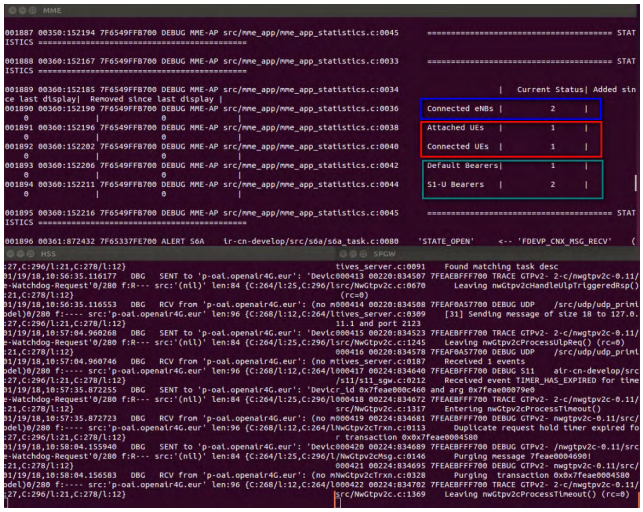

FIGURE 54. The information shown in MME screen when in the "Handover Execution" phase.

As the mobile phone moving, the Fig.54 demonstrates that the UE step into the ''Handover Execution'' phase described in Fig.3 and Fig.4. Specifically, the number of the ''S1-U Bearers'' is 2 shown in the green rectangle in Fig.54, which has proved that the UE has stepped into the ''Handover Execution'' phase.

As the UE keep moving, we can note that there are some changes demonstrated on the traffic observation screen, which is shown in Fig.55. Note that there is a valley in the traffic observation screen which indicates the handover triggering point.

Based on experiment procedures (1) - (5), we carry out many groups intra-frequency X2 handover experiments with diverse combinations of handover parameters setting, such as different distances between eNB #1 and eNB #2, different Tx powers of eNB #1 and eNB #2, and different combinations

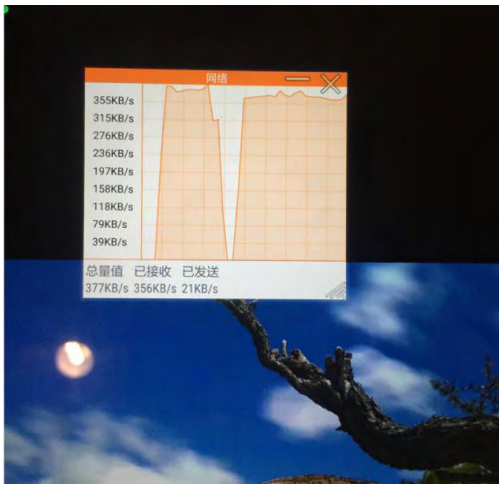

FIGURE 55. The traffic observation screen.

of the handover parameters shown in Table 2. Since we can place the two eNBs at different positions and we can use the timer to record the time period UE moves from eNB #1 to eNB #2, therefore we can roughly estimate and control our moving speed. We focus on four evaluation metrics, which are no handover probabilities, macrocell UE handover failure probabilities, femtocell UE handover failure probabilities, and ping-pong probabilities. Specifically, we statistic the no handover times, the macrocell UE handover failure times, the femtocell UE handover failure times, and ping-pong times based on the observation of the signaling message in Wireshark and the observation of the application session on mobile phone. Then we can obtain the probabilities via dividing the total experiment times.

B. NUMERICAL RESULTS AND DISCUSSIONS

We conduct three groups of experiments to evaluate the two-tier infra-frequency X2 handover performance under diverse cellular base station (i.e., the eNB #1 and eNB #2) parameter setting. Specifically, in the first group of experiments, we respectively change the RF Tx power of eNB #1 from 18 dBm to 24 dBm, change the RF Tx power of eNB #2 from 9 dBm to 3dBm, and change the TTT of eNB # (1, 2) from 320 ms to 40ms, while setting the A3 offset of eNB # (1, 2) = 1dB and the Hysteresis of eNB # (1, 2) =0. Then, we respectively vary the RF Tx power of eNB #1 from 18 dBm to 24 dBm, change the RF Tx power of eNB #2 from 9 dBm to 3dB, and change the TTT of eNB # (1, 2) from 320 ms to 40ms, while setting the A3 offset of eNB (#1, 2) =6dB and the Hysteresis of eNB # (1, 2) =0, in the second group of experiments. Finally, we respectively vary the RF Tx power of eNB #1 from 18 dBm to 24 dBm, change the RF Tx power of eNB #2 from 9 dBm to 3dB, and change the TTT of eNB # (1, 2) from 320 ms to 40ms, while modifying the A3 offset of each eNB =12dB and the Hysteresis of eNB # (1, 2) =0, in the third group of experiments. In all of the experiments, based on the collected experiments records,

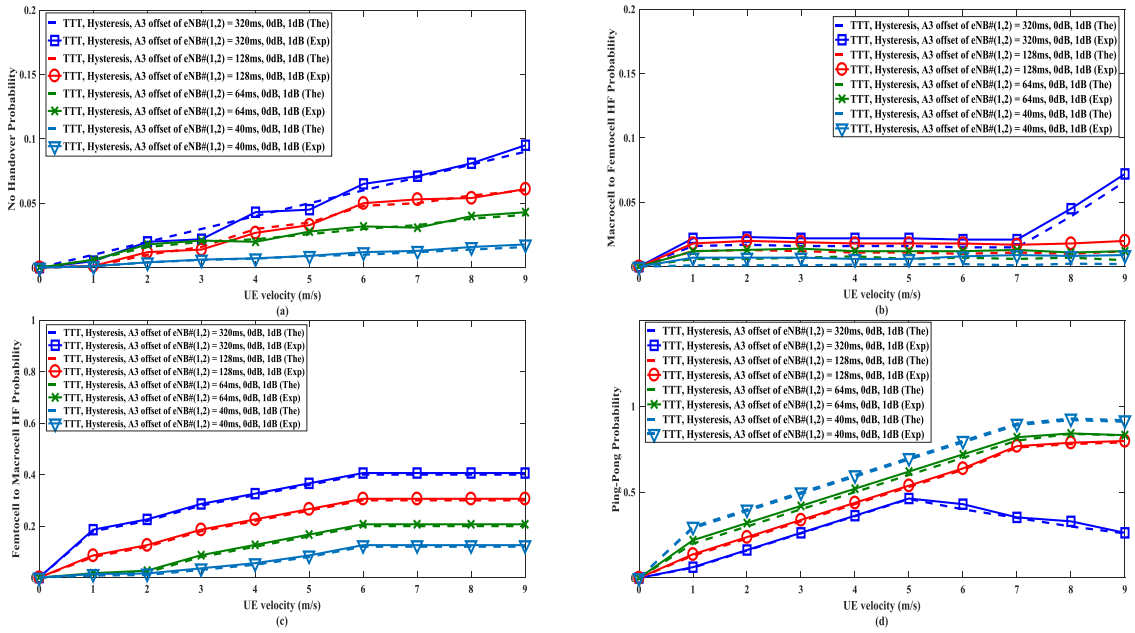

FIGURE 56. Experiment (solid lines with markers) and theoretical (dashed lines) results as a function of UE velocity for the RF Tx power of eNB #1=18dBm, the RF Tx power of eNB #2=9 dBm and the A3 offset of eNB #(1, 2) =1dB. (a) The no handover probability; (b) The Macrocell UE handover failure probability; (c) The Femtocell UE handover failure probability; (d) The ping-pong probability.

we calculate the no handover probability, the macrocell UE handover failure probability (i.e., the UE handover from macrocell to femtocell), the femtocell UE handover failure probability (i.e., the UE handover from femtocell to macrocell), and the ping-pong probability.

1) PERFORMANCE UNDER THE FIRST GROUP EXPERIMENT PARAMETER SETTING

a: NO HANDOVER PROBABILITIES

Fig.56 (a), Fig.57 (a), Fig.58 (a), and Fig.59 (a) demonstrate the mobile UE no handover probabilities under the first group experiment parameter setting. From those four figures, we see that the no handover probabilities follow (eNB #1=(18, 20, 22, 24) dBm, eNB #2=(9, 7, 5, 3) dBm, (A3 offset, Hysteresis) = (1, 0) dB, TTT=320 ms) > (eNB #1=(18, 20, 22, 24) dBm, eNB #2=(9, 7, 5, 3) dBm, (A3 offset, Hysteresis) = (1, 0) dB, TTT=128 ms) > (eNB #1=(18, 20, 22, 24) dBm, eNB #2=(9, 7, 5, 3) dBm, (A3 offset, Hysteresis) = (1, 0) dB, TTT=64 ms) > (eNB #1=(18, 20, 22, 24) dBm, eNB #2=(9, 7, 5, 3) dBm, (A3 offset, Hysteresis) = (1, 0) dB, TTT=40 ms).

Note that the theoretical no handover probabilities are roughly aligned with experiment results in all considered cases. The reason for some deviations between the theoretical and experiment results is due to the fact that the Femtocell and the Macrocell coverage areas is not an ideal circle in real experiment scenarios.

We find that the parameters combination (eNB #1=(18, 20, 22, 24) dBm, eNB #2=(9, 7, 5, 3) dBm, (A3 offset, Hysteresis) = (1, 0) dB, TTT=320 ms) shows the highest no handover probability while the parameters combination (eNB #1=(18, 20, 22, 24) dBm, eNB #2=(9, 7, 5, 3) dBm, (A3 offset, Hysteresis) = (1, 0) dB, TTT=40 ms) shows the lowest no handover probability. This is because as the TTT increase (i.e., the TC_m and TC_f increase), the (vTC_m, vTC_f, no handover probability) increase accordingly. Therefore, the larger TTT setting, the larger no handover probabilities for the mobile UE. Also, the no handover probability increases with UE velocity, because the chance that the UE moves out of the femtocell coverage before TTT expires gets larger.

Moreover, when we vary the Tx power of the eNB while fixing other parameters, the no handover probability increases with the eNB Tx power increase (i.e., the same color curves in those four figures follow Fig.56 (a) < Fig.57 (a) < Fig.58 (a) < Fig.59 (a)). The reason contributes to this is because the femtocell coverage area becomes smaller (i.e., turn lower the eNB #2 Tx power) and the macrocell coverage area becomes larger (i.e., turn larger the eNB #2 Tx power).

b: MACROCELL TO FEMTOCELL HANDOVER FAILURE PROBABILITIES

Fig.56 (b), Fig.57 (b), Fig.58 (b), and Fig.59 (b) demonstrate the macrocell UE handover failure probabilities under the first group experiment parameter setting. From those four figures, we see that the macrocell UE handover failure probabilities follow (eNB #1=(18, 20, 22, 24) dBm, eNB #2=(9, 7, 5, 3) dBm, (A3 offset, Hysteresis) = (1, 0) dB, TTT=320 ms) > (eNB #1=(18, 20, 22, 24) dBm, eNB #2=(9, 7, 5, 3) dBm, (A3 offset, Hysteresis) = (1, 0) dB, TTT=128 ms) > (eNB #1=(18, 20, 22, 24) dBm, eNB #2=(9, 7, 5, 3) dBm,

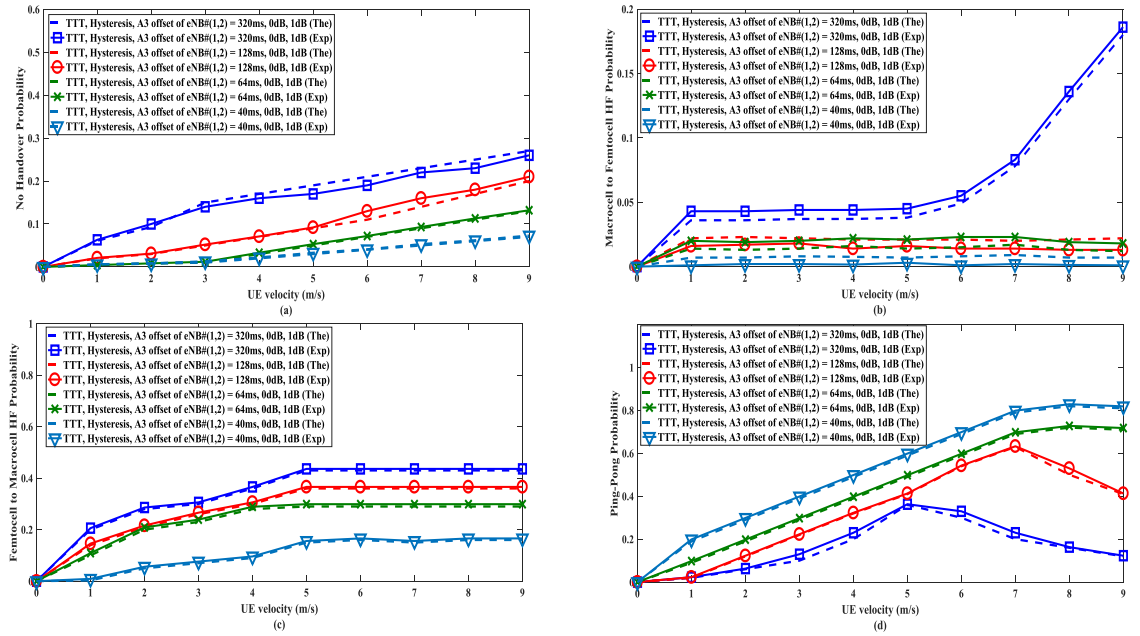

FIGURE 57. Experiment (solid lines with markers) and theoretical (dashed lines) results as a function of UE velocity for the RF Tx power of eNB #1=20dBm, the RF Tx power of eNB #2=7 dBm, and the A3 offset of eNB #(1, 2)=1dB. (a) The no handover probability; (b) The Macrocell UE handover failure probability; (c) The Femtocell UE handover failure probability; (d) The ping-pong probability.

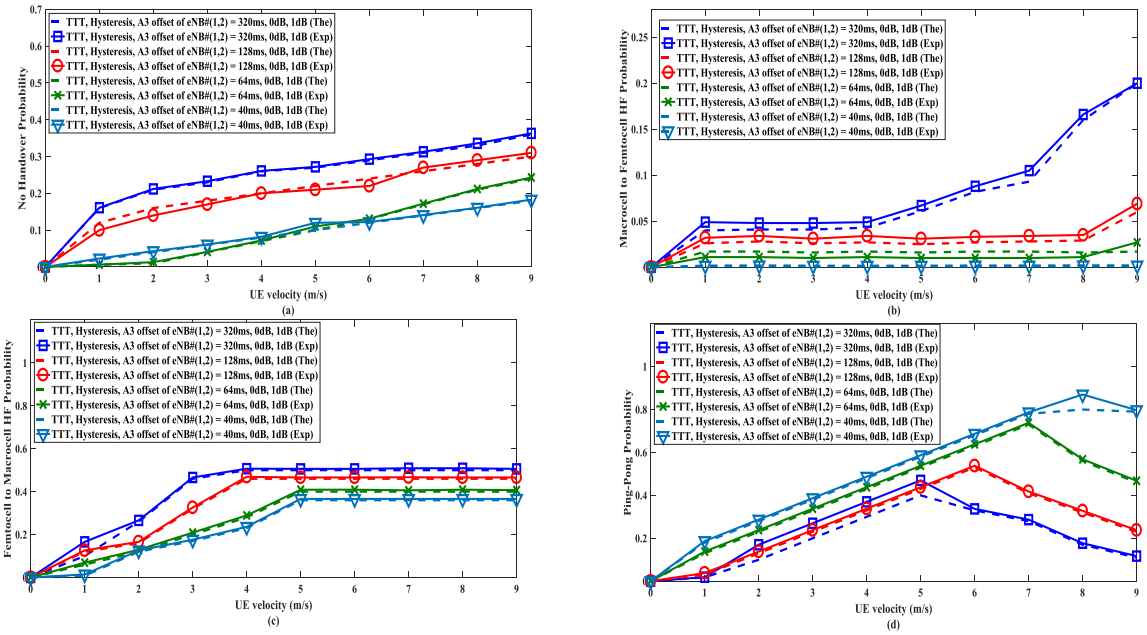

FIGURE 58. Experiment (solid lines with markers) and theoretical (dashed lines) results as a function of UE velocity for the RF Tx power of eNB #1=22dBm, the RF Tx power of eNB #2=5 dBm, and the A3 offset of eNB #(1, 2)=1dB. (a) The no handover probability; (b) The Macrocell UE handover failure probability; (c) The Femtocell UE handover failure probality; (d) The ping-pong probability.

(A3 offset, Hysteresis) = (1, 0) dB, TTT=64 ms) > (eNB #1=(18, 20, 22, 24) dBm, eNB #2=(9, 7, 5, 3) dBm, (A3 offset, Hysteresis) = (1, 0) dB, TTT=40 ms).

We observe that the parameters combination (eNB #1=(18, 20, 22, 24) dBm, eNB #2=(9, 7, 5, 3) dBm, (A3 offset, Hysteresis) = (1, 0) dB, TTT=320 ms) shows the highest Macrocell UE handover failure probability while the parameters combination (eNB #1=(18, 20, 22, 24) dBm, eNB #2=(9, 7, 5, 3) dBm, (A3 offset, Hysteresis) = (1, 0) dB, TTT=40 ms) shows the lowest macrocell UE handover

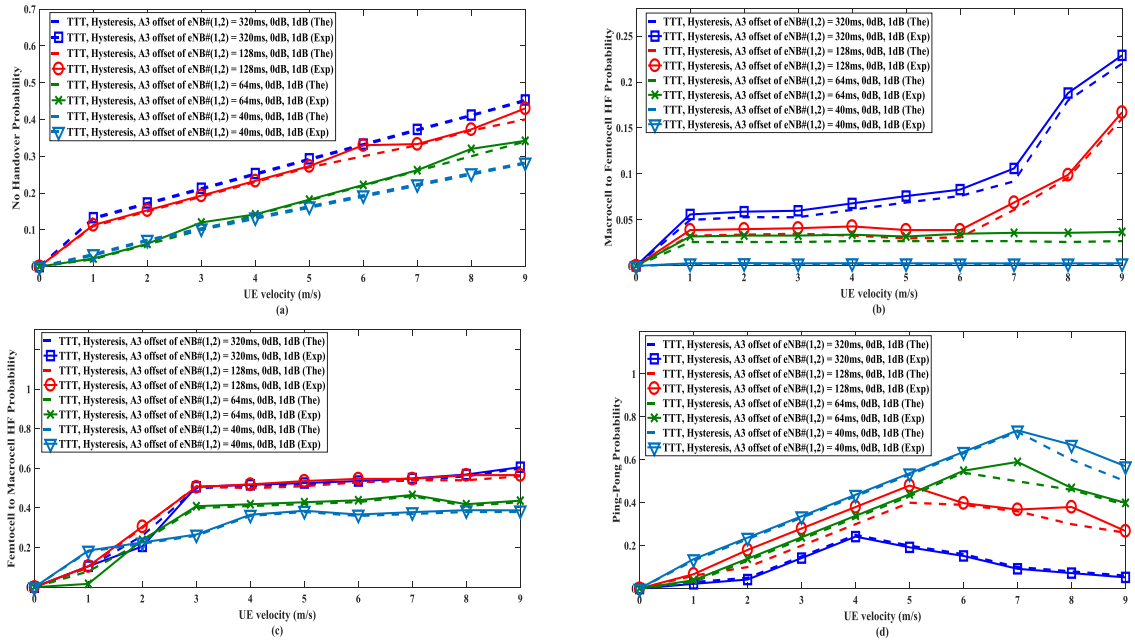

FIGURE 59. Experiment (solid lines with markers) and theoretical (dashed lines) results as a function of UE velocity for the RF Tx power of eNB #1=24dBm, the RF Tx power of eNB #2=3 dBm, and the A3 offset of eNB # (1, 2) =1dB. (a) The no handover probability; (b) The Macrocell UE handover failure probability; (c) The Femtocell UE handover failure probality; (d) The ping-pong probability.

failure probability. This is because as the TTT increase (i.e., the TC_m and TC_f increase), the (vTC_m, vTC_f, macrocell UE handover failure probability) increase accordingly. Therefore, the larger TTT setting, the larger macrocell UE handover failure probability. In addition, we can see that the macrocell UE handover failure probability grows with the UE velocity, since the chance that a high mobility UE runs into the femtocell handover failure circle increasing before TTT expires. Furthermore, when we vary the Tx power of the eNB while fixing other parameters, the Macrocell UE handover failure probability increases with the eNB Tx power increase (i.e., the same color curves in those four figures follow Fig.56 (b)< Fig.57(b)< Fig.58(b)< Fig.59(b)). The reason contributes to this is because the Femtocell coverage area becomes smaller and the macrocell coverage area becomes larger.

c: FEMTOCELL TO MACROCELL HANDOVER FAILURE PROBABILITIES

Fig.56(c), Fig.57(c), Fig.58(c), and Fig.59(c) demonstrate the Femtocell UE handover failure probabilities under the first group experiment parameter setting. From those four figures, we see that the femtocell UE handover failure probabilities follow (eNB #1=(18, 20, 22, 24) dBm, eNB #2=(9, 7, 5, 3) dBm, (A3 offset, Hysteresis) = (1, 0) dB, TTT=320 ms) > (eNB #1=(18, 20, 22, 24) dBm, eNB #2=(9, 7, 5, 3) dBm, (A3 offset, Hysteresis) = (1, 0) dB, TTT=128 ms) > (eNB #1=(18, 20, 22, 24) dBm, eNB #2=(9, 7, 5, 3) dBm, (A3 offset, Hysteresis) = (1, 0) dB, TTT=64 ms) > (eNB #1=(18, 20, 22, 24) dBm, eNB #2=(9, 7, 5, 3) dBm, (A3 offset, Hysteresis) = (1, 0) dB, TTT=40 ms).

We find that the parameters combination (eNB #1=(18, 20, 22, 24) dBm, eNB #2=(9, 7, 5, 3) dBm, (A3 offset, Hysteresis) = (1, 0) dB, TTT=320 ms) shows the highest femtocelll UE handover failure probability while the parameters combination (eNB #1=(18, 20, 22, 24) dBm, eNB #2=(9, 7, 5, 3) dBm, (A3 offset, Hysteresis) = (1, 0) dB, TTT=40 ms) shows the lowest femtocell UE handover failure probability. This is because as the TTT increase (i.e., the TC_m and TC_f increase), the (v TC_m, v TC_f, femtocell UE handover failure probability) increase accordingly. Therefore, the larger TTT setting, the larger femtocell UE handover failure probability. In addition, we can see that the Femtocell UE handover failure probability grows with the UE velocity for the reason that the chance of a high mobility UE runs into the macrocell handover failure circle before TTT expires increases.

Furthermore, when we vary the Tx power of the eNB while fixing other parameters, the femtocell UE handover failure probability increases with the eNB Tx power increase (i.e., the same color curves in those four figures follow Fig.56(c)< Fig.57(c)< Fig.58(c)< Fig.59(c)). The reason contributes to this is because the femtocell coverage area becomes smaller and the macrocell coverage area becomes larger.

d: PING-PANG PROBABILITY

Fig.56 (d), Fig.57 (d), Fig.58 (d), and Fig.59 (d) demonstrate the ping-pang probabilities under the first group experiment parameter setting. From those four figures, we observe that the ping-pang probabilities follow (eNB #1=(18, 20, 22, 24) dBm, eNB #2=(9, 7, 5, 3) dBm, (A3 offset, Hysteresis) = (1, 0) dB, TTT=320 ms) < (eNB #1=(18, 20, 22, 24) dBm,

eNB #2=(9, 7, 5, 3) dBm, (A3 offset, Hysteresis) = (1, 0) dB, TTT=128 ms) < (eNB #1=(18, 20, 22, 24) dBm, eNB #2=(9, 7, 5, 3) dBm, (A3 offset, Hysteresis) = (1, 0) dB, TTT=64 ms) < (eNB #1=(18, 20, 22, 24) dBm, eNB #2=(9, 7, 5, 3) dBm, (A3 offset, Hysteresis) = (1, 0) dB, TTT=40 ms).

We see that the parameters combination (eNB #1=(18, 20, 22, 24) dBm, eNB #2=(9, 7, 5, 3) dBm, (A3 offset, Hysteresis) = (1, 0) dB, TTT=40 ms) shows the highest ping-pang probability while the parameters combination (eNB #1=(18, 20, 22, 24) dBm, eNB #2=(9, 7, 5, 3) dBm, (A3 offset, Hysteresis) = (1, 0) dB, TTT=320 ms) shows the lowest ping-pang probability. This is because as the TTT increase (i.e., the TC_m and TC_f increase), the ping-pang probability decreases accordingly. Therefore, the larger TTT setting, the lower ping-pang probability. In addition the PP probability also grows with the UE velocity. Because the high mobility UEs traverse the femtocell coverage faster and the chance that they do it before the ping-pang time threshold T_{pp} increases. Note that for very high-velocity UEs, the ping-pang probability decreases due to the increase of no handover probabilities and handover failure probabilities, which prevents the adequate handovers and thus incurs the ping-pangs.

Furthermore, when we vary the Tx power of the eNB while fixing other parameters, the ping-pang probability decreases wi-th the eNB Tx power increase (i.e., the same color curves in th-ose four figures follow Fig.56(d)< Fig.57(d)< Fig.58(d)< Fig.59(d)).

2) PERFORMANCE UNDER THE SECOND GROUP EXPERIMENT PARAMETER SETTING

a: NO HANDOVER PROBABILITIES

Fig.60 (a), Fig.61 (a), Fig.62 (a), and Fig.63 (a) demonstrate the mobile UE no handover probabilities under the second group experiment parameter setting. From those four figures, we note that the no handover probabilities follow (eNB #1=(18, 20, 22, 24) dBm, eNB #2=(9, 7, 5, 3) dBm, (A3 offset, Hysteresis) = (6, 0) dB, TTT=320 ms) > (eNB #1=(18, 20, 22, 24) dBm, eNB #2=(9, 7, 5, 3) dBm, (A3 offset, Hysteresis) = (6, 0) dB, TTT=128 ms) > (eNB #1=(18, 20, 22, 24) dBm, eNB #2=(9, 7, 5, 3) dBm, (A3 offset, Hysteresis) = (6, 0) dB, TTT=64 ms) > (eNB #1=(18, 20, 22, 24) dBm, eNB #2=(9, 7, 5, 3) dBm, (A3 offset, Hysteresis) = (6, 0) dB, TTT=40 ms).

According to the experiment results obtained in Figures 60, 61, 62 and 63, the numerical experiment results match the derived analytical closed-form expressions approximately, which verify the accuracy of the analytical analyses. However, there is still a small gap between the analytical and simulation results. This is because we assume a typical UE with a uniform speed moving crosses the small cell coverage during one trace movement in the analysis, and we assume the femtocell and the macrocell coverage areas is ideal circle. However, those assumptions could not obtain in real scenarios.

We notice that the parameters combination (eNB #1= (18, 20, 22, 24) dBm, eNB #2= (9, 7, 5, 3) dBm, (A3 offset, Hysteresis) = (6, 0) dB, TTT=320 ms) shows the highest no handover probability while the parameters combination (eNB #1= (18, 20, 22, 24) dBm, eNB #2= (9, 7, 5, 3) dBm, (A3 offset, Hysteresis) = (6, 0) dB, TTT=40 ms) shows the lowest no handover probability. The reason contributes to this result is same as that in A. (1). Also, the no handover probability increases with UE velocity with the same reason illustrated in A. (1).

Moreover, when we vary the Tx power of the eNB while fixing other parameters, the no handover probability increases with the eNB Tx power increase (i.e., the same color curves in those four figures follow Fig.60 (a) < Fig.61 (a) < Fig.62 (a) < Fig.63 (a)). The reason contributes to this is same as described in A. (1).

Compared with the first group experiment, we set the A3 offset =6 dB in the second group experiment. From the results in Fig.60 (a)-Fig.63 (a), it can be found that the no handover probability increases with increasing A3 offset (i.e., the results shown in Fig.60(a)-Fig.63(a) > the results in Fig.56(a)-Fig.59(a)). This is because the mobile UE is more difficult to make handover under the larger A3 offset.

b: MACROCELL TO FEMTOCELL HANDOVER FAILURE PROBABILITIES

Fig.60 (b), Fig.61 (b), Fig.62 (b), and Fig.63 (b) show the macrocell UE handover failure probabilities under the second group experiment parameter setting. From those four figures, we see that the macrocell UE handover failure probabilities follow (eNB #1=(18, 20, 22, 24) dBm, eNB #2=(9, 7, 5, 3) dBm, (A3 offset, Hysteresis) = (6, 0) dB, TTT=320 ms) > (eNB #1=(18, 20, 22, 24) dBm, eNB #2=(9, 7, 5, 3) dBm, (A3 offset, Hysteresis) = (6, 0) dB, TTT=128 ms) > (eNB #1=(18, 20, 22, 24) dBm, eNB #2=(9, 7, 5, 3) dBm, (A3 offset, Hysteresis) = (6, 0) dB, TTT=64 ms) > (eNB #1=(18, 20, 22, 24) dBm, eNB #2=(9, 7, 5, 3) dBm, (A3 offset, Hysteresis) = (6, 0) dB, TTT=40 ms).

Note that the parameters combination (eNB #1= (18, 20, 22, 24) dBm, eNB #2= (9, 7, 5, 3) dBm, (A3 offset, Hysteresis) = (6, 0) dB, TTT=320 ms) shows the highest macrocell UE handover failure probability while the parameters combination (eNB #1= (18, 20, 22, 24) dBm, eNB #2= (9, 7, 5, 3) dBm, (A3 offset, Hysteresis) = (6, 0) dB, TTT=40 ms) shows the lowest macrocell UE handover failure probability. It can be obviously observed that the handover failure rate increases dramatically with the growth of TTT duration. This result is intuitively understood because as the TTT duration grows, UEs are more likely to enter a femtocell handover failure boundary before the TTT timer expires, which leads to the radio link failure. In addition, we can see that the macrocell UE handover failure probability grows with the UE velocity with the same reasons described in A. (2).

Furthermore, when we vary the Tx power of the eNB while fixing other parameters, the macrocell UE handover

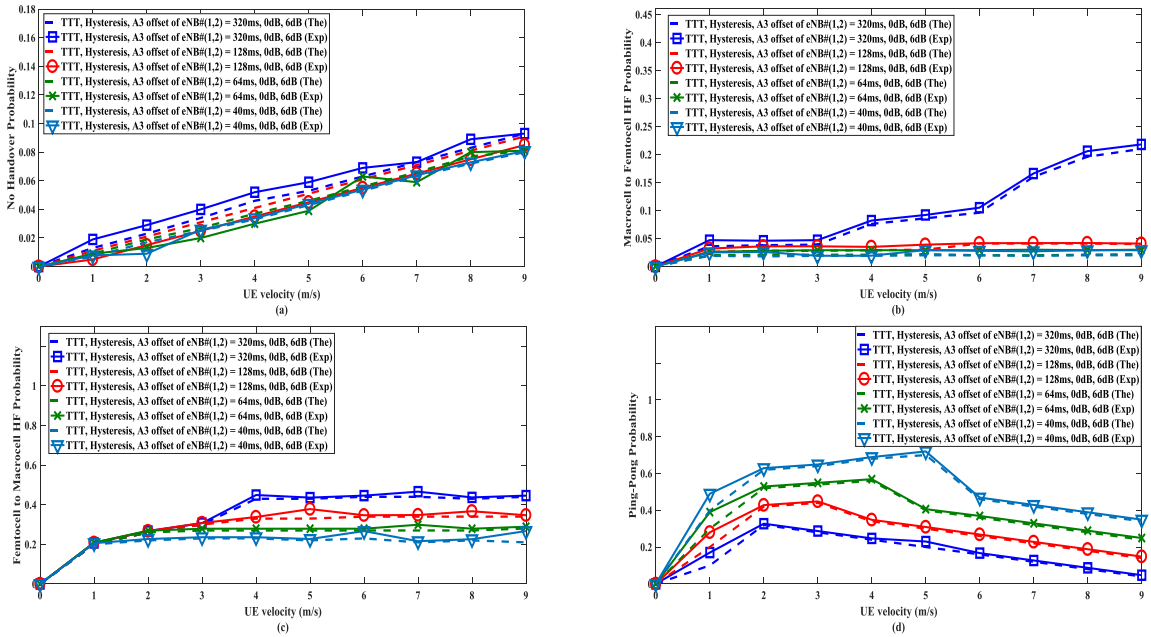

FIGURE 60. Experiment (solid lines with markers) and theoretical (dashed lines) results as a function of UE velocity for the RF Tx power of eNB #1=18dBm, the RF Tx power of eNB #2=9 dBm and the A3 offset of eNB # (1, 2) =6dB. (a) The no handover probability; (b) The Macrocell UE handover failure probability; (c) The Femtocell UE handover failure probality; (d) The ping-pong probability.

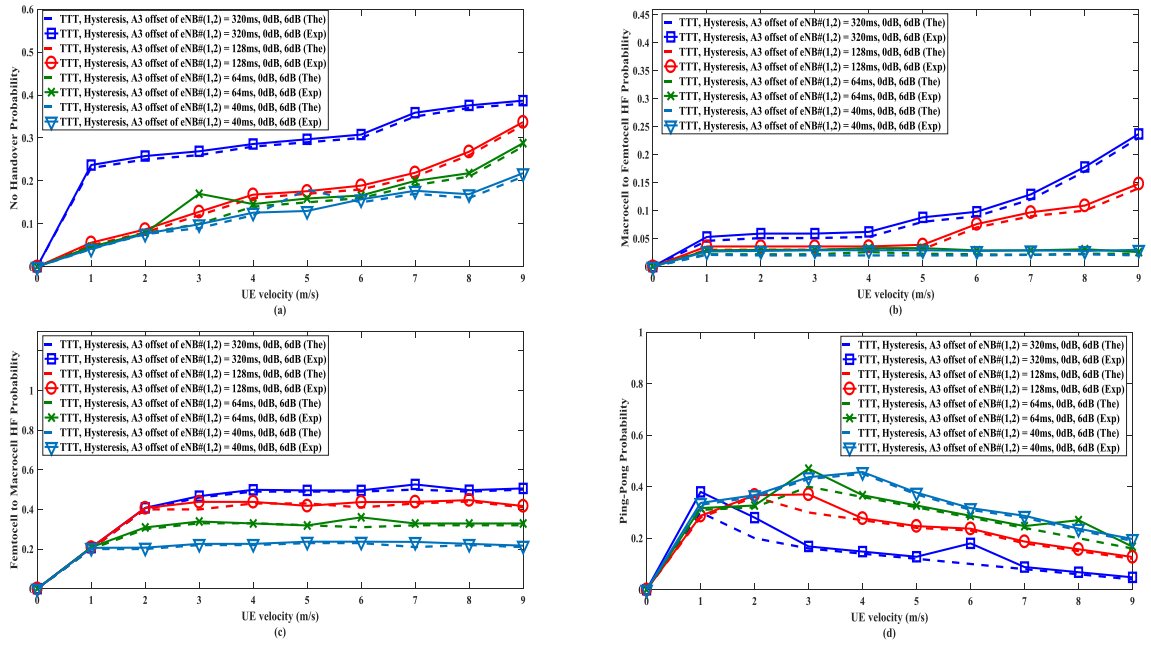

FIGURE 61. Experiment (solid lines with markers) and theoretical (dashed lines) results as a function of UE velocity for the RF Tx power of eNB #1=20dBm, the RF Tx power of eNB #2=7 dBm, and the A3 offset of eNB # (1, 2) =6dB. (a) The no handover probability; (b) The Macrocell UE handover failure probability; (c) The Femtocell UE handover failure probality; (d) The ping-pong probability.

failure probability increases with the eNB Tx power increase (i.e., the same color curves in those four figures follow Fig.60(b)< Fig.61(b)< Fig.62(b)< Fig.63(b)). The reason contributes to this is same as that in A. (2). In addition, compared with the first group experiment, it can be found that the macrocell UE handover failure probability increases with increasing A3 offset (i.e., the results shown in Fig.60(b)-Fig.63(b) > the results in Fig.56(b)-Fig.59(b)).

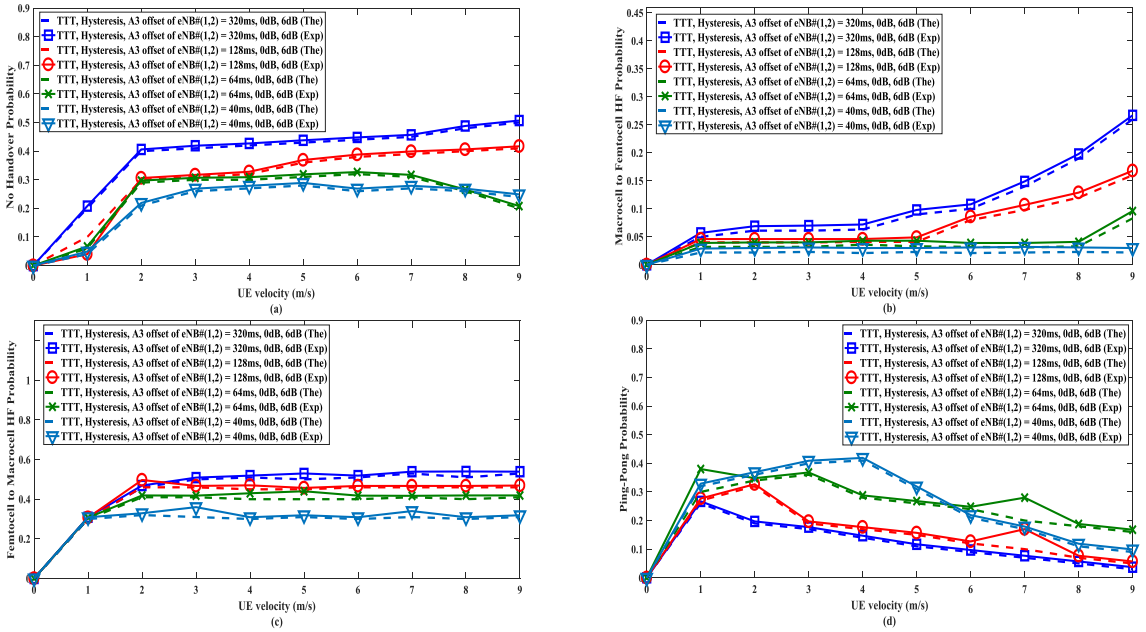

FIGURE 62. Experiment (solid lines with markers) and theoretical (dashed lines) results as a function of UE velocity for the RF Tx power of eNB #1=22dBm, the RF Tx power of eNB #2=5 dBm, and the A3 offset of eNB # (1, 2) =6dB. (a) The no handover probability; (b) The Macrocell UE handover failure probability; (c) The Femtocell UE handover failure probality; (d) The ping-pong probability.

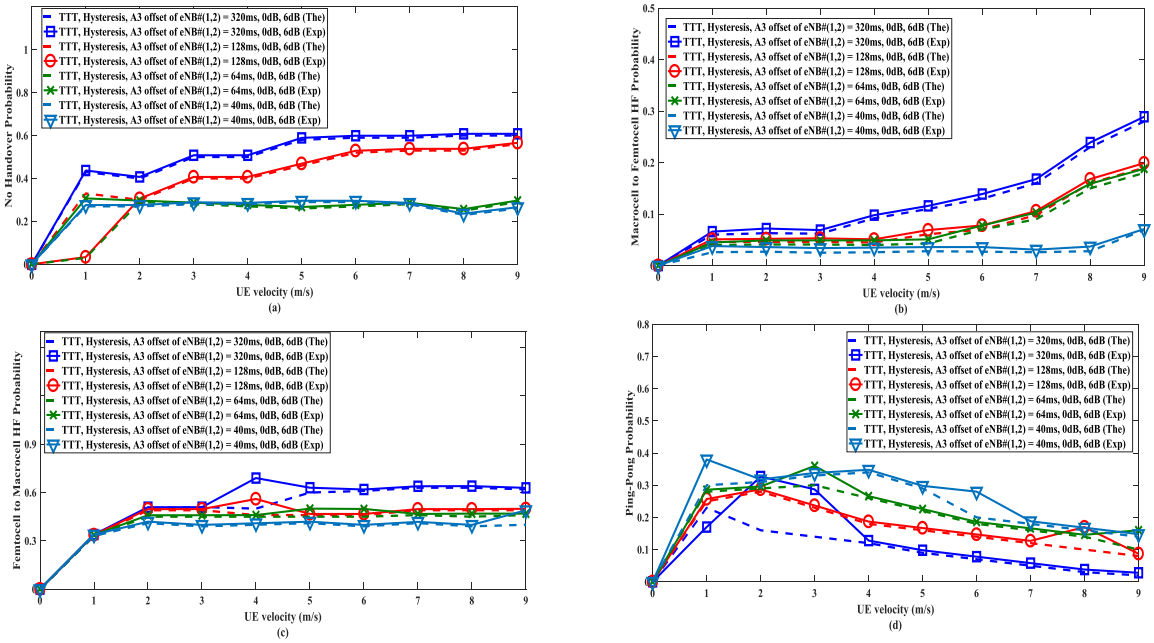

FIGURE 63. Experiment (solid lines with markers) and theoretical (dashed lines) results as a function of UE velocity for the RF Tx power of eNB #1=24dBm, the RF Tx power of eNB #2=3 dBm, and the A3 offset of eNB # (1, 2) =6dB. (a) The no handover probability; (b) The Macrocell UE handover failure probability; (c) The Femtocell UE handover failure probality; (d) The ping-pong probability.

c: FEMTOCELL TO MACROCELL HANDOVER FAILURE PROBABILITIES

Fig.60(c), Fig.61(c), Fig.62(c), and Fig.63(c) demonstrate the femtocell UE handover failure probabilities under the second group experiment parameter setting. From those four figures, we see that the femtocell UE handover failure probabilities follow (eNB #1=(18, 20, 22, 24) dBm, eNB #2=(9, 7, 5, 3) dBm, (A3 offset, Hysteresis) = (6, 0) dB, TTT=320 ms) > (eNB #1=(18, 20, 22, 24) dBm, eNB #2=(9, 7, 5, 3) dBm, (A3 offset, Hysteresis) = (6, 0) dB, TTT=128 ms) > (eNB #1=(18, 20, 22, 24) dBm, eNB #2=(9, 7, 5, 3) dBm, (A3 offset, Hysteresis) = (6, 0) dB,

TTT=64 ms) > (eNB #1=(18, 20, 22, 24) dBm, eNB #2=(9, 7, 5, 3) dBm, (A3 offset, Hysteresis) = (6, 0) dB, TTT=40 ms).

We find that the parameters combination (eNB #1= (18, 20, 22, 24) dBm, eNB #2= (9, 7, 5, 3) dBm, (A3 offset, Hysteresis) = (6, 0) dB, TTT=320 ms) shows the highest femtocelll UE handover failure probability while the parameters combination (eNB #1= (18, 20, 22, 24) dBm, eNB #2= (9, 7, 5, 3) dBm, (A3 offset, Hysteresis) = (6, 0) dB, TTT=40 ms) shows the lowest femtocell UE handover failure probability. This is because as the TTT increase (i.e., the TC_m and TC_f increase), the (v TC_m, v TC_f, Femtocell UE handover failure probability) increase accordingly. In addition, we can see that the Femtocell UE handover failure probability grows with the UE velocity for the same reason illustrated in A. (3).

Furthermore, when we vary the Tx power of the eNB while fixing other parameters, the femtocell UE handover failure probability increases with the eNB Tx power increase (i.e., the same color curves in those four figures follow Fig.60(c)< Fig.61(c)< Fig.62(c)< Fig.63(c)). The reason contributes to this is same as that described in A. (3). In addition, compared with the first group experiment, it can be found that the femtocell UE handover failure probability increases with increasing A3 offset (i.e., the results shown in Fig.60(c)-Fig.63(c) > the results in Fig.56(c)-Fig.59(c)).

d: PING-PANG PROBABILITY

Fig.60 (d), Fig.61 (d), Fig.62 (d), and Fig.63 (d) show the ping-pang probabilities under the second group experiment parameter setting. In contrast to the handover failure probabilities, we observe that the ping-pang probabilities follow (eNB #1=(18, 20, 22, 24) dBm, eNB #2=(9, 7, 5, 3) dBm, (A3 offset, Hysteresis) = (6, 0) dB, TTT=320 ms) < (eNB #1=(18, 20, 22, 24) dBm, eNB #2=(9, 7, 5, 3) dBm, (A3 offset, Hysteresis) = (6, 0) dB, TTT=128 ms) < (eNB #1=(18, 20, 22, 24) dBm, eNB #2=(9, 7, 5, 3) dBm, (A3 offset, Hysteresis) = (6, 0) dB, TTT=64 ms) < (eNB #1=(18, 20, 22, 24) dBm, eNB #2=(9, 7, 5, 3) dBm, (A3 offset, Hysteresis) = (6, 0) dB, TTT=40 ms).

We see that the parameters combination (eNB #1= (18, 20, 22, 24) dBm, eNB #2= (9, 7, 5, 3) dBm, (A3 offset, Hysteresis) = (6, 0) dB, TTT=40 ms) shows the highest ping-pang probability while the parameters combination (eNB #1= (18, 20, 22, 24) dBm, eNB #2= (9, 7, 5, 3) dBm, (A3 offset, Hysteresis) = (6, 0) dB, TTT=320 ms) shows the lowest ping-pang probability. In addition, the ping-pang probability also grows with the UE velocity, and for very high-velocity UEs, the ping-pang probability decreases due to the increase of no handover probabilities and handover failure probabilities, which prevents the adequate handovers and thus incurs the ping-pangs. The reasons contribute to the above-mentioned results are same as that described in A. (4).

Furthermore, when we vary the Tx power of the eNB while fixing other parameters, the ping-pang probability decreases with the eNB Tx power increase (i.e., the same color curves in those four figures follow Fig.60(d)< Fig.61(d)< Fig.62(d)< Fig. (d)). In addition, compared with the first group experiment, it can be found that the ping-pang probability decreases with increasing A3 offset (i.e., the results shown in Fig.60 (d)-Fig.63 (d) < the results in Fig.56 (d)-Fig.59 (d)).

3) PERFORMANCE UNDER THE THIRD GROUP EXPERIMENT PARAMETER SETTING

a: NO HANDOVER PROBABILITIES

Fig.64 (a), Fig.65 (a), Fig.66 (a), and Fig.67 (a) show the mobile UE no handover probabilities under the third group experiment parameter setting. From the four figures, we find that the no handover probabilities follow (eNB #1=(18, 20, 22, 24) dBm, eNB #2=(9, 7, 5, 3) dBm, (A3 offset, Hysteresis) = (12, 0) dB, TTT=320 ms) > (eNB #1=(18, 20, 22, 24) dBm, eNB #2=(9, 7, 5, 3) dBm, (A3 offset, Hysteresis) = (12, 0) dB, TTT=128 ms) > (eNB #1=(18, 20, 22, 24) dBm, eNB #2=(9, 7, 5, 3) dBm, (A3 offset, Hysteresis) = (12, 0) dB, TTT=64 ms) > (eNB #1=(18, 20, 22, 24) dBm, eNB #2=(9, 7, 5, 3) dBm, (A3 offset, Hysteresis) = (12, 0) dB, TTT=40 ms).

Note that the parameters combination (eNB #1= (18, 20, 22, 24) dBm, eNB #2= (9, 7, 5, 3) dBm, (A3 offset, Hysteresis) = (12, 0) dB, TTT=320 ms) shows the highest no handover probability while the parameters combination (eNB #1= (18, 20, 22, 24) dBm, eNB #2= (9, 7, 5, 3) dBm, (A3 offset, Hysteresis) = (12, 0) dB, TTT=40 ms) shows the lowest no handover probability. The reason contributes to this experiment result is same as that in A. (1). Also, the no handover probability increases with UE velocity with the same reason illustrated in A. (1).

Moreover, when we vary the Tx power of the eNB while fixing other parameters, the no handover probability increases with the eNB Tx power increase (i.e., the same color curves in those four figures follow Fig.64 (a) < Fig.65 (a) < Fig.66 (a) < Fig.67 (a)). The reason contributes to this is same as described in A. (1).

Compared with the first group and second group experiments, we set the A3 offset =12 dB in the third group experiment. From the results in Fig.64 (a)-Fig.67 (a), it can be found that the no handover probability increases with increasing A3 offset (i.e., the results shown in Fig.64 (a)-Fig.67 (a) > the results in Fi-g.60 (a)-Fig.63 (a) > the results in Fig.56 (a)-Fig.59 (a)). This is because the mobile UE is more difficult to make handover under the larger A3 offset.

b: MACROCELL TO FEMTOCELL HANDOVER FAILURE PROBABILITIES

Fig.64 (b), Fig.65 (b), Fig.66 (b), and Fig.67 (b) show the Macrocell UE handover failure probabilities under the third group experiment parameter setting. From those four figures, we see that the macrocell UE handover failure probabilities follow (eNB #1=(18, 20, 22, 24) dBm,

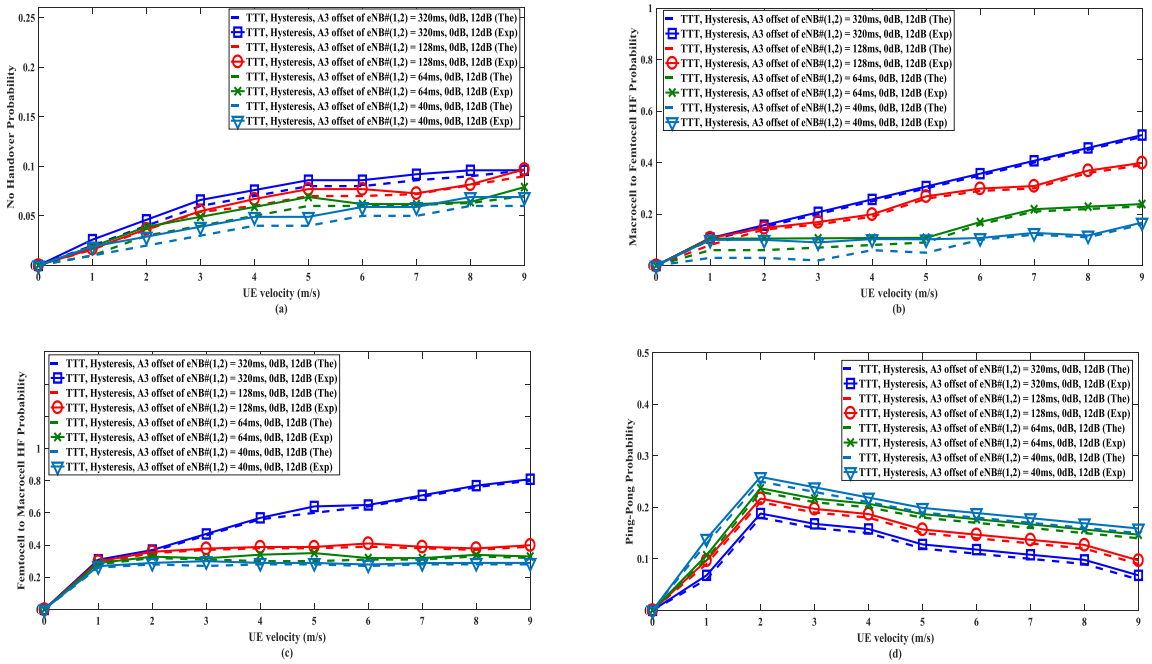

FIGURE 64. Experiment (solid lines with markers) and theoretical (dashed lines) results as a function of UE velocity for the RF Tx power of eNB #1=18dBm, the RF Tx power of eNB #2=9 dBm and the A3 offset of eNB # (1, 2) =12dB. (a) The no handover probability; (b) The Macrocell UE handover failure probability; (c) The Femtocell UE handover failure probality; (d) The ping-pong probability.

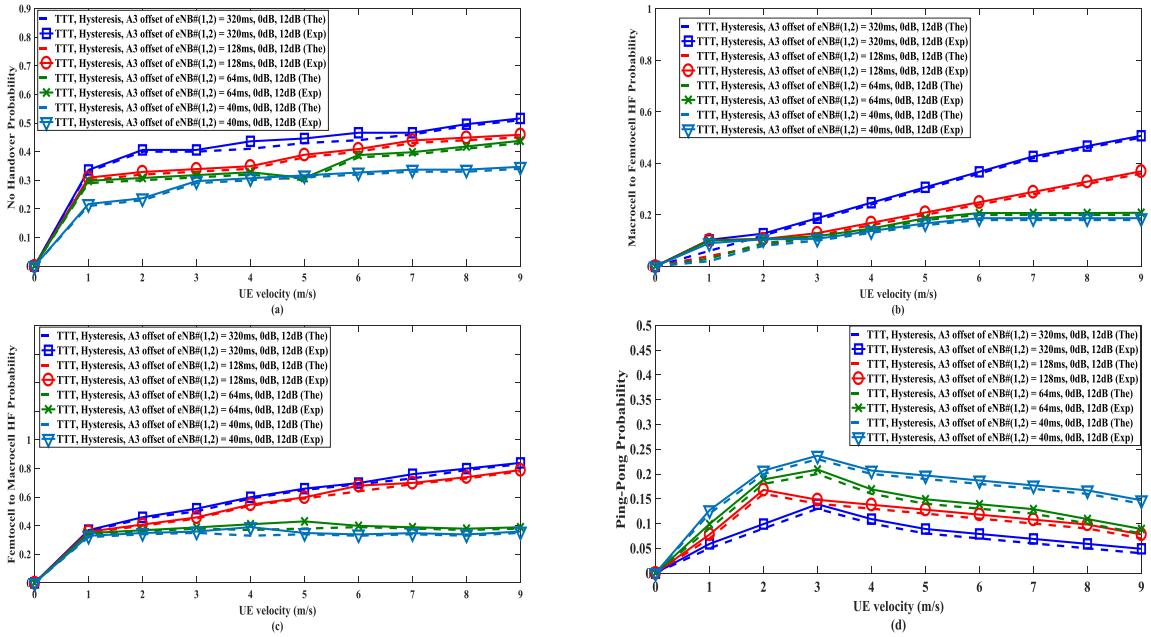

FIGURE 65. Experiment (solid lines with markers) and theoretical (dashed lines) results as a function of UE velocity for the RF Tx power of eNB #1=20dBm, the RF Tx power of eNB #2=7 dBm, and the A3 offset of eNB # (1, 2) =12dB. (a) The no handover probability; (b) The Macrocell UE handover failure probability; (c) The Femtocell UE handover failure probality; (d) The ping-pong probability.

eNB #2=(9, 7, 5, 3) dBm, (A3 offset, Hysteresis) = (12, 0) dB, TTT=320 ms) > (eNB #1=(18, 20, 22, 24) dBm, eNB #2=(9, 7, 5, 3) dBm, (A3 offset, Hysteresis) = (12, 0) dB, TTT=128 ms) > (eNB #1=(18, 20, 22, 24) dBm, eNB #2=(9, 7, 5, 3) dBm, (A3 offset, Hysteresis) = (12, 0) dB, TTT=64 ms) > (eNB #1=(18, 20, 22, 24) dBm, eNB #2=(9, 7, 5, 3) dBm, (A3 offset, Hysteresis) = (12, 0) dB, TTT=40 ms).

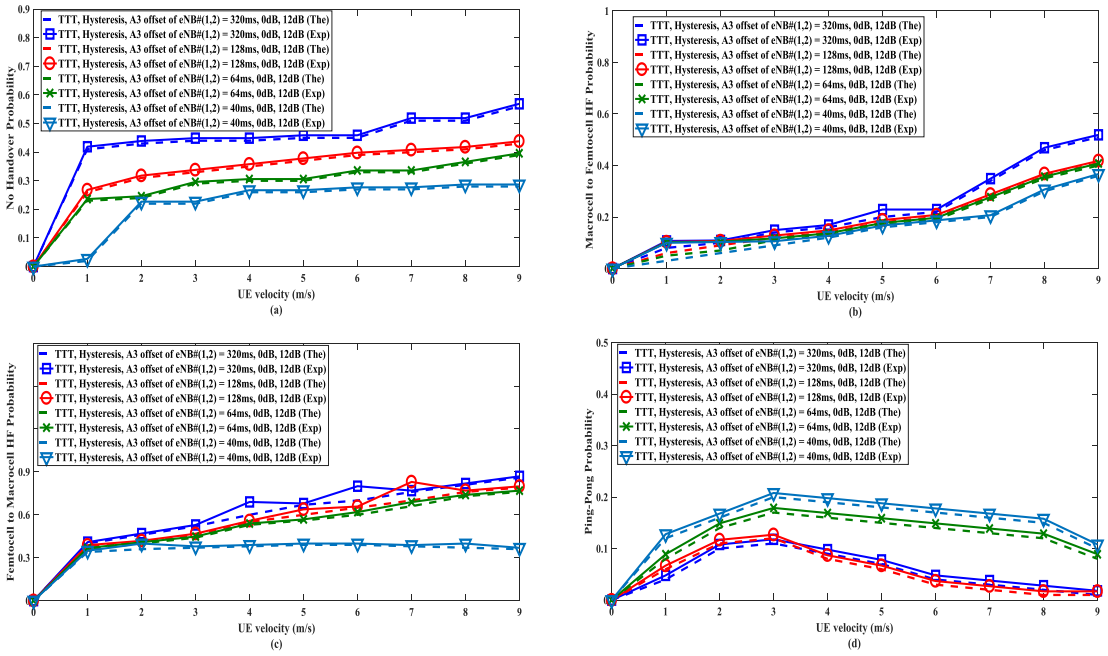

FIGURE 66. Experiment (solid lines with markers) and theoretical (dashed lines) results as a function of UE velocity for the RF Tx power of eNB #1=22dBm, the RF Tx power of eNB #2=5 dBm, and the A3 offset of eNB # (1, 2) =12dB. (a) The no handover probability; (b) The Macrocell UE handover failure probability; (c) The Femtocell UE handover failure probality; (d) The ping-pong probability.

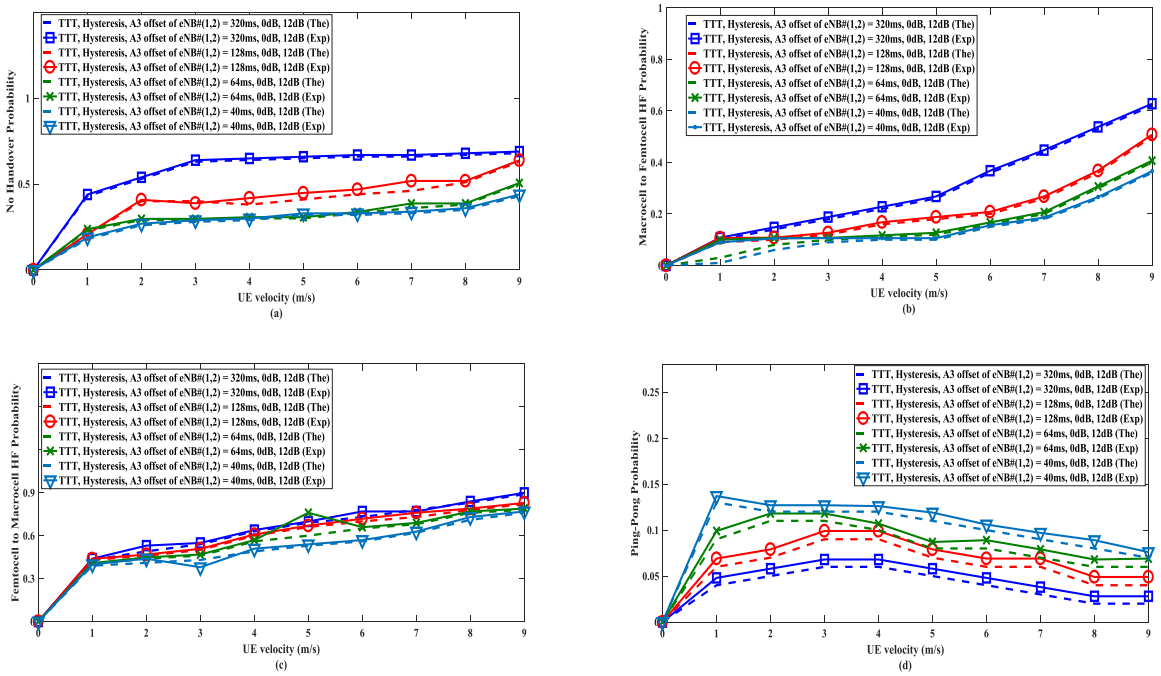

FIGURE 67. Experiment (solid lines with markers) and theoretical (dashed lines) results as a function of UE velocity for the RF Tx power of eNB #1=24dBm, the RF Tx power of eNB #2=3 dBm, and the A3 offset of eNB # (1, 2) =12dB. (a) The no handover probability; (b) The Macrocell UE handover failure probability; (c) The Femtocell UE handover failure probality; (d) The ping-pong probability.

Note that the parameters combination (eNB #1= (18, 20, 22, 24) dBm, eNB #2= (9, 7, 5, 3) dBm, (A3 offset, Hysteresis) = (12, 0) dB, TTT=320 ms) shows the highest macrocell UE handover failure probability while the parameters combination (eNB #1= (18, 20, 22, 24) dBm, eNB #2= (9, 7, 5, 3) dBm, (A3 offset, Hysteresis) = (12, 0) dB, TTT=40 ms)

shows the lowest macrocell UE handover failure probability. It can be apparently observed that the handover failure rate increases dramatically with the growth of TTT duration for the same reason described in A. (2). In addition, we can see that the macrocell UE handover failure probability grows with the UE velocity with the same reasons described in A. (2).

Furthermore, when we vary the Tx power of the eNB while fixing other parameters, the macrocell UE handover failure probability increases with the eNB Tx power increase (i.e., the same color curves in those four figures follow Fig.64(b)< Fig.65(b)< Fig.66(b)< Fig.67(b)). The reason contributes to this is same as that in A. (2). In addition, compared with the first group and the second group experiments, it can be found that the macrocell UE handover failure probability increases with increasing A3 offset (i.e., the results shown in Fig.64(b)-Fig.67(b) > the results in Fig.60(b)-Fig.63(b) > the results in Fig.56(b)-Fig.59(b)).

c: FEMTOCELL TO MACROCELL HANDOVER FAILURE PROBABILITIES

Fig.64(c), Fig.65(c), Fig.66(c), and Fig.67(c) demonstrate the femtocell UE handover failure probabilities under the third group experiment parameter setting. From those four figures, we see that the femtocell UE handover failure probabilities follow (eNB #1=(18, 20, 22, 24) dBm, eNB #2=(9, 7, 5, 3) dBm, (A3 offset, Hysteresis) = (12, 0) dB, TTT=320 ms) > (eNB #1=(18, 20, 22, 24) dBm, eNB #2=(9, 7, 5, 3) dBm, (A3 offset, Hysteresis) = (12, 0) dB, TTT=128 ms) > (eNB #1=(18, 20, 22, 24) dBm, eNB #2=(9, 7, 5, 3) dBm, (A3 offset, Hysteresis) = (12, 0) dB, TTT=64 ms) > (eNB #1=(18, 20, 22, 24) dBm, eNB #2=(9, 7, 5, 3) dBm, (A3 offset, Hysteresis) = (12, 0) dB, TTT=40 ms).

We find that the parameters combination (eNB #1= (18, 20, 22, 24) dBm, eNB #2= (9, 7, 5, 3) dBm, (A3 offset, Hysteresis) = (12, 0) dB, TTT=320 ms) shows the highest femtocelll UE handover failure probability while the parameters combination (eNB #1= (18, 20, 22, 24) dBm, eNB #2= (9, 7, 5, 3) dBm, (A3 offset, Hysteresis) = (12, 0) dB, TTT=40 ms) shows the lowest Femtocell UE handover failure probability. This is because as the TTT increase (i.e., the TC_m and TC_f increase), the (v TC_m, v TC_f, femtocell UE handover failure probability) increase accordingly. In addition, we can see that the femtocell UE handover failure probability grows with the UE velocity for the same reason illustrated in A. (3).

Furthermore, when we vary the Tx power of the eNB while fixing other parameters, the femtocell UE handover failure probability increases with the eNB Tx power increase (i.e., the same color curves in those four figures follow Fig.64(c)< Fig.65(c)< Fig.66(c)< Fig.67(c)). The reason contributes to this is same as that described in A. (3). In addition, compared with the first group and the second group experiments, it can be found that the femtocell UE handover failure probability increases with increasing A3 offset (i.e., the results shown in Fig.64(c)-Fig.67(c) > the results in Fig.60(c)-Fig.63(c) > the results in Fig.56(c)-Fig.59(c)).

d: PING-PANG PROBABILITY

Fig.64 (d), Fig.65 (d), Fig.66 (d), and Fig.67 (d) show the ping-pang probabilities under the third group experiment parameter setting. In contrast to the handover failure probabilities, we see that the ping-pang probabilities follow (eNB #1=(18, 20, 22, 24) dBm, eNB #2=(9, 7, 5, 3) dBm, (A3 offset, Hysteresis) = (12, 0) dB, TTT=320 ms) < (eNB #1=(18, 20, 22, 24) dBm, eNB #2=(9, 7, 5, 3) dBm, (A3 offset, Hysteresis) = (12, 0) dB, TTT=128 ms) < (eNB #1=(18, 20, 22, 24) dBm, eNB #2=(9, 7, 5, 3) dBm, (A3 offset, Hysteresis) = (12, 0) dB, TTT=64 ms) < (eNB #1=(18, 20, 22, 24) dBm, eNB #2=(9, 7, 5, 3) dBm, (A3 offset, Hysteresis) = (12, 0) dB, TTT=40 ms).

We see that the parameters combination (eNB #1= (18, 20, 22, 24) dBm, eNB #2= (9, 7, 5, 3) dBm, (A3 offset, Hysteresis) = (12, 0) dB, TTT=40 ms) shows the highest ping-pang probability while the parameters combination (eNB #1= (18, 20, 22, 24) dBm, eNB #2= (9, 7, 5, 3) dBm, (A3 offset, Hysteresis) = (12, 0) dB, TTT=320 ms) shows the lowest ping-pang probability. In addition, the ping-pang probability also grows with the UE velocity, and for very high-velocity UEs, the ping-pang probability decreases due to the increase of no handover probabilities and handover failure probabilities, which prevents the adequate handovers and thus incurs the ping-pangs. The reasons contribute to the above-mentioned results are same as that described in A. (4).

Furthermore, when we vary the Tx power of the eNB while fixing other parameters, the ping-pang probability decreases wi-th the eNB Tx power increase (i.e., the same color curves in t-hose four figures follow Fig.64(d)< Fig.65(d)< Fig.66(d)< Fig.6-7(d)). In addition, compared with the first group experiment, it can be found that the ping-pang probability decreases with incr-easing A3 offset (i.e., the results shown in Fig.9 (d)-Fig.12 (d) < the results in Fig.5 (d)-Fig.8 (d) < the results in Fig.1 (d)-Fig.4 (d)).

Based on the above-mentioned analysis, it can be observed that TTT controls the trade-off between handover failure probabilities (i.e., the macrocell UE handover failure and the femtocell UE handover failure) and ping-pang probabilities. Since the handover failure rate is a function of the product of UE velocity v and TTT (including the TC_m and TC_f), but not their individual values, it is critical how fast the UE travels while the TTT timer is running. A short TTT can reduce the handover failure probability, but increases the ping-pang probability and vice versa, which indicates that the parameter TTT should be carefully optimized according to the UE velocities and the cell coverage size which is proportioned to the base station's RF Tx power. In case of TTT and A3 offset, and Hysteresis being fixed, different handover strategies can be applied to UEs with different velocities. For instance, high mobility users can always connect to the macrocell eNBs and avoid macrocell to femtocell handover due to its possible high handover rate and handover failure rate.

VII. CONCLUSION

In order to depict the two-tier intra-frequency X2 handover performance in macro-femto HetNets, in this paper, we analyze the key performance metrics for macro-to-femto cell handovers with closed-form expressions. To be specific, we first construct a software defined open LTE platform. Based on software-defined open LTE platform, we then proposed an analytical model, including the coverage models which represent the small cell boundary and the cross-tier handover failure boundary by two biased circles, the accuracy of which have been proved by experiments. Based on the analytical model, we further derived the closed-form expressions of macrocell to femtocell cross-tier handover failure probabilities and ping-pong probabilities as functions of relevant system parameters. These expressions show that the Time To Trigger (TTT) and user velocity (UE) have great influences on the two-tier intra-frequency X2 handover performance. The handover failure probability declines with the decrease of TTT while the ping-pong probability grows, which means that a tradeoff between the handover failure probability and the ping-pong probability should be achieved. Experiment results verify the accuracy of the proposed analytical model and closed-form theoretical analyses, which provide guidance for actual network planning as well as handover optimizations in densely deployed macro-femto HetNets. Currently, the current version software-defined open LTE platform is composed by the commercial UEs, commercial eNBs, and updated soft EPC, which is not completely software defined and opening. In the future, we will continue to develop the soft UE and the soft eNB, and will utilize those software-defined equipment to substitute the commercial hard-coded equipment in the open LTE platform (i.e., evolve to the final version).

ACKNOWLEDGMENT

The authors would like to thank the anonymous reviewers for their helpful comments and suggestions for their work.

APPENDIX A
DERIVATION FROM EQUATION (3) TO EQUATION (2)

The detailed derivation process from equation (3) to equation (2) is shown as follows. To be specific, we get the derivative of equation (3) with respect to the variable ch.

$$\begin{aligned}
&[\frac{2}{\pi}\arctan(\frac{ch}{\sqrt{4R_{at}^2-ch^2}})]' \\
&\Rightarrow \frac{1}{1+\frac{ch^2}{4R_{at}^2-ch^2}} \times (\frac{ch}{\sqrt{4R_{at}^2-ch^2}})' \\
&\Rightarrow \frac{1}{\frac{4R_{at}^2-ch^2+ch^2}{4R_{at}^2-ch^2}} \times (\frac{ch}{\sqrt{4R_{at}^2-ch^2}})' \\
&\Rightarrow \frac{4R_{at}^2-ch^2}{4R_{at}^2} \times \frac{\sqrt{4R_{at}^2-ch^2}-ch(\sqrt{4R_{at}^2-ch^2})'}{4R_{at}^2-ch^2} \\
&\Rightarrow \frac{\sqrt{4R_{at}^2-ch^2}-ch(\sqrt{4R_{at}^2-ch^2})'}{4R_{at}^2} \\
&\Rightarrow \frac{\sqrt{4R_{at}^2-ch^2}-ch\times\frac{-ch}{\sqrt{4R_{at}^2-ch^2}}}{4R_{at}^2} \\
&\Rightarrow \frac{\sqrt{4R_{at}^2-ch^2}+\frac{ch^2}{\sqrt{4R_{at}^2-ch^2}}}{4R_{at}^2} \\
&\Rightarrow \frac{4R_{at}^2-ch^2+ch^2}{\sqrt{4R_{at}^2-ch^2}} \times \frac{1}{4R_{at}^2} \\
&\Rightarrow \frac{1}{\sqrt{4R_{at}^2-ch^2}}
\end{aligned} \tag{30}$$

APPENDIX B
DERIVATION FROM THE SECOND ITEM IN EQUATION (9) TO EQUATION (10)

The detailed derivation process from the second item in equation (9) to equation (10) is shown as follows. To be specific, based on equation (8), we can get the following derivation process.

$$\begin{aligned}
vTC_m &\geq \mathrm{X}_{\text{HF-M}}(\psi, R_{at}, R_{am}) \\
&\Rightarrow vTC_m \geq R_{at}\cos\psi - \sqrt{R_{am}^2 - R_{at}^2\sin^2\psi} \\
&\Rightarrow vTC_m \geq R_{at}\cos\psi - \sqrt{R_{am}^2 - R_{at}^2(1-\cos^2\psi)} \\
&\Rightarrow vTC_m \geq R_{at}\cos\psi - \sqrt{R_{am}^2 - R_{at}^2 + R_{at}^2\cos^2\psi} \\
&\Rightarrow \sqrt{R_{am}^2 - R_{at}^2 + R_{at}^2\cos^2\psi} \geq R_{at}\cos\psi - vTC_m \\
&\Rightarrow R_{am}^2 - R_{at}^2 + R_{at}^2\cos^2\psi \geq R_{at}\cos\psi^2 \\
&\quad - 2R_{at}\cos\psi vTC_m + v^2TC_m^2 \\
&\Rightarrow 2R_{at}\cos\psi vTC_m \geq v^2TC_m^2 - R_{am}^2 + R_{at}^2 \\
&\Rightarrow \cos\psi \geq \frac{v^2TC_m^2 - R_{am}^2 + R_{at}^2}{2R_{at}vTC_m} \psi \in [-\frac{\pi}{2}, \frac{\pi}{2}] \\
&\Rightarrow \psi \in [-\arccos\frac{v^2TC_m^2 - R_{am}^2 + R_{at}^2}{2R_{at}vTC_m}, \\
&\qquad \arccos\frac{v^2TC_m^2 - R_{am}^2 + R_{at}^2}{2R_{at}vTC_m}]
\end{aligned} \tag{31}$$

Then, we get the derivative of equation (1) with respect to the variable ψ, we can obtain the following equation.

$$\frac{\mathrm{d}(ch)}{\mathrm{d}(\psi)} = 2R_{at}(-\sin\psi) \tag{32}$$

Then, based on equation (2), equation (3), and equation (32). We can obtain the following equation.

$$\begin{aligned}
\frac{\mathrm{d}(ch)}{\mathrm{d}(\psi)} &= 2R_{at}(-\sin\psi), \mathrm{g}(ch) \\
&= \frac{2}{\pi\sqrt{4R_{at}^2 - ch^2}}
\end{aligned}$$

$$
\begin{aligned}
&\mathrm{P}(ch_1 < ch(\psi) < ch_2) \\
&\quad = \frac{2}{\pi}\arctan(\frac{ch}{\sqrt{4R_{at}^2 - ch^2}})|_{ch_1}^{ch_2} \\
&\therefore\ \mathrm{P}(\psi_1 < \psi < \psi_2) \\
&\quad = \int_{\psi_1}^{\psi_2} \frac{2}{\pi} \times \frac{1}{\sqrt{4R_{at}^2 - 4R_{at}^2\cos\psi^2}} \times 2R_{at}(-\sin\psi)\mathrm{d}\psi \\
&\quad \Rightarrow \int_{\psi_1}^{\psi_2} \frac{2}{\pi} \times \frac{1}{2R_{at}\sin\psi} \times 2R_{at}(-\sin\psi)\mathrm{d}\psi \\
&\quad \Rightarrow \int_{\psi_1}^{\psi_2} \frac{2}{\pi} \times (-1)\mathrm{d}\psi \qquad (33)
\end{aligned}
$$

Then, based on the above-mentioned process, we can finally obtain the equation (10).

APPENDIX C
DERIVATION FROM EQUATION (13) TO EQUATION (15)

The detailed derivation process from equation (13) to equation (15) is shown as follows.

$$
\begin{aligned}
vTC_f &> X_{HF-F}(\psi, R_{at}, R_{af}) \\
&\Rightarrow vTC_f > R_{at}\cos\psi + \sqrt{R_{af}^2 - R_{at}^2\sin^2\psi} - ch(\psi) \\
&\Rightarrow vTC_f + ch(\psi) - R_{at}\cos\psi > \sqrt{R_{af}^2 - R_{at}^2\sin^2\psi} \\
R_{at}\cos\psi &= \frac{1}{2}ch(\psi) \\
&\Rightarrow vTC_f + ch(\psi) - \frac{1}{2}ch(\psi) > \sqrt{R_{af}^2 - R_{at}^2\sin^2\psi} \\
&\Rightarrow vTC_f + \frac{1}{2}ch(\psi) > \sqrt{R_{af}^2 - R_{at}^2\sin^2\psi} \\
&\Rightarrow v^2(TC_f)^2 + 2vTC_f \times \frac{1}{2}ch(\psi) + \frac{1}{4}(ch(\psi))^2 \\
&> R_{af}^2 - R_{at}^2\sin^2\psi \\
&\Rightarrow v^2(TC_f)^2 + vTC_f ch(\psi) + \frac{1}{4}(ch(\psi))^2 \\
&> R_{af}^2 - R_{at}^2(1 - \cos^2\psi) \\
&\Rightarrow v^2(TC_f)^2 + vTC_f ch(\psi) + \frac{1}{4}(ch(\psi))^2 \\
&> R_{af}^2 - R_{at}^2 + R_{at}^2\cos^2\psi \\
&\Rightarrow v^2(TC_f)^2 + vTC_f ch(\psi) + \frac{1}{4}(ch(\psi))^2 \\
&> R_{af}^2 - R_{at}^2 + \frac{1}{4}(ch(\psi))^2 \\
&\Rightarrow v^2(TC_f)^2 + vTC_f ch(\psi) \\
&> R_{af}^2 - R_{at}^2 \\
&\Rightarrow ch(\psi) > \frac{R_{af}^2 - R_{at}^2 - v^2(TC_f)^2}{vTC_f} \\
&\Rightarrow ch(\psi) > \frac{R_{af}^2 - R_{at}^2}{vTC_f} - vTC_f \qquad (34)
\end{aligned}
$$

REFERENCES

[1] J. G. Andrews, H. Claussen, M. Dohler, S. Rangan, and M. C. Reed, "Femtocells: Past, present, and future," *IEEE J. Sel. Areas Commun.*, vol. 30, no. 3, pp. 497–508, Apr. 2012.

[2] Nokia Siemens Networks. (Aug. 2011). *2020: Beyond 4G, Radio Evolution for The Gig-Abit Experience*. [Online]. Available: http://nsn.com/?le/15036/2020-beyond-4g-radio-evolution-for-thegigabit-experience

[3] D. L. Perez, I. Guvenc, and X. Chu, "Mobility management challenges in 3GPP heterogeneous networks wireless medium access control protocols," *IEEE Commun. Mag.*, vol. 50, no. 12, pp. 70–78, Dec. 2012.

[4] Y. Hong, X. Xu, and M. Tao, "Predictive connection time based small cell discovery strategy for LTE-advanced and beyond," in *Proc. IEEE Wireless Commun. Netw. Conf. (WCNC)*, Istanbul, Turkey, Apr. 2014, pp. 2061–2066.

[5] *E-UTRA; Mobility Enhancements in Heterogeneous Networks*, document TS 36.839, 3GPP, Valbonne, France, Jan. 2013.

[6] *Evolved Universal Terrestrial Radio Access (E-UTRA); Mobility Enhancements in Heterogeneous Networks*, document TS 36.839, 3GPP, Valbonne, France, Sep. 2012.

[7] *Protocol Specification; Radio Resource Control*, document TS 36.331, 3GPP, Valbonne, France, Dec.2011.

[8] S. Ramanath, V. Kavitha, and E. Altman, "Impact of mobility on call block, call drops and optimal cell size in small cell networks," in *Proc. IEEE Workshop Indoor Outdoor Femto Cells (IOFC)*, Istanbul, Turkey, Sep. 2010, pp. 156–161.

[9] K. Balachandran, J. H. Kang, K. Karakayali, and K. Rege, "Seamless macro-cell anchored radio transmission for enhanced downlink performance in heterogeneous networks," in *Proc. IEEE Int. Conf. Comput. Commun. Netw. (ICCCN)*, Maui, HI, USA, Aug. 2011, pp. 1–5.

[10] K. Yagyu *et al.*, "Investigation on mobility management for carrier aggregation in LTE-advanced," in *Proc. IEEE Veh. Technol. Conf. (VTC)*, San Francisco, CA, USA, Sep. 2011, pp. 1–5.

[11] *Technical Specification Group Radio Access Network; Evolved Universal Terrestrial Radio Access (E-UTRA); Mobility Enhancements in Heterogeneous Networks (Release 11)*, document TS 36.839, 3GPP, Valbonne, France, Jun. 2011.

[12] S. Oh, B. Ryu, and Y. Shin, "EPC signaling load impact over S1 and X2 handover on LTE-advanced system," in *Proc. 3D World Congr. Inf. Commun. Technol. (WICT)*, Dec. 2013, pp. 183–188.

[13] S. Oh, H. Kim, B. Ryu, and N. Park, "Inbound mobility management on LTE-advanced femtocell topology using x2 interface," in *Proc. 20th Int. Conf. Comput. Commun. Netw. (ICCCN)*, Jul. 2011, pp. 1–5.

[14] T. Bai, Y. Wang, Y. Liu, and L. Zhang, "A policy-based handover mechanism between femtocell and macrocell for LTE based networks," in *Proc. IEEE 13th Int. Conf. Commun. Tech.*, Jinan, China, 2011, pp. 916–920.

[15] S. J. Wu, "A new handover strategy between femtocell and macrocell for LTE-based network," in *Proc. 4th Int. Conf. Ubi-Media Comput.*, São Paulo, Brazil, 2011, pp. 203–208.

[16] C. Liu, J. Wei, S. Huang, and Y. Cao, "A distance-based handover scheme for femtocell and macrocell overlaid networks," in *Proc. 8th Int. Conf. Wireless Commun.*, Shanghai, China, 2012, pp. 1–4.

[17] K. Kitagawa, T. Komine, T. Yamamoto, and S. Konishi, "A handover optimization algorithm with mobility robustness for LTE systems," in *Proc. IEEE 22nd Int. Symp. Pers. Indoor Mobile Radio Commun. (PIMRC)*, Sep. 2011, pp. 1647–1651.

[18] M. Z. Chowdhury and Y. M. Jang, "Handover management in high-dense femtocellular networks," *EURASIP J. Wireless Commun. Netw.*, vol. 2013, no. 1, pp. 1–21, 2013.

[19] K. Kitagawa, T. Komine, T. Yamamoto, and S. Konishi, "Performance evaluation of handover in LTE-advanced systems with pico cell range expansion," in *Proc. IEEE 23rd Int. Symp. Pers. Indoor Mobile Radio Commun. (PIMRC)*, Sep. 2012, pp. 1071–1076.

[20] B. Jeong, S. Shin, I. Jang, N. W. Sung, and H. Yoon, "A smart handover decision algorithm using location prediction for hierarchical macro/femtocell networks," in *Proc. IEEE Veh. Technol. Conf. (VTC Fall)*, Sep. 2011, pp. 1–5.

[21] S. Barbera, P. H. Michaelsen, M. Saily, and K. Pedersen, "Improved mobility performance in LTE co-channel HetNets through speed differentiated enhancements," in *Proc. IEEE Globecom*, Dec. 2012, pp. 426–430.

[22] A. Lobinger, S. Stefanski, T. Jansen, and I. Balan, "Coordinating handover parameter optimization and load balancing in LTE self-optimizing networks," in *Proc. IEEE Veh. Technol. Conf.*, May 2011, pp. 1–5.

[23] A. Roy, J. Shin, and N. Saxena, "Multi-objective handover in LTE macro/femto-cell networks," *J. Commun. Netw.*, vol. 15, no. 5, pp. 578–587, 2012.
[24] J. Choi, W.-K. Seo, J.-C. Nam, I.-S. Park, and Y.-Z. Cho, "Handover decision algorithm based on available data volume in hierarchical macro/femto-cell networks," in *Proc. 14th Int. Conf. Commun. Electron.*, Hue, Vietnam, 2012, pp. 145–149.
[25] X. Lin, R. K. Ganti, P. J. Fleming, and J. G. Andrews, "Towards understanding the fundamentals of mobility in cellular networks," *IEEE Trans. Wireless Commun.*, vol. 12, no. 4, pp. 1686–1698, Apr. 2013.
[26] *E-UTRAN—X2 General Aspects and Principles*, document TS 36.420, 3GPP, Valbonne, France, Sep. 2011.
[27] *E-UTRAN X2 Interface: X2 Application Protocol (X2AP)*, document TS 36.423, 3GPP, Valbonne, France, Mar. 2012.
[28] *E-UTRAN—S1 General Aspects and Principles*, document TS 36.410, 3GPP, Valbonne, France, Sep. 2011.
[29] *S1 Application Protocol (S1AP)*, document TS 36.413, 3GPP, Valbonne, France, Mar. 2012.
[30] M. Sesia, M. Toufik, and M. Baker, *LTE—The UMTS Long Term Evolution: From Theory to Practice*. Hoboken, NJ, USA: Wiley, Jan. 2009.
[31] *Radio Resource Control (RRC)*, document TS 36.331, 3GPP, Valbonne, France, Oct. 2013.
[32] *OpenAirInterface*. [Online]. Available: http://www.openairinterface.org/?page_id=72
[33] R. C. Larson and A. R. Odoni, "Bertrand paradox," in *Urban Operations Research*. New York, NY, USA: Prentice-Hall, 1981. [Online]. Available: http://web.mit.edu/urban_or_book/www/book/chapter3/3.3.2.html
[34] *Evolved Universal Terrestrial Radio Access (E-UTRA); Mobility Enhancements in Heterogeneous Networks*, document TS 36.839, 3GPP, Valbonne, France, Jun. 2011.
[35] *Evolved Universal Terrestrial Radio Access (E-UTRA) and Evolved Universal Terrestrial Radio Access Network (E-UTRAN); Overall Description; Stage 2*, document TS 36.300, 3GPP, Valbonne, France, Jun. 2015.
[36] *E-UTRA—Physical Layer Measurements*, document TS 36.214, 3GPP, Valbonne, France, Jun. 2015.
[37] *Radio Resource Control (RRC)*, document TS 36.331, 3GPP, Valbonne, France, Dec. 2010.

JIANXIN JIA received the M.S. degree in computer science and engineering from Shanghai Maritime University, where he is currently pursuing the Ph.D. degree. In 2013, he received the Qualification Certificate of Computer and Software Technology Proficiency as a Database System Engineer, the Qualification Certificate of Computer and Software Technology Proficiency as a Networking Engineer, the Qualification Certificate of Computer and Software Technology Proficiency as a Software Designer in 2014, the Qualification Certificate of Computer and Software Technology Proficiency as a Software Testing Engineer in 2015, and the Honorable Certificate related to the Qualification Certificate of Computer and Software Technology Proficiency (top 3 in Zhejiang province) in 2016. His main research interests include wireless communication, distributed computing, mobile networking, underwater acoustic communication technology, and cloud security.

GUANGZHONG LIU received the B.S. degree from Southwest Jiaotong University and the Ph.D. degree from the China University of Mining and Technology. He is currently a Professor of computer science and engineering with Shanghai Maritime University. His specific research interests include underwater acoustic communication technology, mobile networking, wireless communication, and network security.

DEZHI HAN received the Ph.D. degree from the Huazhong University of Science and Technology. He is currently a Professor of computer science and engineering with Shanghai Maritime University. His research interests include cloud computing, mobile networking, wireless communication, and cloud security.

JUN WANG received the Ph.D. degree from the University of Cincinnati in 2002. He is currently a Professor with the University of Central Florida. His research interests include cloud computing, mobile networking, and cloud security.